Cell Reports

Identification of protein aggregates in the aging vertebrate brain with prion-like and phase-separation properties

Graphical abstract

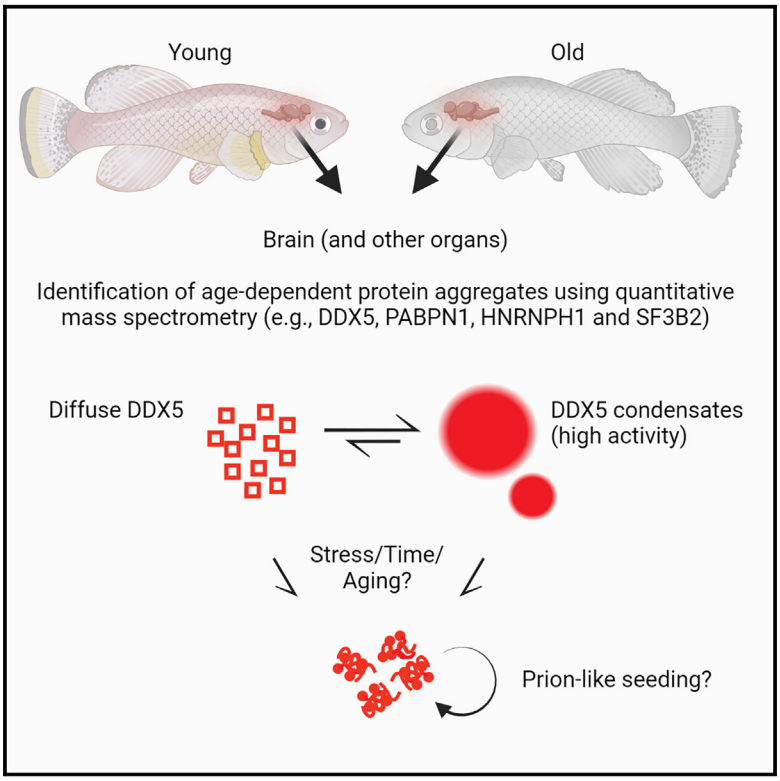

Highlights

- Quantitative identification of proteins that aggregate in old killifish brains
- The RNA helicase DDX5 forms aggregate-like puncta in old vertebrate brains
- DDX5 aggregates exhibit prion-like behavior and seed the formation of new aggregates
- DDX5 forms condensates that enhance its activity but mature into inactive aggregates

Authors

Itamar Harel, Yiwen R. Chen, Inbal Ziv, ..., Alejandro Sánchez Alvarado, Daniel F. Jarosz, Anne Brunet

Correspondence

itamarh@mail.huji.ac.il (I.H.), jarosz@stanford.edu (D.F.J.), abrunet1@stanford.edu (A.B.)

In brief

Harel, Chen, and colleagues describe the systematic identification of proteins that aggregate in old vertebrate brains. Interestingly, one of these proteins, the RNA helicase DDX5, seeds the formation of new aggregates in a "prion-like" behavior. These findings could have implications for the age dependency of cognitive decline.

Harel et al., 2024, Cell Reports ■■, 112787 ■■, 2024
https://doi.org/10.1016/j.celrep.2023.112787

CellPress

Cell Reports

CellPress
OPEN ACCESS

Report

Identification of protein aggregates in the aging vertebrate brain with prion-like and phase-separation properties

Itamar Harel,[1,3,11,*] Yiwen R. Chen,[2,11] Inbal Ziv,[2,12] Param Priya Singh,[1,8,9,12] Daniel Heinzer,[1,12] Paloma Navarro Negredo,[1] Uri Goshtchevsky,[3] Wei Wang,[4,10] Gwendoline Astre,[3] Eitan Moses,[3] Andrew McKay,[1] Ben E. Machado,[1] Katja Hebestreit,[1] Sifei Yin,[2] Alejandro Sánchez Alvarado,[4,5] Daniel F. Jarosz,[2,6,13,*] and Anne Brunet[1,7,13,14,*]

[1]Department of Genetics, Stanford University, Stanford, CA 94305, USA
[2]Department of Chemical and Systems Biology, Stanford University, Stanford, CA 94305, USA
[3]The Silberman Institute, the Hebrew University of Jerusalem, Givat Ram, Jerusalem 91904, Israel
[4]Stowers Institute for Medical Research, Kansas City, MO 64110, USA
[5]Howard Hughes Medical Institute
[6]Department of Developmental Biology, Stanford University, Stanford, CA 94305, USA
[7]Glenn Laboratories for the Biology of Aging, Stanford University, Stanford, CA 94305, USA
[8]Present address: Department of Anatomy, University of California, San Francisco, San Francisco, CA 94143, USA
[9]Present address: Bakar Aging Research Institute, University of California, San Francisco, San Francisco, CA 94143, USA
[10]Present address: National Institute of Biological Sciences, Beijing 102206, China
[11]These authors contributed equally
[12]These authors contributed equally
[13]Senior author
[14]Lead contact
*Correspondence: itamarh@mail.huji.ac.il (I.H.), jarosz@stanford.edu (D.F.J.), abrunet1@stanford.edu (A.B.)
https://doi.org/10.1016/j.celrep.2023.112787

SUMMARY

Protein aggregation, which can sometimes spread in a prion-like manner, is a hallmark of neurodegenerative diseases. However, whether prion-like aggregates form during normal brain aging remains unknown. Here, we use quantitative proteomics in the African turquoise killifish to identify protein aggregates that accumulate in old vertebrate brains. These aggregates are enriched for prion-like RNA-binding proteins, notably the ATP-dependent RNA helicase DDX5. We validate that DDX5 forms aggregate-like puncta in the brains of old killifish and mice. Interestingly, DDX5's prion-like domain allows these aggregates to propagate across many generations in yeast. *In vitro*, DDX5 phase separates into condensates. Mutations that abolish DDX5 prion propagation also impair the protein's ability to phase separate. DDX5 condensates exhibit enhanced enzymatic activity, but they can mature into inactive, solid aggregates. Our findings suggest that protein aggregates with prion-like properties form during normal brain aging, which could have implications for the age-dependency of cognitive decline.

INTRODUCTION

Aging is accompanied by a striking increase in the incidence of neurodegenerative diseases. Many of these diseases are characterized by progressive accumulation of protein aggregates in the brain—amyloid-β and τ for Alzheimer's disease, α-synuclein for Parkinson's disease, and Huntingtin for Huntington's disease.[1,2] Some of these proteins (e.g., TMEM106B) can also aggregate during physiological aging.[3] Protein aggregates accumulate during normal aging in several non-vertebrate organisms, such as yeast and *C. elegans*.[4–11] But vertebrates have more complex tissues. While the aging soluble proteome has been characterized in vertebrates tissues, including the brain,[12–17] a systematic and quantitative evaluation of protein aggregates in the vertebrate brain during normal aging has not been done.

Prion-like properties have been proposed to drive the progression of several neurodegenerative pathologies by facilitating the transmission of protein aggregates from affected to unaffected areas of the brain.[18–22] Long viewed as a rare biological oddity, prions have recently been discovered throughout evolution, from yeast to humans.[23–25] Prions and prion-like self-assembly have been implicated in normal physiological functions, such as metabolism, cell fate determination, antiviral responses, and inflammation.[23,24,26–31] Although proteins with prion-like properties were identified in old *C. elegans*,[4] whether prion-like protein aggregates accumulate during physiological vertebrate aging, notably in the brain, is unknown.

Please cite this article in press as: Harel et al., Identification of protein aggregates in the aging vertebrate brain with prion-like and phase-separation properties, Cell Reports (2023), https://doi.org/10.1016/j.celrep.2023.112787

A Experimental design

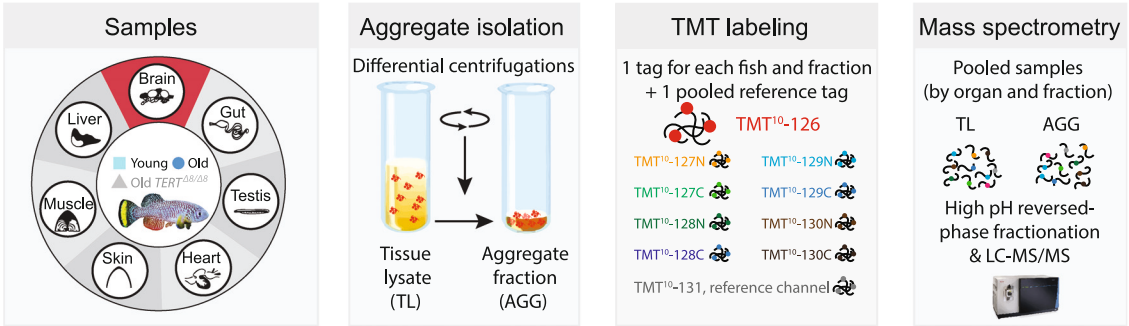

B Aggregates in young and old brains

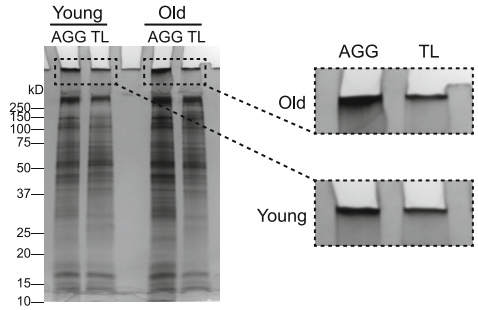

C PCA for protein levels in the brain

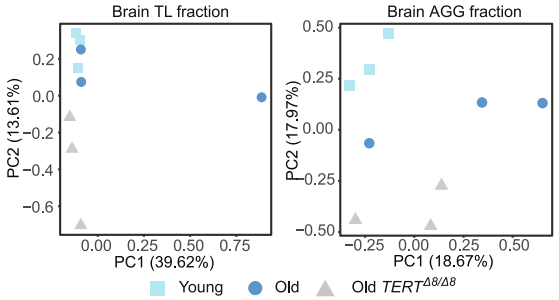

D Aggregation propensity in the aging brain

Killifish protein	Human protein	FC score	Prion score	Fraction of disordered AAs
PABPN1 (2 of 2)	PABPN1	3.8	-12.5	0.42
SLC27A1 (1 of 2)	SLC27A1	2.4	-18.7	0.06
SNMP70	SNRNP70	2.3	-14.7	0.57
ANK2 (1 of 3)	ANK2	2.3	4.9	0.57
ATP5J (1 of 2)	ATP5J	2.3	-24.5	0.95
MAGI2 (2 of 3)	MAGI2	2.3	3.0	0.70
CLASP2	CLASP2	2.2	0.7	0.42
MARK4 (2 of 4)	MARK4	2.2	-4.8	0.48
EVL (3 of 4)	EVL	2.1	7.9	0.76
WASF1	WASF1	2	-4.8	0.63
NONO	NONO	1.9	9.6	0.30
CASKIN1 (3 of 5)	CASKIN1	1.9	-7.9	0.70
SCARB2 (2 of 3)	SCARB2	1.9	-14.7	0.14
MPI	MPI	1.8	-17.8	0.00
SOD2	SOD2	1.8	-12.3	0.13
NCOA5 (2 of 2)	NCOA5	1.8	2.6	0.48
SF3B2	SF3B2	1.8	-5.6	0.59
TRIO (1 of 2)	TRIO	1.8	11.4	0.41
GYS1	GYS1	1.7	-20.2	0.14
RPL10	RPL10	1.7	-20.8	0.00
EXOC1 (1 of 2)	EXOC1	1.6	-12.1	0.13
ATP8A1	ATP8A1	1.6	-11.0	0.10
LOC107379131	No homolog	1.6	-20.2	0.00
CAST	CAST	1.6	-18.3	1.00
DYNLL2 (1 of 3)	DYNLL2	1.5	-27.0	0.00
HMOX2	HMOX2	1.5	-21.3	0.17
FAM91A1	FAM91A1	1.5	-16.8	0.21
CAMK2D (3 of 3)	CAMK2D	1.5	-17.4	0.22
TMOD3	TMOD3	1.5	-13.7	0.25
RPL13A	RPL13A	1.5	-15.2	0.00
DDX5 (2 of 2)	DDX5	1.5	35.0	0.30
HNRNPH1 (2 of 2)	HNRNPH1	1.5	24.4	0.26
EML1 (2 of 3)	EML1	1.5	-18.0	0.03
ABLIM2	ABLIM2	1.5	-6.1	0.56

E GSEA enrichment for aggregation propensity in the aging brain

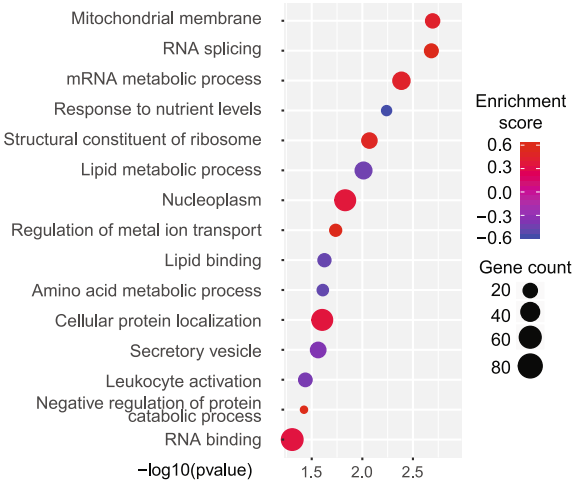

F Enrichment for prion-like domains (PrD)

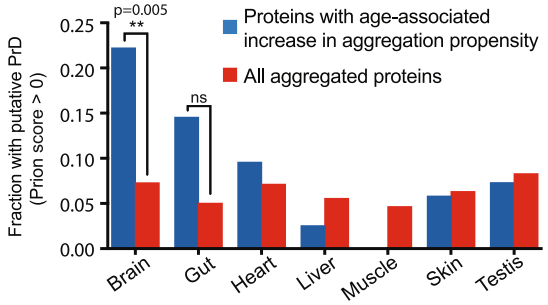

(legend on next page)

Please cite this article in press as: Harel et al., Identification of protein aggregates in the aging vertebrate brain with prion-like and phase-separation properties, Cell Reports (2023), https://doi.org/10.1016/j.celrep.2023.112787

The African turquoise killifish *Nothobranchius furzeri* is an ideal vertebrate model to investigate protein aggregation in the aging brain. Its lifespan is 6–10 times shorter than mice or zebrafish.[32,33] Within this short time frame, the killifish recapitulates defining features of vertebrate aging—cognitive decline and neurodegeneration in the brain.[34–39] The killifish responds to conserved lifespan interventions, including dietary restriction.[40,41] Moreover, integrative genomic and genome-editing toolkits have been developed in the organism.[42–48] Some protein aggregates have been examined qualitatively in aged killifish brains, such as ribosome subunits.[17] However, the identity of specific protein aggregates in old brains and whether they have a prion-like behavior remains uncharacterized.

Here, we leverage the killifish as a powerful model to unbiasedly identify proteins that aggregate during normal brain aging. Using quantitative proteomics, we identify many proteins with an increased propensity to aggregate in the aging brain. One of these proteins, the RNA helicase DDX5, forms aggregate-like puncta in old brains of both killifish and mice and has prion-like seeding properties in cells. DDX5 rapidly undergoes phase separation *in vitro*, and these condensates mature into solid aggregates that are inactive and potentially infectious. The aggregation of key proteins during normal vertebrate brain aging could contribute to the age dependency of cognitive decline.

RESULTS

Proteomic identification of proteins that aggregate in the old vertebrate brain

The identity of protein aggregates that arise during normal brain aging is poorly understood. To discover such aggregates, we used a protocol that separates them from large protein complexes and membraneless organelles based on molecular weight[49]—an approach that can detect amyloids[50] and other types of protein aggregates.[49] We collected seven tissues (brain, heart, liver, gut, muscle, skin, testis) from three young (3.5 months), three old (7 months), and three old telomerase ($TERT^{\Delta 8/\Delta 8}$, 7 months) mutant male killifish (Figure 1A). $TERT^{\Delta 8/\Delta 8}$ mutant fish exhibit signs of premature aging, especially in proliferative organs (e.g., gut, testis).[45] Using differential centrifugation, we isolated a fraction enriched for high molecular weight protein aggregates (AGG) and another fraction of matched native tissue lysate (TL) (STAR Methods).[49] The aged brain aggregate fraction displayed substantially more SDS-resistant species than the young counterpart (Figure 1B, inset), suggesting that protein aggregation is enhanced in the aged killifish brain.

To quantitatively characterize protein aggregation in old brains (and other tissues), we used tandem mass tag (TMT)-based quantitative mass spectrometry (MS) (Figure 1A).[49] Focusing on the brain, principal-component analysis (PCA) revealed stronger separation of the aggregate fractions compared with total lysate fractions between young, old, and old $TERT^{\Delta 8/\Delta 8}$ mutant killifish (Figure 1C). To identify proteins that are intrinsically more prone to aggregation with old age, we calculated the aggregation propensity—the relative abundance ratio of aggregate versus tissue lysate for each protein expressed in the brain (Figure 1D). Proteins with significant age-dependent increases in aggregation propensity in the brain included many proteins with RNA-binding properties,[23,24,26–31,51,52] including proteins involved in mRNA synthesis (PABPN1) and splicing (DDX5, HNRNPH1, SF3B2) (Figures 1D, 1E, and S1A).

Interestingly, brain proteins with an increased aggregation propensity with age were uniquely enriched for protein sequences that are predicted to have prion-like properties[53] (Figures 1D and 1F). In addition, they also exhibited intrinsically disordered regions[54]—domains that are not predicted to adopt a single three-dimensional structure in solution—another hallmark of prions and prion-like proteins[54] (Figures 1D, 1F, and S1B). Collectively, these data identify many proteins that form aggregates in the vertebrate brains during physiological aging and reveal an enrichment for proteins with disordered and prion-like domains.

The RNA helicase DDX5 forms aggregate-like puncta in old vertebrate brains

Among the proteins that aggregate with age in the killifish brain, we focused on DDX5—an ATP-dependent RNA helicase (Figure S2A)—because of its high prion-like score (Figure 1D) and role in RNA splicing.[55] DDX5 has a C-terminal intrinsically

Figure 1. Quantitative identification of age-related protein aggregation in the vertebrate brain

(A) Quantitative proteomic analysis pipeline for the brain (and other organs) from young, old, and old $TERT^{\Delta 8/\Delta 8}$ male fish. For each organ, a tissue lysate (TL) and an aggregate (AGG) fraction were isolated, and tandem mass tag (TMT) labeling and mass spectrometry were performed. Workflow and tags: Table S1A.

(B) Silver stain of SDS-PAGE gel with TL and AGG samples from young and old brains. Similar amounts (~1 μg) of TL and the AGG fraction from brain were used. Note that the protein quantity for the AGG fraction was underestimated. A version of the gel with additional organs is in Chen et al.[49]

(C) Principal-component analysis (PCA) on protein abundance in TL or AGG fractions from the brain of young (light blue square), old (dark blue circle), and old $TERT^{\Delta 8/\Delta 8}$ (gray triangles) fish. Each symbol represents an individual fish. There was an outlier for the old brain sample due to quantification prior to mass spectrometry analysis. Another version of this PCA is in Chen et al.[49]

(D) Ranked list of proteins with increased aggregation propensity in old versus young brains based on descending fold change (FC)—i.e., the relative abundance ratio of AGG over TL averaged across three fish in old versus young killifish brain ($p < 0.05$, Student's t test). Predicted prion-like domain (PrD) scores (PLAAC) and fraction of disordered amino acids (aa) (DISOPRED3) are presented (Table S1D). Red: PrD score > 0 and fraction of disordered aa > 0.3 (30%) are considered to be prion-like proteins or intrinsically disordered proteins, respectively. Paralogs are indicated as "X of Y" ("2 of 3" means the second paralog out of three identified paralogs) (Table S1D). See also Table S1B.

(E) Selected GO enrichment using gene set enrichment analysis (GSEA) for proteins with an increased aggregation propensity in old brains. Complete set in Figure S1A. Enrichment score, the score for enrichment/depletion of GO terms in this gene set. Counts, number of genes. p values were not false discovery rate (FDR) corrected.

(F) Enrichment for PrDs in proteins with increased aggregation propensity with age in the brain and other tissues. Data represent the fraction of proteins with putative PrD (PrD score > 0). Red: all detected aggregated proteins; blue: proteins with increased aggregation propensity with aging ($t \geq 0.75$, $p < 0.05$ from Student's t test). Age-associated differences in aggregation propensity were assessed using Fisher's exact test. Numbers in Table S3A.

Please cite this article in press as: Harel et al., Identification of protein aggregates in the aging vertebrate brain with prion-like and phase-separation properties, Cell Reports (2023), https://doi.org/10.1016/j.celrep.2023.112787

A Prion-like domain (PrD) in DDX5

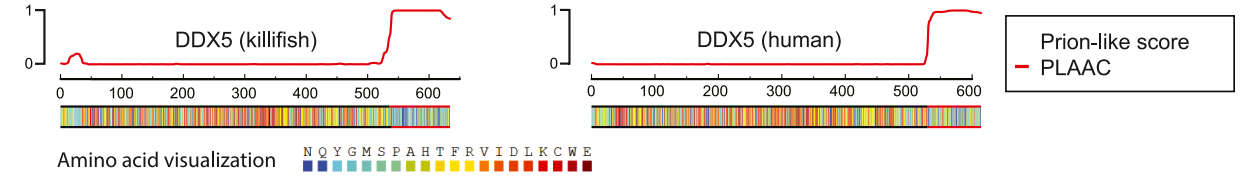

B Intrinsically disordered region (IDR) in DDX5

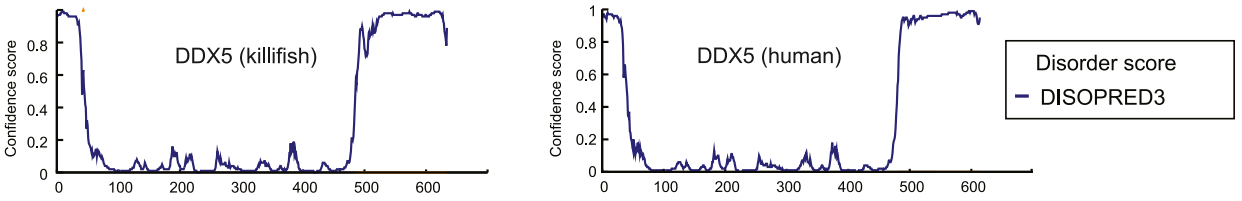

C Immunohistochemistry of **killifish** brain sections

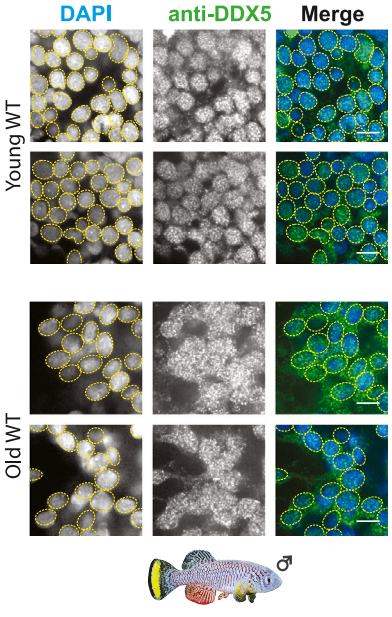

D Immunohistochemistry of **mouse** brain sections

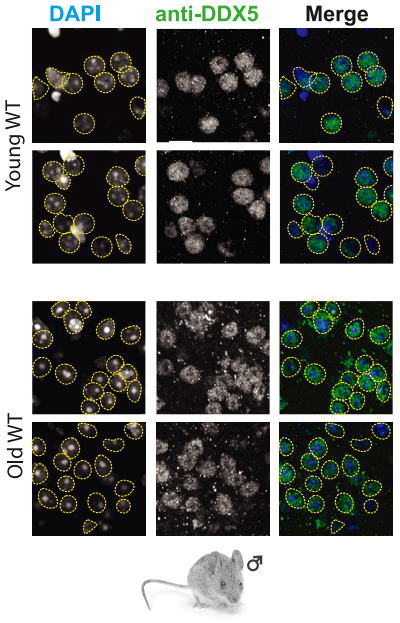

E Generation of transgenic killifish: *Tg(ddx5:DDX5-GFP)*

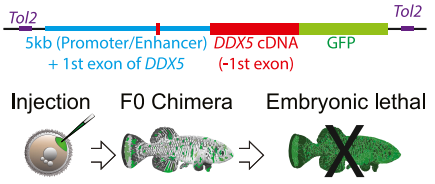

F Immunohistochemistry of **killifish** brain sections

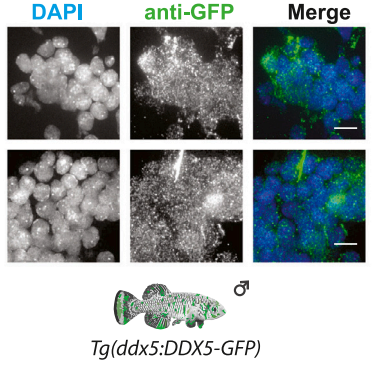

G Aggregation of killifish DDX5 and truncation mutants in human 293T cells

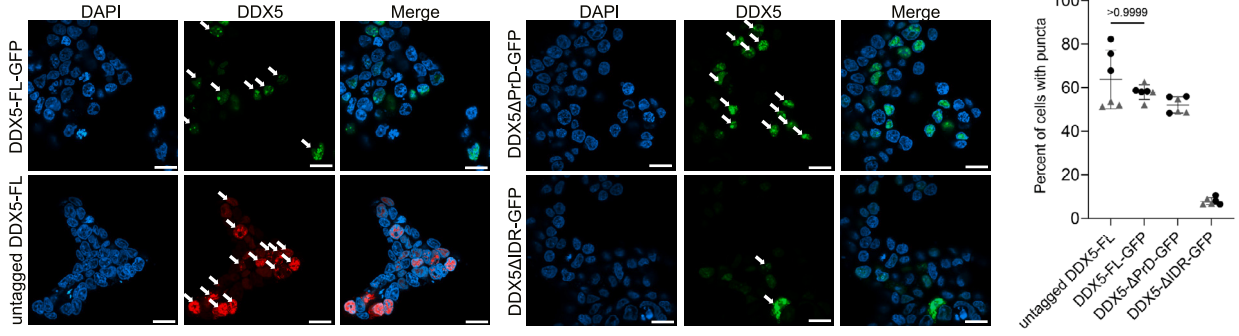

(legend on next page)

Please cite this article in press as: Harel et al., Identification of protein aggregates in the aging vertebrate brain with prion-like and phase-separation properties, Cell Reports (2023), https://doi.org/10.1016/j.celrep.2023.112787

disordered region (IDR), which encompasses a domain with a strong prion-like score (prion-like domain [PrD]) (Figures 2A, 2B, S2B, and S2C). Both the entire IDR region and the specific PrD are conserved in human DDX5 (Figures 2A and 2B).

To independently test whether DDX5 forms aggregates in the aging killifish brain, we generated an antibody to killifish DDX5 (Figure S2D) and performed immunostaining on brain sections. While DDX5 formed nuclear puncta in young killifish brains, DDX5 was present in both nuclear and cytoplasmic puncta in old killifish brains, and qualitatively, these puncta became more "disorganized" (Figures 2C and S2E, quantified in Figure S2F). Interestingly, immunostaining of young and old mouse brains also showed that mammalian DDX5 formed both nuclear and cytoplasmic/peri-nuclear puncta in old mouse brains and that these puncta were more disorganized (Figure 2D). Differences in DDX5 puncta appearance between killifish and mice could be due to protein homeostasis milieu or protein sequences.

Additionally, we generated transgenic fish founders expressing killifish DDX5 fused to GFP driven by *DDX5* regulatory regions (Figures 2E, and S3A). Overexpressed DDX5-GFP formed disorganized puncta both in the cytoplasm and the nucleus in old killifish brains (Figure 2F). DDX5 knockout killifish were not viable, highlighting the importance of this RNA helicase at the organismal level (Figure S3B). Thus, DDX5 is an essential protein that assembles in nuclear puncta in young animals, but these puncta become mislocalized and disorganized in old vertebrate brains.

We then asked if killifish DDX5 overexpressed in a heterologous system can form aggregate-like puncta. When overexpressed in human 293T cells, killifish DDX5 fused to GFP formed nuclear puncta, and in rare cases, these puncta were cytoplasmic (Figures 2G, S3C, and S3D). Overexpressed killifish DDX5 without any fused fluorescent protein also formed nuclear puncta (Figure 2G). Truncation of the entire IDR of DDX5 significantly reduced the formation of puncta (Figures 2G and S3C). In contrast, truncation of the PrD alone still allowed puncta formation (Figure 2G). Finally, human DDX5 fused to GFP also formed nuclear puncta (Figure S3E), indicating that the ability of DDX5 to form aggregate-like puncta is conserved.

Hence, DDX5 forms aggregate-like puncta *in vivo* in old vertebrate brains and in mammalian cells, and the disordered domain of DDX5 is a critical molecular determinant of its aggregation capacity.

DDX5 aggregates act as prions that can seed the formation of new aggregates

We asked whether DDX5 aggregates have "infectious" prion-like properties—i.e., the ability to "seed" the formation of larger protein aggregates. To this end, we used an inducible system[56] in which yeast cells are switched from raffinose- to galactose-containing media to drive the expression of fluorescently tagged fusion proteins (Figure 3A). A hallmark of prion proteins is that their overexpression induces their aggregation.[57] When overexpressed in yeast, killifish DDX5-EGFP (and other proteins that aggregated in old brains such as MARK4 and SCARB2) formed aggregate-like fluorescent puncta, whereas EGFP (or mRuby3) fused to other proteins (PABPN1 and HNRNPH1) did not (Figures 3B, 3C, and S4A).

To test whether DDX5 aggregates are "infectious," we used a 2-color system in which yeast cells are switched from raffinose- to galactose-containing media to induce the expression of mRuby3-tagged proteins (induction) and then switched back to raffinose-containing media and allowed to propagate for twenty generations (outgrowth). This systems dilutes pre-existing aggregates beyond detection levels and allows the detection of protein aggregation seeded across generations onto the low-expressed EGFP-tagged version (Figure 3D). We verified that killifish DDX5 protein inducibly aggregated in this 2-color system (Figures 3E, induction, red puncta, and S4B), whereas other control proteins did not (Figures S4C and S4D). Interestingly, killifish DDX5 tagged with EGFP (DDX5-EGFP) still formed puncta after propagation over multiple generations (Figures 3E, outgrowth, green puncta, and 3F), consistent with an infectious prion-like behavior.

We asked whether the disordered PrD within DDX5 is required for its aggregation and prion-like propagation. Truncating the entire IDR abolished DDX5 aggregation in this assay and, consequently, any ability to seed (Figures S4F and S4G). Interestingly, truncation of just the PrD still resulted in DDX5 aggregation (Figures 3G, S4E, and S4F), similar to our observations in human cells. However, this PrD truncation construct could not act as a template for prion-like seeding (Figures 3G and S4F–S4H). These results identify separable molecular drivers of DDX5 aggregation and prion-like seeding.

Figure 2. The RNA helicase DDX5 has a conserved PrD and shows increased aggregate-like puncta in old vertebrate brains

(A and B) Presence and location of predicted PrD (A) and intrinsically disordered region (IDR; B) in DDX5 in killifish and humans. Red line: PLAAC score. DDX5 amino acid positions are indicated at the bottom. Amino acid composition is color coded. Blue line: local disorder score (DISOPRED3).

(C) Immunohistochemistry for DDX5 in brain sections from young (3.5 months) and old (7 months) male killifish. Green: DDX5; blue: DAPI (nuclei). Image representative of 3 individual fish for each age group. Staining was performed twice independently, ~7 sections per fish per experiment. Scale bar: 10 μm. Quantification of the subcellular localization of DDX5 puncta is in Figure S2F.

(D) Immunohistochemistry for DDX5 in brain sections from young (4 months) and old (28 months) male mice. Green: DDX5; blue: DAPI (nuclei). Image representative of 2 mice per age group, 6 sections per mouse. Scale bar: 20 μm.

(E) Generation of *Tg(ddx5:DDX5-GFP)* transgenic F0 founders (there was no germline transmission).

(F) Immunohistochemistry for GFP in brain sections from old (~6–7 months) male *Tg(ddx5:DDX5-GFP)* F0 founders (which can have variable protein expression). Green: GFP; blue: DAPI (nuclei). Image representative of 3 individual fish, ~6 sections per fish. Scale bar: 10 μm.

(G) Immunocytochemistry in human 293T cells for untagged killifish DDX5 full length (red, antibody to killifish DDX5) or GFP-tagged killifish DDX5 (full length [FL] and two different truncation mutants [ΔIDR and ΔPrD] [green, antibody to GFP]). Left: representative images from two independent experiments, each performed in triplicate. White arrows indicate cells with puncta (determined by signal intensity over a pre-defined maximum). Scale bar: 10 μm. Right: mean ± SD of the percentage of transfected cells showing DDX5 puncta. Each dot represents the average of ~240 cells from 3 fields of view over two independent experiments. Circles: experiment #1; triangles: experiment #2. p values: Kruskal-Wallis with Dunn's correction.

Please cite this article in press as: Harel et al., Identification of protein aggregates in the aging vertebrate brain with prion-like and phase-separation properties, Cell Reports (2023), https://doi.org/10.1016/j.celrep.2023.112787

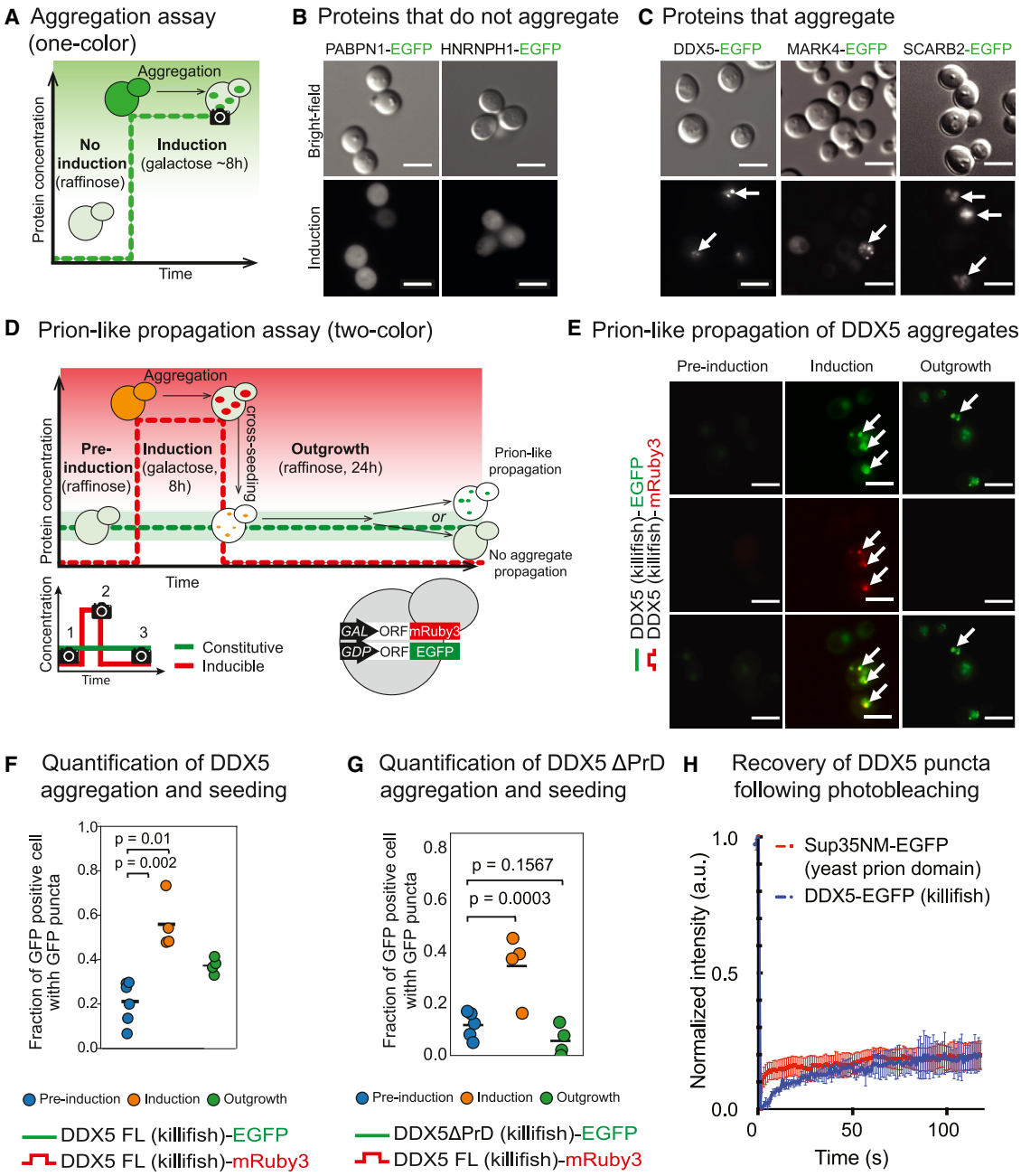

Figure 3. DDX5 exhibits prion-like seeding properties

(A) "1-color" experimental design to assess protein aggregation in yeast by conditionally expressing C-terminally EGFP-tagged killifish protein candidates under a galactose-inducible promoter. Protein aggregation is scored by quantification of the EGFP fluorescent puncta.

(B and C) Identification of killifish candidate proteins that do not aggregate (B) or that do aggregate (C) following galactose-inducible overexpression in yeast. White arrows: fluorescent puncta (aggregates). Scale bar: 5 μm.

(D) "2-color" experimental design to assess prion-like aggregate propagation in yeast. This design tests whether brief overexpression ("induction") of a killifish candidate (C-terminally tagged with mRuby3 and under the control of a galactose-inducible promoter) can induce a cross-generational prion-like propagation of a constitutively expressed candidate (C-terminally tagged with EGFP and under the control of the glyceraldehyde 3-phosphate dehydrogenase (GPD) promoter with a single-copy-number plasmid). The cross-generational effect was tested during "outgrowth" (i.e., 200-fold dilution), highlighting aggregates that can stably propagate for 7–8 generations in yeast cells. Protein aggregation is scored by quantification of mRuby3 (red) or EGFP (green) fluorescent puncta.

(E) Using the 2-color system, killifish DDX5-EGFP aggregates were visible in both induction and outgrowth phases, indicating prion-like propagation. Representative of 4 independent experiments. White arrows: fluorescent puncta (aggregates). Scale bar: 5 μm.

(F) Quantification of DDX5 aggregates and prion-like seeding potential by calculating the fraction of EGFP-positive cells with EGFP puncta during pre-induction, induction, and outgrowth. Black bar indicates mean values from 4–6 independent experiments (6 independent pre-induction measurements and 4 independent

(legend continued on next page)

Please cite this article in press as: Harel et al., Identification of protein aggregates in the aging vertebrate brain with prion-like and phase-separation properties, Cell Reports (2023), https://doi.org/10.1016/j.celrep.2023.112787

A hallmark of prion-like propagation is its specificity. In our 2-color seeding assay, DDX5 puncta were efficiently propagated when killifish DDX5-EGFP was expressed with DDX5-mRuby3 (Figure 3). However, such an effect did not occur with the expression of mRuby3 protein or polyQ-mRuby3 aggregates, demonstrating that propagation is specific to DDX5 (Figures S4I and S4J).

Another characteristic of many prions is their ability to form relatively immobile aggregates. To investigate the dynamics of DDX5 aggregation, we used fluorescence recovery after photobleaching (FRAP).[58–61] In FRAP, traditional prion aggregates have poor recovery, consistent with their immobile nature (Figure 3H). We photobleached fluorescent puncta formed by overexpression of killifish DDX5-EGFP in live yeast cells. Fluorescence recovery was extremely slow and similar to the amyloid aggregates formed by the archetypical yeast prion protein Sup35 (Figure 3H). Thus, DDX5 aggregates have several prion-like properties.

DDX5 has phase-separation behavior that depends upon its disordered and prion-like domains

Some proteins with prion-like properties can also exhibit phase-separation behavior, in which a recombinant protein spontaneously forms large condensates within an aqueous solution.[58,59,62–69] We characterized the phase-separation properties of DDX5 *in vitro* by generating recombinant killifish DDX5 from *E. coli* (Figure S5A). Purified killifish DDX5 could easily phase separate to form condensates under physiological protein and salt concentrations (1–10 μM and ∼150 mM, respectively) (Figure 4A). These condensates were round, increased in size with time (Figure 4B), and could be dissolved at elevated salt concentrations (Figure 4A). Condensates formed equally well with unlabeled protein (Figure 4B, top right), establishing that the behavior was not an artifact of the fluorophore. Thus, killifish DDX5 exhibits phase-separation behavior *in vitro*, with the formation of large condensates.

We asked which domains of DDX5 are necessary for its *in vitro* phase-separation properties. Truncation of the entire IDR completely abolished phase separation (Figure 4A). Truncation of only the PrD did not entirely abolish DDX5's phase-separation behavior, but it did shift the phase boundary (Figure 4A). Indeed, DDX5 ΔPrD mutant protein remained mostly diffuse under physiological concentrations (Figure 4A) and formed only small droplets in non-physiological (high protein concentration) conditions (Figure 4B). Thus, the PrD is critical for phase separation at physiological conditions and for the formation of large condensates. Given that the PrD is essential for the propagation of aggregates *in vivo* in yeast, the phase separation properties of DDX5 may play an important role in driving its prion-like propagation.

DDX5 condensates enhance activity but can mature into inactive, potentially infectious aggregates

DDX5 is an ATP-dependent RNA helicase. We measured DDX5 ATPase activity in the diffuse versus condensate states. To this end, we isolated diffuse DDX5 in pre-steady-state condition (Figure 4C) by quickly dialyzing the protein in low-salt buffer and removing any nucleated condensate that might have formed through centrifugation. We performed an RNA-dependent ATPase activity assay on half of the diffuse DDX5 sample. In parallel, we waited for the other half of the DDX5 sample to mature, forming a mixture of diffuse proteins and condensates, and we performed the same assay on this fraction (Figures 4D and S5B). Interestingly, in conditions that favor condensate formation, DDX5 had a greater ATP hydrolysis activity than in diffuse conditions (Figure 4D). We next examined the ATPase activity of the DDX5 ΔPrD mutant protein. DDX5 ΔPrD did not form condensates at the concentrations used and did not exhibit a change in ATPase activity as a function of increased protein concentration (Figure S5C). In the diffuse state, the ATPase activities of DDX5 and the DDX5 ΔPrD truncation mutant were similar (Figures S5D and S5E). Thus, the condensate state may be physiologically important for DDX5 function.

Finally, we asked whether the physiological phase-separation properties of DDX5 could come at a price over time and underlie the emergence of a prion-like seeding behavior. Over time, DDX5 condensates matured into less spherical (more disorganized) aggregates (Figure 4E). Interestingly, these solid DDX5 aggregates had much less ATPase activity than the diffuse form (Figure 4F). These solid aggregates also efficiently seeded the formation of additional aggregates *in vitro* (Figure 4G). Thus, the condensate form of DDX5 may enhance its physiological activity but could, over time, lead to irreversible aggregation, loss of function, and potentially seeding.

DISCUSSION

Our study identifies many proteins that form aggregates in the vertebrate brain during normal aging. Protein aggregates were known to increase with age in *C. elegans*,[4–6,9,11,70] but whether this applied to vertebrates, which have more complex organs and tissues, was not characterized quantitatively. While older killifish have been shown to exhibit aggregation of α-synuclein[38] or ribosomal subunits,[17] our study reveals that many proteins that were not previously associated with diseases aggregate during physiological aging. One of these proteins, the RNA helicase DDX5, forms aggregates in old brains both in killifish and in mice, indicating that the aggregation of this protein is conserved throughout evolution. Proteins that aggregate in old brains

experiments with matched pre-induction, induction, and outgrowth measurements). Each dot represents the average value within each experiment (an average of 135 GFP-positive yeast cells were quantified for each strain under each experimental condition). p values: Student's t test.

(G) Quantification of DDX5 ΔPrD aggregation and prion-like seeding potential by calculating the fraction of EGFP-positive cells with EGFP puncta during pre-induction, induction with DDX5 FL-mRuby3, and outgrowth. Black bar indicates mean values from 4–5 independent experiments (5 independent pre-induction measurements and 4 independent experiments with matched pre-induction, induction, and outgrowth measurements). p values: Student's t test.

(H) Fluorescence recovery after photobleaching (FRAP) of killifish DDX5 (blue line) and yeast Sup35NM (a *bona fide* yeast prion, red line) puncta in yeast. Representative of 2 independent experiments. Mean ± SEM of the normalized intensity of the photobleached area at each time point (10 s interval with photobleaching performed at the 4th frame).

Please cite this article in press as: Harel et al., Identification of protein aggregates in the aging vertebrate brain with prion-like and phase-separation properties, Cell Reports (2023), https://doi.org/10.1016/j.celrep.2023.112787

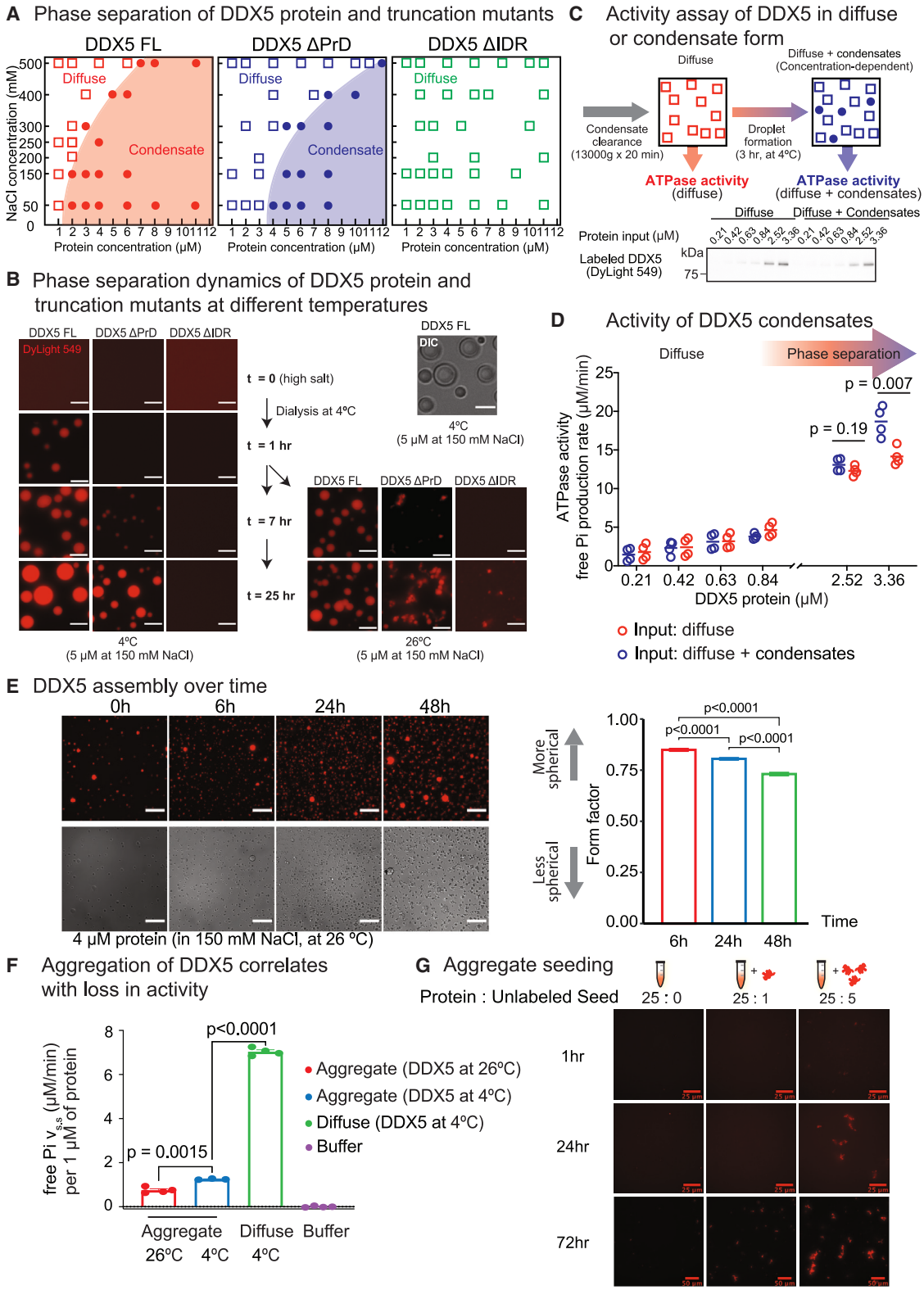

Figure 4. DDX5 phase separates and can form aggregates

(A) Phase diagrams for purified killifish DDX5 recombinant protein FL and truncation mutants (ΔPrD and ΔIDR) under variable NaCl (y axis) and protein concentrations (x axis). Empty squares: diffuse state; full circle: condensate state.

(legend continued on next page)

Please cite this article in press as: Harel et al., Identification of protein aggregates in the aging vertebrate brain with prion-like and phase-separation properties, Cell Reports (2023), https://doi.org/10.1016/j.celrep.2023.112787

exhibit enrichment for disordered regions and PrDs, suggesting a protein-autonomous mode of aggregate formation (though the protein homeostasis environment of the aged brain could also contribute).[49,71–73]

DDX5 is an ATP-dependent RNA helicase that is involved in RNA splicing. DDX5 associates with RNA foci in mammalian cells[74] and forms nuclear speckles, which are likely important for its function as a splicing helicase.[75] We show that DDX5 can self-assemble into condensates *in vitro*, with increased ATP hydrolysis activity, suggesting a physiological role for DDX5 nuclear speckles. This property could also render DDX5 more susceptible to aggregation during aging, which could result in RNA-splicing defects and altered cellular functions. As DDX5 is involved in the splicing of Tau (MAPT) in Alzheimer's disease,[76] aggregation properties might contribute to defects during aging and possibly neurodegenerative diseases.

Strikingly, DDX5 exhibits phase separation *in vitro* and prion-like behavior *in vivo* in yeast. The PrD of DDX5 is critical for its phase-separation and prion-like properties. Other RNA-binding proteins (from yeast and mammals) have been recently shown to exhibit phase-separation behavior (FUS, TDP-43, SUP35, etc.), and their PrDs are important for this transition,[58,59,77–79] though not all proteins that contain these domains behave like *bona fide* prions. Prion-like phase-separation properties could contribute to the spread of cognitive defects during aging and neurodegenerative diseases.

Limitations of the study

Here, we assess protein aggregates in the whole brain during aging, which does not provide regional or cellular resolution. In addition, the method we use to enrich for protein aggregates may not capture all types of aggregates and, conversely, may enrich for some proteins that are not aggregated. It will be important to independently validate the aggregation properties of the proteins identified here, beside DDX5. Finally, the *in vivo* relevance of DDX5 aggregation remains unclear. It will be interesting to examine DDX5 puncta in brains of patients with neurodegenerative diseases and to explore the link between DDX5 subcellular localization and aggregation. It will also be important to characterize DDX5 aggregate characteristics and seeding properties in the brain and determine if expression of DDX5 lacking its PrD *in vivo* affects age-dependent cognitive defects.

STAR★METHODS

Detailed methods are provided in the online version of this paper and include the following:

- KEY RESOURCES TABLE
- RESOURCE AVAILABILITY
  - Lead contact
  - Material availability
  - Data and code availability
- EXPERIMENTAL MODEL AND STUDY PARTICIPANT DETAILS
  - S. *cerevisiae*
  - Mice
  - African turquoise killifish strain, husbandry, and maintenance
- METHOD DETAILS
  - Isolation of tissue lysate (TL) and aggregate-enriched (AGG) fractions from brain tissues
  - Mass spectrometry sample preparation and analysis
  - Annotation of the NCBI genes models of turquoise killifish
  - Mass spectrometry data normalization and analysis of age-associated changes
  - Principal component analysis (PCA)
  - Gene ontology enrichment analysis
  - Statistics for enrichment for PLAAC and DISOPRED
  - CRISPR/Cas9 target prediction and gRNA synthesis
  - Production of Cas9 mRNA
  - Microinjection of turquoise killifish embryos and sequencing of targeted sites
  - Generation of DDX5-GFP transgenic fish
  - GFP antibody staining in brain tissue
  - Generation of killifish DDX5 antibodies
  - Tissue extracts and western-blot for DDX5 antibodies
  - Immunostaining of DDX5 in killifish brain sections
  - Immunostaining of DDX5 in mouse brain sections
  - Cloning of killifish cDNAs
  - Cloning and exogenous expression of killifish proteins in 293T cells
  - Cloning of DDX5 wild-type and mutants in yeast vectors
  - Exogenous expression of killifish proteins in *Saccharomyces cerevisiae* (one color overexpression assay)
  - Exogenous expression of killifish proteins in *Saccharomyces cerevisiae* (two-color seeding assay)
  - Fluorescence recovery after photo bleaching
  - DDX5-SNAP *E. coli* expression and purification
  - DDX5(1–535)-SNAP *E. coli* expression and purification
  - DDX5(1–483)-SNAP *E. coli* expression and purification
  - His10-DDX5-SNAP *E. coli* expression and purification
  - Protein labeling reaction
  - Phase diagrams
  - Salt, protein concentration, temperature, and time effects on DDX5 assembly

(B) Left: phase separation temporal dynamics of DDX5 FL or truncation mutants (ΔPrD and ΔIDR) at various temperatures. Red: DyLight 549-labeled C-terminally SNAP-tagged recombinant protein. Representative of 2 independent experiments. Scale bar: 5 μm. Top right: Differential interference contrast (DIC) representative image of DDX5 condensates.

(C) Experimental design to measure DDX5 ATPase activity in diffuse or condensate states. Empty squares: diffuse state; full circle: condensates. Bottom: western blot to verify DDX5 protein concentration.

(D) Assessment of ATPase activity of the killifish DDX5 protein in diffuse (red circles) or condensate (blue circles, above 2 μM) forms. ATPase activity is measured as a function of the free phosphate (Pi) release rate (μM/min) at indicated DDX5 protein concentrations (μM). Values of 4 replicates from one representative experiment. Two independent experiments were performed (2nd experiment in Figure S5B). DDX5 has no activity in the absence of RNA.

(E) Formation of more disorganized DDX5 aggregates over time. SNAP-tagged recombinant DDX5 labeled with the DyLight 549 dye (left panels). Quantification of the form factor (sphericality of the condensates/aggregates) (right panel). p values: Student's t test.

(F) Comparison of ATPase activity of killifish DDX5: aggregate (red or blue bars), diffuse (green bar), and buffer only (purple bar). ATPase activity is measured as in (D). Representative of 2 independent experiments (mean ± SD from one experiment).

(G) DDX5 aggregates upon seeding with aggregated DDX5 protein at indicated molar ratios (top) and time post-seeding (left). SNAP-tagged recombinant DDX5 labeled with DyLight 549 dye (Protein). His10- and SNAP-tagged recombinant DDX5 aggregates labeled with Alexa 488 (Seed). Scale bar: 25 μm (top) or 50 μm (bottom). Representative of 2 independent experiments.

SUPPLEMENTAL INFORMATION

Supplemental information can be found online at https://doi.org/10.1016/j.celrep.2023.112787.

ACKNOWLEDGMENTS

We thank Steven Boeynaems, Serena Sanulli, and Reut Shalgi for critical reading of the manuscript. We thank the Brunet, Jarosz, and Harel labs, particularly Olivia Zhou, for stimulating discussion and feedback on the manuscript. We thank T. Kelly Rainbolt and Judith Frydman for guidance on protein homeostasis. We thank Christine Yeh for help with mass spectrometry analyses. We thank Stanford's mass spectrometry facility, notably Christopher M. Adams and Ryan Leib, for processing samples. We thank Parag Mallick and Josh Elias for feedback on mass spectrometry analyses. We thank Kiran Chandrasekher and Ray Futia for independent protein aggregation quantification in yeast and Anupam Chakravarty for feedback on DDX5 *in vitro* experiments. We thank Susan Murphy (Stanford) and Ashayma Abu-tair (HUJI) for killifish maintenance. Mass spectrometry experiments were supported by the Vincent Coates Foundation Mass Spectrometry Laboratory, Stanford University (RRID:SCR_017801) and NIH P30CA124435 (Stanford Cancer Institute Proteomics/Mass Spectrometry Shared Resource). FRAP experiments were supported in part by NIH S10OD01227601 (National Center for Research Resources). This work was supported by NIH RF1AG057334 (A.B. and D.F.J.) and R01AG063418 (A.B. and D.F.J.); Stanford Alzheimer's Disease Research Center and Zaffaroni Alzheimer's Disease Translational Program (A.B. and D.F.J.); the Stanford Brain Rejuvenation Project (A.B.); the Glenn Foundation for Medical Research (A.B.); a Stanford Systems Biology Seed Grant (I.H., Y.R.C., and I.Z.); ERC StG #101078188 (I.H.); the Zuckerman Program (I.H.); NIH R21AG063739 (I.H.); ISF 2178/19 (I.H.); Israel Ministry of Science 3-17631 and 3-16872 (I.H.); Moore Foundation GBMF9341 (I.H.); BSF-NSF 2020611 (I.H.); the Israel Ministry of Agriculture 12-16-0010 (I.H.); Damon Runyon, Rothschild, and Human Frontiers long-term post-doctoral fellowships (I.H.); an EMBO post-doctoral fellowship (D.H.); and a Stanford Graduate Student Fellowship (Y.R.C.).

AUTHOR CONTRIBUTIONS

I.H., Y.R.C., I.Z., A.B., and D.F.J. designed mass spectrometry experiments. I.H. isolated killifish organs, and Y.R.C. and I.Z. isolated samples for mass spectrometry with the help of I.H. and performed silver stain analysis. Y.R.C. designed and implemented mass spectrometry data analysis and performed domain enrichment analyses with input from I.H., P.P.S., A.B., and D.F.J. I.H. generated mammalian constructs, performed and analyzed killifish immunocytochemistry experiments and some 293T experiments, and generated DDX5 CRISPR knockout and and DDX5 antibody. Y.R.C. generated yeast constructs with help from I.H. and B.E.M. and performed and analyzed yeast aggregation and FRAP experiments. Y.R.C. generated and purified recombinant killifish DDX5 proteins and performed and analyzed phase-separation and activity assays. P.P.S. conducted PCA and GO term analyses. D.H. performed and analyzed 293T experiments and assembled the revised version of the manuscript. P.N.N. performed and analyzed DDX5 immunocytochemistry experiments in mice. U.G. and G.A. performed and analyzed immunocytochemistry experiments in killifish and western blot for DDX5, respectively, under the supervision of I.H. I.H. generated the transgenic DDX5 construct, and W.W. generated the transgenic killifish overexpressing DDX5 under the supervision of A.S.A. E.M. and A.M. provided young and old killifish brain sections. K.H. performed initial analysis of mass spectrometry data. S.Y. helped with sequence verification and cloning of killifish constructs. I.H., Y.R.C., D.F.J., and A.B. wrote the paper, and all authors commented on the manuscript.

DECLARATION OF INTERESTS

The authors declare no competing interests.

Received: March 21, 2022
Revised: April 23, 2023
Accepted: June 26, 2023
Published: May 28, 2024

REFERENCES

1. Forman, M.S., Trojanowski, J.Q., and Lee, V.M.Y. (2004). Neurodegenerative diseases: a decade of discoveries paves the way for therapeutic breakthroughs. Nat. Med. *10*, 1055–1063. https://doi.org/10.1038/nm1113.
2. Dugger, B.N., and Dickson, D.W. (2017). Pathology of Neurodegenerative Diseases. Cold Spring Harbor Perspect. Biol. *9*, a028035. https://doi.org/10.1101/cshperspect.a028035.
3. Schweighauser, M., Arseni, D., Bacioglu, M., Huang, M., Lövestam, S., Shi, Y., Yang, Y., Zhang, W., Kotecha, A., Garringer, H.J., et al. (2022). Age-dependent formation of TMEM106B amyloid filaments in human brains. Nature *605*, 310–314. https://doi.org/10.1038/s41586-022-04650-z.
4. Huang, C., Wagner-Valladolid, S., Stephens, A.D., Jung, R., Poudel, C., Sinnige, T., Lechler, M.C., Schlörit, N., Lu, M., Laine, R.F., et al. (2019). Intrinsically aggregation-prone proteins form amyloid-like aggregates and contribute to tissue aging in Caenorhabditis elegans. Elife *8*, e43059. https://doi.org/10.7554/eLife.43059.
5. Lechler, M.C., Crawford, E.D., Groh, N., Widmaier, K., Jung, R., Kirstein, J., Trinidad, J.C., Burlingame, A.L., and David, D.C. (2017). Reduced Insulin/IGF-1 Signaling Restores the Dynamic Properties of Key Stress Granule Proteins during Aging. Cell Rep. *18*, 454–467. https://doi.org/10.1016/j.celrep.2016.12.033.
6. David, D.C., Ollikainen, N., Trinidad, J.C., Cary, M.P., Burlingame, A.L., and Kenyon, C. (2010). Widespread protein aggregation as an inherent part of aging in C. elegans. PLoS Biol. *8*, e1000450. https://doi.org/10.1371/journal.pbio.1000450.
7. Wolff, S., Weissman, J.S., and Dillin, A. (2014). Differential scales of protein quality control. Cell *157*, 52–64. https://doi.org/10.1016/j.cell.2014.03.007.
8. López-Otín, C., Blasco, M.A., Partridge, L., Serrano, M., and Kroemer, G. (2013). The hallmarks of aging. Cell *153*, 1194–1217. https://doi.org/10.1016/j.cell.2013.05.039.
9. Ben-Zvi, A., Miller, E.A., and Morimoto, R.I. (2009). Collapse of proteostasis represents an early molecular event in Caenorhabditis elegans aging. Proc. Natl. Acad. Sci. USA *106*, 14914–14919. https://doi.org/10.1073/pnas.0902882106.
10. Labbadia, J., and Morimoto, R.I. (2014). Proteostasis and longevity: when does aging really begin? F1000Prime Rep. *6*, 7. https://doi.org/10.12703/P6-7.
11. Walther, D.M., Kasturi, P., Zheng, M., Pinkert, S., Vecchi, G., Ciryam, P., Morimoto, R.I., Dobson, C.M., Vendruscolo, M., Mann, M., and Hartl, F.U. (2015). Widespread Proteome Remodeling and Aggregation in Aging C. elegans. Cell *161*, 919–932. https://doi.org/10.1016/j.cell.2015.03.032.
12. Yu, Q., Xiao, H., Jedrychowski, M.P., Schweppe, D.K., Navarrete-Perea, J., Knott, J., Rogers, J., Chouchani, E.T., and Gygi, S.P. (2020). Sample multiplexing for targeted pathway proteomics in aging mice. Proc. Natl. Acad. Sci. USA *117*, 9723–9732. https://doi.org/10.1073/pnas.1919410117.

13. Xiao, H., Jedrychowski, M.P., Schweppe, D.K., Huttlin, E.L., Yu, Q., Heppner, D.E., Li, J., Long, J., Mills, E.L., Szpyt, J., et al. (2020). A Quantitative Tissue-Specific Landscape of Protein Redox Regulation during Aging. Cell *180*, 968–983.e24. https://doi.org/10.1016/j.cell.2020.02.012.

14. Gebert, N., Cheng, C.W., Kirkpatrick, J.M., Di Fraia, D., Yun, J., Schädel, P., Pace, S., Garside, G.B., Werz, O., Rudolph, K.L., et al. (2020). Region-Specific Proteome Changes of the Intestinal Epithelium during Aging and Dietary Restriction. Cell Rep. *31*, 107565. https://doi.org/10.1016/j.celrep.2020.107565.

15. Angelidis, I., Simon, L.M., Fernandez, I.E., Strunz, M., Mayr, C.H., Greiffo, F.R., Tsitsiridis, G., Ansari, M., Graf, E., Strom, T.M., et al. (2019). An atlas of the aging lung mapped by single cell transcriptomics and deep tissue proteomics. Nat. Commun. *10*, 963. https://doi.org/10.1038/s41467-019-08831-9.

16. Ori, A., Toyama, B.H., Harris, M.S., Bock, T., Iskar, M., Bork, P., Ingolia, N.T., Hetzer, M.W., and Beck, M. (2015). Integrated Transcriptome and Proteome Analyses Reveal Organ-Specific Proteome Deterioration in Old Rats. Cell Syst. *1*, 224–237. https://doi.org/10.1016/j.cels.2015.08.012.

17. Kelmer Sacramento, E., Kirkpatrick, J.M., Mazzetto, M., Baumgart, M., Bartolome, A., Di Sanzo, S., Caterino, C., Sanguanini, M., Papaevgeniou, N., Lefaki, M., et al. (2020). Reduced proteasome activity in the aging brain results in ribosome stoichiometry loss and aggregation. Mol. Syst. Biol. *16*, e9596. https://doi.org/10.15252/msb.20209596.

18. Brundin, P., Melki, R., and Kopito, R. (2010). Prion-like transmission of protein aggregates in neurodegenerative diseases. Nat. Rev. Mol. Cell Biol. *11*, 301–307. https://doi.org/10.1038/nrm2873.

19. Collinge, J. (2016). Mammalian prions and their wider relevance in neurodegenerative diseases. Nature *539*, 217–226. https://doi.org/10.1038/nature20415.

20. Laferrière, F., Maniecka, Z., Pérez-Berlanga, M., Hruska-Plochan, M., Gilhespy, L., Hock, E.M., Wagner, U., Afroz, T., Boersema, P.J., Barmettler, G., et al. (2019). TDP-43 extracted from frontotemporal lobar degeneration subject brains displays distinct aggregate assemblies and neurotoxic effects reflecting disease progression rates. Nat. Neurosci. *22*, 65–77. https://doi.org/10.1038/s41593-018-0294-y.

21. Brundin, P., and Melki, R. (2017). Prying into the Prion Hypothesis for Parkinson's Disease. J. Neurosci. *37*, 9808–9818. https://doi.org/10.1523/JNEUROSCI.1788-16.2017.

22. Walker, L.C., and Jucker, M. (2015). Neurodegenerative diseases: expanding the prion concept. Annu. Rev. Neurosci. *38*, 87–103. https://doi.org/10.1146/annurev-neuro-071714-033828.

23. Harvey, Z.H., Chen, Y., and Jarosz, D.F. (2018). Protein-Based Inheritance: Epigenetics beyond the Chromosome. Mol. Cell. *69*, 195–202. https://doi.org/10.1016/j.molcel.2017.10.030.

24. Halfmann, R. (2016). A glass menagerie of low complexity sequences. Curr. Opin. Struct. Biol. *38*, 18–25. https://doi.org/10.1016/j.sbi.2016.05.002.

25. Halfmann, R., Alberti, S., and Lindquist, S. (2010). Prions, protein homeostasis, and phenotypic diversity. Trends Cell Biol. *20*, 125–133. https://doi.org/10.1016/j.tcb.2009.12.003.

26. Hervas, R., Rau, M.J., Park, Y., Zhang, W., Murzin, A.G., Fitzpatrick, J.A.J., Scheres, S.H.W., and Si, K. (2020). Cryo-EM structure of a neuronal functional amyloid implicated in memory persistence in Drosophila. Science *367*, 1230–1234. https://doi.org/10.1126/science.aba3526.

27. Chakrabortee, S., Byers, J.S., Jones, S., Garcia, D.M., Bhullar, B., Chang, A., She, R., Lee, L., Fremin, B., Lindquist, S., and Jarosz, D.F. (2016). Intrinsically Disordered Proteins Drive Emergence and Inheritance of Biological Traits. Cell *167*, 369–381.e12. https://doi.org/10.1016/j.cell.2016.09.017.

28. Garcia, D.M., Dietrich, D., Clardy, J., and Jarosz, D.F. (2016). A common bacterial metabolite elicits prion-based bypass of glucose repression. Elife *5*, e17978. https://doi.org/10.7554/eLife.17978.

29. Jarosz, D.F., and Khurana, V. (2017). Specification of Physiologic and Disease States by Distinct Proteins and Protein Conformations. Cell *171*, 1001–1014. https://doi.org/10.1016/j.cell.2017.10.047.

30. Holmes, D.L., Lancaster, A.K., Lindquist, S., and Halfmann, R. (2013). Heritable remodeling of yeast multicellularity by an environmentally responsive prion. Cell *153*, 153–165. https://doi.org/10.1016/j.cell.2013.02.026.

31. Cai, X., Chen, J., Xu, H., Liu, S., Jiang, Q.X., Halfmann, R., and Chen, Z.J. (2014). Prion-like polymerization underlies signal transduction in antiviral immune defense and inflammasome activation. Cell *156*, 1207–1222. https://doi.org/10.1016/j.cell.2014.01.063.

32. Valdesalici, S., and Cellerino, A. (2003). Extremely short lifespan in the annual fish Nothobranchius furzeri. Proc. Biol. Sci. *270* (*Suppl 2*), S189–S191. https://doi.org/10.1098/rsbl.2003.0048.

33. Cellerino, A., Valenzano, D.R., and Reichard, M. (2016). From the bush to the bench: the annual Nothobranchius fishes as a new model system in biology. Biol. Rev. Camb. Phil. Soc. *91*, 511–533. https://doi.org/10.1111/brv.12183.

34. Valenzano, D.R., Terzibasi, E., Genade, T., Cattaneo, A., Domenici, L., and Cellerino, A. (2006). Resveratrol prolongs lifespan and retards the onset of age-related markers in a short-lived vertebrate. Curr. Biol. *16*, 296–300. https://doi.org/10.1016/j.cub.2005.12.038.

35. Kim, Y., Nam, H.G., and Valenzano, D.R. (2016). The short-lived African turquoise killifish: an emerging experimental model for ageing. Dis. Model. Mech. *9*, 115–129. https://doi.org/10.1242/dmm.023226.

36. Harel, I., and Brunet, A. (2015). The African Turquoise Killifish: A Model for Exploring Vertebrate Aging and Diseases in the Fast Lane. Cold Spring Harb. Symp. Quant. Biol. *80*, 275–279. https://doi.org/10.1101/sqb.2015.80.027524.

37. Terzibasi, E., Valenzano, D.R., and Cellerino, A. (2007). The short-lived fish Nothobranchius furzeri as a new model system for aging studies. Exp. Gerontol. *42*, 81–89. https://doi.org/10.1016/j.exger.2006.06.039.

38. Matsui, H., Kenmochi, N., and Namikawa, K. (2019). Age- and alpha-Synuclein-Dependent Degeneration of Dopamine and Noradrenaline Neurons in the Annual Killifish Nothobranchius furzeri. Cell Rep. *26*, 1727–1733.e6. https://doi.org/10.1016/j.celrep.2019.01.015.

39. Valenzano, D.R., Terzibasi, E., Cattaneo, A., Domenici, L., and Cellerino, A. (2006). Temperature affects longevity and age-related locomotor and cognitive decay in the short-lived fish Nothobranchius furzeri. Aging Cell *5*, 275–278. https://doi.org/10.1111/j.1474-9726.2006.00212.x.

40. Terzibasi, E., Lefrançois, C., Domenici, P., Hartmann, N., Graf, M., and Cellerino, A. (2009). Effects of dietary restriction on mortality and age-related phenotypes in the short-lived fish Nothobranchius furzeri. Aging Cell *8*, 88–99. https://doi.org/10.1111/j.1474-9726.2009.00455.x.

41. McKay, A., Costa, E.K., Chen, J., Hu, C.K., Chen, X., Bedbrook, C.N., Khondker, R.C., Thielvoldt, M., Priya Singh, P., Wyss-Coray, T., et al. (2022). An automated feeding system for the African killifish reveals the impact of diet on lifespan and allows scalable assessment of associative learning. Elife *11*. https://doi.org/10.7554/eLife.69008.

42. Valenzano, D.R., Benayoun, B.A., Singh, P.P., Zhang, E., Etter, P.D., Hu, C.K., Clément-Ziza, M., Willemsen, D., Cui, R., Harel, I., et al. (2015). The African Turquoise Killifish Genome Provides Insights into Evolution and Genetic Architecture of Lifespan. Cell *163*, 1539–1554. https://doi.org/10.1016/j.cell.2015.11.008.

43. Valenzano, D.R., Sharp, S., and Brunet, A. (2011). Transposon-Mediated Transgenesis in the Short-Lived African Killifish Nothobranchius furzeri, a Vertebrate Model for Aging. G3 *1*, 531–538. https://doi.org/10.1534/g3.111.001271.

44. Harel, I., Valenzano, D.R., and Brunet, A. (2016). Efficient genome engineering approaches for the short-lived African turquoise killifish. Nat. Protoc. *11*, 2010–2028. https://doi.org/10.1038/nprot.2016.103.

45. Harel, I., Benayoun, B.A., Machado, B., Singh, P.P., Hu, C.K., Pech, M.F., Valenzano, D.R., Zhang, E., Sharp, S.C., Artandi, S.E., and Brunet, A. (2015). A platform for rapid exploration of aging and diseases in a naturally short-lived vertebrate. Cell *160*, 1013–1026. https://doi.org/10.1016/j.cell.2015.01.038.

46. Reichwald, K., Petzold, A., Koch, P., Downie, B.R., Hartmann, N., Pietsch, S., Baumgart, M., Chalopin, D., Felder, M., Bens, M., et al. (2015). Insights into Sex Chromosome Evolution and Aging from the Genome of a Short-Lived Fish. Cell *163*, 1527–1538. https://doi.org/10.1016/j.cell.2015.10.071.

47. Bedbrook, C.N., Nath, R.D., Nagvekar, R., Deisseroth, K., and Brunet, A. (2023). Rapid and precise genome engineering in a naturally short-lived vertebrate. Elife *12*, e80639. https://doi.org/10.7554/eLife.80639.

48. Krug, J., Perner, B., Albertz, C., Mörl, H., Hopfenmüller, V.L., and Englert, C. (2023). Generation of a transparent killifish line through multiplex CRISPR/Cas9mediated gene inactivation. Elife *12*, e81549. https://doi.org/10.7554/eLife.81549.

49. Chen, Y.R., Harel, I., Singh, P.P., Ziv, I., Moses, E., Goshtchevsky, U., Machado, B.E., Brunet, A., and Jarosz, D.F. (2022). Tissue-specific landscape of protein aggregation and quality control in an aging vertebrate. bioRxiv. https://doi.org/10.1101/2022.1102.1126.482120.

50. Kryndushkin, D., Pripuzova, N., Burnett, B.G., and Shewmaker, F. (2013). Non-targeted identification of prions and amyloid-forming proteins from yeast and mammalian cells. J. Biol. Chem. *288*, 27100–27111. https://doi.org/10.1074/jbc.M113.485359.

51. Gebauer, F., Schwarzl, T., Valcárcel, J., and Hentze, M.W. (2021). RNA-binding proteins in human genetic disease. Nat. Rev. Genet. *22*, 185–198. https://doi.org/10.1038/s41576-020-00302-y.

52. Sharma, D., Zagore, L.L., Brister, M.M., Ye, X., Crespo-Hernández, C.E., Licatalosi, D.D., and Jankowsky, E. (2021). The kinetic landscape of an RNA-binding protein in cells. Nature *591*, 152–156. https://doi.org/10.1038/s41586-021-03222-x.

53. Lancaster, A.K., Nutter-Upham, A., Lindquist, S., and King, O.D. (2014). PLAAC: a web and command-line application to identify proteins with prion-like amino acid composition. Bioinformatics *30*, 2501–2502. https://doi.org/10.1093/bioinformatics/btu310.

54. Jones, D.T., and Cozzetto, D. (2015). DISOPRED3: precise disordered region predictions with annotated protein-binding activity. Bioinformatics *31*, 857–863. https://doi.org/10.1093/bioinformatics/btu744.

55. Dardenne, E., Polay Espinoza, M., Fattet, L., Germann, S., Lambert, M.P., Neil, H., Zonta, E., Mortada, H., Gratadou, L., Deygas, M., et al. (2014). RNA helicases DDX5 and DDX17 dynamically orchestrate transcription, miRNA, and splicing programs in cell differentiation. Cell Rep. *7*, 1900–1913. https://doi.org/10.1016/j.celrep.2014.05.010.

56. Weinhandl, K., Winkler, M., Glieder, A., and Camattari, A. (2014). Carbon source dependent promoters in yeasts. Microb. Cell Factories *13*, 5. https://doi.org/10.1186/1475-2859-13-5.

57. Wickner, R.B. (1994). [URE3] as an altered URE2 protein: evidence for a prion analog in Saccharomyces cerevisiae. Science *264*, 566–569. https://doi.org/10.1126/science.7909170.

58. Maharana, S., Wang, J., Papadopoulos, D.K., Richter, D., Pozniakovsky, A., Poser, I., Bickle, M., Rizk, S., Guillén-Boixet, J., Franzmann, T.M., et al. (2018). RNA buffers the phase separation behavior of prion-like RNA binding proteins. Science *360*, 918–921. https://doi.org/10.1126/science.aar7366.

59. Franzmann, T.M., Jahnel, M., Pozniakovsky, A., Mahamid, J., Holehouse, A.S., Nüske, E., Richter, D., Baumeister, W., Grill, S.W., Pappu, R.V., et al. (2018). Phase separation of a yeast prion protein promotes cellular fitness. Science *359*, eaao5654. https://doi.org/10.1126/science.aao5654.

60. Frederick, K.K., Debelouchina, G.T., Kayatekin, C., Dorminy, T., Jacavone, A.C., Griffin, R.G., and Lindquist, S. (2014). Distinct prion strains are defined by amyloid core structure and chaperone binding site dynamics. Chem. Biol. *21*, 295–305. https://doi.org/10.1016/j.chembiol.2013.12.013.

61. Wu, Y.X., Masison, D.C., Eisenberg, E., and Greene, L.E. (2006). Application of photobleaching for measuring diffusion of prion proteins in cytosol of yeast cells. Methods *39*, 43–49. https://doi.org/10.1016/j.ymeth.2006.04.004.

62. Molliex, A., Temirov, J., Lee, J., Coughlin, M., Kanagaraj, A.P., Kim, H.J., Mittag, T., and Taylor, J.P. (2015). Phase separation by low complexity domains promotes stress granule assembly and drives pathological fibrillization. Cell *163*, 123–133. https://doi.org/10.1016/j.cell.2015.09.015.

63. Boeynaems, S., Bogaert, E., Kovacs, D., Konijnenberg, A., Timmerman, E., Volkov, A., Guharoy, M., De Decker, M., Jaspers, T., Ryan, V.H., et al. (2017). Phase Separation of C9orf72 Dipeptide Repeats Perturbs Stress Granule Dynamics. Mol. Cell. *65*, 1044–1055.e5. https://doi.org/10.1016/j.molcel.2017.02.013.

64. Boeynaems, S., Alberti, S., Fawzi, N.L., Mittag, T., Polymenidou, M., Rousseau, F., Schymkowitz, J., Shorter, J., Wolozin, B., Van Den Bosch, L., et al. (2018). Protein Phase Separation: A New Phase in Cell Biology. Trends Cell Biol. *28*, 420–435. https://doi.org/10.1016/j.tcb.2018.02.004.

65. Hardenberg, M., Horvath, A., Ambrus, V., Fuxreiter, M., and Vendruscolo, M. (2020). Widespread occurrence of the droplet state of proteins in the human proteome. Proc. Natl. Acad. Sci. USA *117*, 33254–33262. https://doi.org/10.1073/pnas.2007670117.

66. Sanders, D.W., Kedersha, N., Lee, D.S.W., Strom, A.R., Drake, V., Riback, J.A., Bracha, D., Eeftens, J.M., Iwanicki, A., Wang, A., et al. (2020). Competing Protein-RNA Interaction Networks Control Multiphase Intracellular Organization. Cell *181*, 306–324.e28. https://doi.org/10.1016/j.cell.2020.03.050.

67. Riback, J.A., Zhu, L., Ferrolino, M.C., Tolbert, M., Mitrea, D.M., Sanders, D.W., Wei, M.T., Kriwacki, R.W., and Brangwynne, C.P. (2020). Composition-dependent thermodynamics of intracellular phase separation. Nature *581*, 209–214. https://doi.org/10.1038/s41586-020-2256-2.

68. van Mierlo, G., Jansen, J.R.G., Wang, J., Poser, I., van Heeringen, S.J., and Vermeulen, M. (2021). Predicting protein condensate formation using machine learning. Cell Rep. *34*, 108705. https://doi.org/10.1016/j.celrep.2021.108705.

69. Riback, J.A., and Brangwynne, C.P. (2020). Can phase separation buffer cellular noise? Science *367*, 364–365. https://doi.org/10.1126/science.aba0446.

70. Labbadia, J., and Morimoto, R.I. (2015). Repression of the Heat Shock Response Is a Programmed Event at the Onset of Reproduction. Mol. Cell. *59*, 639–650. https://doi.org/10.1016/j.molcel.2015.06.027.

71. Gallotta, I., Sandhu, A., Peters, M., Haslbeck, M., Jung, R., Agilkaya, S., Blersch, J.L., Rödelsperger, C., Röseler, W., Huang, C., et al. (2020). Extracellular proteostasis prevents aggregation during pathogenic attack. Nature *584*, 410–414. https://doi.org/10.1038/s41586-020-2461-z.

72. Müller, J.B., Geyer, P.E., Colaço, A.R., Treit, P.V., Strauss, M.T., Oroshi, M., Doll, S., Virreira Winter, S., Bader, J.M., Köhler, N., et al. (2020). The proteome landscape of the kingdoms of life. Nature *582*, 592–596. https://doi.org/10.1038/s41586-020-2402-x.

73. Draceni, Y., and Pechmann, S. (2019). Pervasive convergent evolution and extreme phenotypes define chaperone requirements of protein homeostasis. Proc. Natl. Acad. Sci. USA *116*, 20009–20014. https://doi.org/10.1073/pnas.1904611116.

74. Laurent, F.X., Sureau, A., Klein, A.F., Trouslard, F., Gasnier, E., Furling, D., and Marie, J. (2012). New function for the RNA helicase p68/DDX5 as a modifier of MBNL1 activity on expanded CUG repeats. Nucleic Acids Res. *40*, 3159–3171. https://doi.org/10.1093/nar/gkr1228.

75. Liao, S.E., and Regev, O. (2021). Splicing at the phase-separated nuclear speckle interface: a model. Nucleic Acids Res. *49*, 636–645. https://doi.org/10.1093/nar/gkaa1209.

76. Kar, A., Fushimi, K., Zhou, X., Ray, P., Shi, C., Chen, X., Liu, Z., Chen, S., and Wu, J.Y. (2011). RNA helicase p68 (DDX5) regulates tau exon 10 splicing by modulating a stem-loop structure at the 5' splice site. Mol. Cell Biol. *31*, 1812–1821. https://doi.org/10.1128/MCB.01149-10.

77. Tauber, D., Tauber, G., Khong, A., Van Treeck, B., Pelletier, J., and Parker, R. (2020). Modulation of RNA Condensation by the DEAD-Box Protein eIF4A. Cell *180*, 411–426.e16. https://doi.org/10.1016/j.cell.2019.12.031.

78. Guo, L., Kim, H.J., Wang, H., Monaghan, J., Freyermuth, F., Sung, J.C., O'Donovan, K., Fare, C.M., Diaz, Z., Singh, N., et al. (2018). Nuclear-Import Receptors Reverse Aberrant Phase Transitions of RNA-Binding Proteins with Prion-like Domains. Cell *173*, 677–692.e20. https://doi.org/10.1016/j.cell.2018.03.002.

79. Wang, J., Choi, J.M., Holehouse, A.S., Lee, H.O., Zhang, X., Jahnel, M., Maharana, S., Lemaitre, R., Pozniakovsky, A., Drechsel, D., et al. (2018). A Molecular Grammar Governing the Driving Forces for Phase Separation of Prion-like RNA Binding Proteins. Cell *174*, 688–699.e16. https://doi.org/10.1016/j.cell.2018.06.006.

80. Alberti, S., Gitler, A.D., and Lindquist, S. (2007). A suite of Gateway cloning vectors for high-throughput genetic analysis in Saccharomyces cerevisiae. Yeast *24*, 913–919. https://doi.org/10.1002/yea.1502.

81. McQuin, C., Goodman, A., Chernyshev, V., Kamentsky, L., Cimini, B.A., Karhohs, K.W., Doan, M., Ding, L., Rafelski, S.M., Thirstrup, D., et al. (2018). CellProfiler 3.0: Next-generation image processing for biology. PLoS Biol. *16*, e2005970. https://doi.org/10.1371/journal.pbio.2005970.

82. Kryndushkin, D., Pripuzova, N., and Shewmaker, F.P. (2017). Isolation and Analysis of Prion and Amyloid Aggregates from Yeast Cells. Cold Spring Harb. Protoc. *2017*, pdb.prot089045. https://doi.org/10.1101/pdb.prot089045.

83. Chen, Y.R., Ziv, I., Swaminathan, K., Elias, J.E., and Jarosz, D.F. (2021). Protein aggregation and the evolution of stress resistance in clinical yeast. Philos. Trans. R. Soc. Lond. B Biol. Sci. *376*, 20200127. https://doi.org/10.1098/rstb.2020.0127.

84. Wheeler, J.R., Jain, S., Khong, A., and Parker, R. (2017). Isolation of yeast and mammalian stress granule cores. Methods *126*, 12–17. https://doi.org/10.1016/j.ymeth.2017.04.020.

85. Ingolia, N.T., Brar, G.A., Rouskin, S., McGeachy, A.M., and Weissman, J.S. (2012). The ribosome profiling strategy for monitoring translation in vivo by deep sequencing of ribosome-protected mRNA fragments. Nat. Protoc. *7*, 1534–1550. https://doi.org/10.1038/nprot.2012.086.

86. McAlister, G.C., Nusinow, D.P., Jedrychowski, M.P., Wühr, M., Huttlin, E.L., Erickson, B.K., Rad, R., Haas, W., and Gygi, S.P. (2014). MultiNotch MS3 enables accurate, sensitive, and multiplexed detection of differential expression across cancer cell line proteomes. Anal. Chem. *86*, 7150–7158. https://doi.org/10.1021/ac502040v.

87. Klann, K., Tascher, G., and Münch, C. (2020). Functional Translatome Proteomics Reveal Converging and Dose-Dependent Regulation by mTORC1 and eIF2alpha. Mol. Cell. *77*, 913–925.e4. https://doi.org/10.1016/j.molcel.2019.11.010.

88. Li, J., Paulo, J.A., Nusinow, D.P., Huttlin, E.L., and Gygi, S.P. (2019). Investigation of Proteomic and Phosphoproteomic Responses to Signaling Network Perturbations Reveals Functional Pathway Organizations in Yeast. Cell Rep. *29*, 2092–2104.e4. https://doi.org/10.1016/j.celrep.2019.10.034.

89. Mirzaei, M., Gupta, V.B., Chick, J.M., Greco, T.M., Wu, Y., Chitranshi, N., Wall, R.V., Hone, E., Deng, L., Dheer, Y., et al. (2017). Age-related neurodegenerative disease associated pathways identified in retinal and vitreous proteome from human glaucoma eyes. Sci. Rep. *7*, 12685. https://doi.org/10.1038/s41598-017-12858-7.

90. Navarrete-Perea, J., Yu, Q., Gygi, S.P., and Paulo, J.A. (2018). Streamlined Tandem Mass Tag (SL-TMT) Protocol: An Efficient Strategy for Quantitative (Phospho)proteome Profiling Using Tandem Mass Tag-Synchronous Precursor Selection-MS3. J. Proteome Res. *17*, 2226–2236. https://doi.org/10.1021/acs.jproteome.8b00217.

91. Nusinow, D.P., Szpyt, J., Ghandi, M., Rose, C.M., McDonald, E.R., 3rd, Kalocsay, M., Jané-Valbuena, J., Gelfand, E., Schweppe, D.K., Jedrychowski, M., et al. (2020). Quantitative Proteomics of the Cancer Cell Line Encyclopedia. Cell *180*, 387–402.e16. https://doi.org/10.1016/j.cell.2019.12.023.

92. Zhang, L., and Elias, J.E. (2017). Relative Protein Quantification Using Tandem Mass Tag Mass Spectrometry. Methods Mol. Biol. *1550*, 185–198. https://doi.org/10.1007/978-1-4939-6747-6_14.

93. Yu, G., Wang, L.G., Han, Y., and He, Q.Y. (2012). clusterProfiler: an R package for comparing biological themes among gene clusters. OMICS *16*, 284–287. https://doi.org/10.1089/omi.2011.0118.

94. Montague, T.G., Cruz, J.M., Gagnon, J.A., Church, G.M., and Valen, E. (2014). CHOPCHOP: a CRISPR/Cas9 and TALEN web tool for genome editing. Nucleic Acids Res. *42*, W401–W407. https://doi.org/10.1093/nar/gku410.

95. Jao, L.E., Wente, S.R., and Chen, W. (2013). Efficient multiplex biallelic zebrafish genome editing using a CRISPR nuclease system. Proc. Natl. Acad. Sci. USA *110*, 13904–13909. https://doi.org/10.1073/pnas.1308335110.

96. Kwan, K.M., Fujimoto, E., Grabher, C., Mangum, B.D., Hardy, M.E., Campbell, D.S., Parant, J.M., Yost, H.J., Kanki, J.P., and Chien, C.B. (2007). The Tol2kit: a multisite gateway-based construction kit for Tol2 transposon transgenesis constructs. Dev. Dynam. *236*, 3088–3099. https://doi.org/10.1002/dvdy.21343.

97. Wang, W., Hu, C.K., Zeng, A., Alegre, D., Hu, D., Gotting, K., Ortega Granillo, A., Wang, Y., Robb, S., Schnittker, R., et al. (2020). Changes in regeneration-responsive enhancers shape regenerative capacities in vertebrates. Science *369*, eaaz3090. https://doi.org/10.1126/science.aaz3090.

98. Harel, I., Nathan, E., Tirosh-Finkel, L., Zigdon, H., Guimarães-Camboa, N., Evans, S.M., and Tzahor, E. (2009). Distinct origins and genetic programs of head muscle satellite cells. Dev. Cell *16*, 822–832. https://doi.org/10.1016/j.devcel.2009.05.007.

99. Harel, I., Maezawa, Y., Avraham, R., Rinon, A., Ma, H.Y., Cross, J.W., Leviatan, N., Hegesh, J., Roy, A., Jacob-Hirsch, J., et al. (2012). Pharyngeal mesoderm regulatory network controls cardiac and head muscle morphogenesis. Proc. Natl. Acad. Sci. USA *109*, 18839–18844. https://doi.org/10.1073/pnas.1208690109.

100. Ganz, J., Kaslin, J., Hochmann, S., Freudenreich, D., and Brand, M. (2010). Heterogeneity and Fgf dependence of adult neural progenitors in the zebrafish telencephalon. Glia *58*, 1345–1363. https://doi.org/10.1002/glia.21012.

101. Hirling, H., Scheffner, M., Restle, T., and Stahl, H. (1989). RNA helicase activity associated with the human p68 protein. Nature *339*, 562–564. https://doi.org/10.1038/339562a0.

Please cite this article in press as: Harel et al., Identification of protein aggregates in the aging vertebrate brain with prion-like and phase-separation properties, Cell Reports (2023), https://doi.org/10.1016/j.celrep.2023.112787

STAR★METHODS

KEY RESOURCES TABLE

REAGENT or RESOURCE	SOURCE	IDENTIFIER
Antibodies		
DDX5 C terminus. Antigen: DDX5-625: 625-PYPIPPPFPQ-634	This paper	N/A
Anti-DDX5	Sigma-Aldrich	HPA020043
Anti-Rabbit HRP	Abcam	ab6721
Bacterial and virus strains		
Escherichia coliLOBSTR-BL21(DE3)-RIL	Kerafast	Cat# EC1002
Chemicals, peptides, and recombinant protein		
Acetic acid	Ricca Chemical	Cat# RABA0010500
Ammonium bicarbonate	Acros Organics	Cat# AC393210010
Ampicillin sodium salt	Sigma-Aldrich	Cat# A9518-100G
ATP	Sigma-Aldrich	Cat# A2383-10G
Blotting grade blocker nonfat dry milk	Bio-Rad	Cat# 170-6404XTU
Bovine serum albumin	Calbiochem	Cat# 126575
Bromophenol blue	Acros Organics	Cat# AC40316-0100
Calcium chloride	Sigma-Aldrich	Cat# 223506-500G
Chloramphenicol	RPI	Cat# C61000–25.0
Centrifuge filter unit	EMD Millipore	Cat# UFC903024, Cat# UFC803024, Cat# UFC503024
cOmplete, Mini, EDTA-free protease inhibitor cocktail	Roche	Cat# 11836170001
CSM-Ura powder	Sunrise	Cat# 1004-010
CSM-Leu-Ura powder	Sunrise	Cat# 1038-010
Deoxyribonucleic acid sodium salt from salmon testes	Sigma-Aldrich	Cat# D1626-5G
Dextrose (D-Glucose)	Fisher Scientific	Cat# D16-3
D(+)-Galactose	Fisher Scientific	Cat# BP656-500
D(+)-Raffinose	Fisher Scientific	Cat# 50-494-587
DNase I	New England BioLabs	Cat# M0303S
Dithiothreitol	Gold Biotechnology	Cat# DTT100
Formic acid	Fisher Scientific	Cat# A118P-500
Gateway BP clonase II enzyme mix	Invitrogen	Cat# 11789020
Gateway LR clonase II enzyme mix	Invitrogen	Cat# 11791020
Glass beads, acid-washed, 425–600 μm (30–40 U.S. sieve)	Sigma-Aldrich	Cat# G8772-500G
Glycerol	Fisher scientific	Cat# BP229-4
Hydrogen peroxide solution, 30% in H2O	Sigma-Aldrich	Cat# 216763-100ML
Imidazole	Sigma-Aldrich	Cat# 12399-500G
InstantBlue Protein Stain	Expedeon	Cat# ISB1L
Iodoacetamide	Sigma-Aldrich	Cat# I6125-10G
IPTG	Gold Biotechnology	Cat# I2481C25
Kanamycin monosulfate	Gold Biotechnology	Cat# K-120-10
Lysozyme	Thermo Fisher	Cat# 89833
Luminol	Sigma-Aldrich	Cat# A8511-5G
Luria broth buffered capsules	RPI	Cat# L24045–1000.0
Magnesium chloride hexahydrate	RPI	Cat# M24000–500.0
Methanol	Sigma-Aldrich	Cat# 179337-4L
MS-222	Sigma-Aldrich	A5040

(*Continued on next page*)

Please cite this article in press as: Harel et al., Identification of protein aggregates in the aging vertebrate brain with prion-like and phase-separation properties, Cell Reports (2023), https://doi.org/10.1016/j.celrep.2023.112787

Continued

REAGENT or RESOURCE	SOURCE	IDENTIFIER
N-Ethylmaleimide	Sigma-Aldrich	E3876
NativeMarker Unstained Protein Standard	Thermo Fisher	Cat# LC0725
NativePAGE 3–12% Bis-Tris Protein Gels	Thermo Fisher	Cat# BN10030BOX
NativePAGE 4x sample buffer	Thermo Fisher	Cat# BN2003
NativePAGE 5% G-250 sample additive	Thermo Fisher	Cat# BN2004
Ni-NTA agarose beads	Qiagen	Cat# 30250
Metal beads	Eldan Israel	Cat# RC55 420
Novex WedgeWell 4–20% Tris-Glycine gel	Thermo Fisher	Cat# XP04205BOX
NP-40 Alternative	EMD Millipore	Cat# 492018-50ML
NuSieve GTG Agarose low melting temperature	Lonza	Cat# 50081
p-Coumaric acid	Sigma-Aldrich	Cat# C9008-5G
PageRuler^{TM} Plus protein ladder	Thermo Fisher	Cat# 11832124
PBS, pH 7.4	Gibco	LS10010023
Pepstatin A	Abcam	Cat# ab141416
Poly-D-Lysine	Sigma-Aldrich	7886-10MG
ProLong Gold	ThermoFisher	Cat# P36930
ProteaseMAX Surfactant	Promega	Cat# V2071
Ponceau red	Sigma-Aldrich	P7170
Potassium chloride	Sigma-Aldrich	Cat# P9541-1KG
Potassium ferricyanide (III) powder	Sigma-Aldrich	Cat# 702587-250G
RNase A	Akron Biotech	Cat# 89508-840
Silver nitrate	Sigma-Aldrich	Cat# 209139-25G
SNAP surface 549	New England BioLabs	Cat# S9112S
SNAP surface Alexa Fluor 488	New England BioLabs	Cat# S9129S
Slide-A-Lyzer dialysis cassettes, 20K MWCO, 0.1 mL	Thermo Fisher	Cat# 69590
Slide-A-Lyzer dialysis cassettes, 10K MWCO, 3–12 mL	Thermo Fisher	Cat# 66810
Slide-A-Lyzer dialysis cassettes, 10K MWCO, 30 mL	Thermo Fisher	Cat# 66830
Sodium carbonate	Sigma-Aldrich	Cat# 71345-1KG
Sodium chloride	Thermo Fisher	Cat# S271-1
Sodium dodecyl sulfate	Sigma-Aldrich	Cat# L3771-500G
Sodium thiosulfate pentahydrate	Sigma-Aldrich	Cat# 217247-500G
Spectinomycin sulfate	P212121	Cat# GB-S-150-100
Sucrose	Sigma-Aldrich	Cat# S7903-1KG
Superdex S200 Increase column	GE Healthcare	Cat# 28990944
Tris base	Gold Biotechnology	Cat# T-400-5
Triton X-100	Sigma-Aldrich	Cat# X100-100ML
Tween 20	Bio Basic	Cat# TB0560
Urea	Sigma-Aldrich	Cat# U4884-1KG
Water, Sterile (For RNA work)	Fisher scientific	Cat# BP5611
Yeast nitrogen base w/o amino acids	BD Difco	Cat# BD291920
Yeast ribonucleic acid (yeast total RNA)	Sigma-Aldrich	Cat# R6750-100MG
YPD broth	RPI	Cat# Y20090–5000.0
Smt3-specific protease Ulp1	This paper	N/A
African killifish DDX5-SNAP	This paper	N/A
African killifish DDX5ΔPrD-SNAP	This paper	N/A
African killifish DDX5ΔIDR-SNAP	This paper	N/A

(*Continued on next page*)

Please cite this article in press as: Harel et al., Identification of protein aggregates in the aging vertebrate brain with prion-like and phase-separation properties, Cell Reports (2023), https://doi.org/10.1016/j.celrep.2023.112787

Continued

REAGENT or RESOURCE	SOURCE	IDENTIFIER
Critical commercial assays		
BIOMOL® GREEN	Enzo Life Science	Cat# BML-AK111-1000
EZ-ECL	Biological Industries	Cat#20-500-500
Bio-Rad Protein Assay	BioRad	Cat#500-0006
GeneJet Plasmid Miniprep Kit	Thermo Scientific	Cat# K0503
Pierce BCA Protein Assay Kit – Reducing Agent Compatible	Thermo Scientific	Cat# 23250
Pierce Quantitative Fluorometric Peptide Assay	Thermo Scientific	Cat# 23290
QuickChange Lightning Site-Directed Mutagenesis Kit	Agilent	Cat# 210518
TMT10plex™ Isobaric Label Reagent Set	Thermo Scientific	Cat# 90110
Deposited data		
Tandem mass spectrometry data (raw and analyzed data)	This paper	MassIVE MSV000086315
Experimental models: Organisms/strains		
BY4741 (*S. cerevisiae*)	Dharmacon	YSC1048
[*RNQ*$^{+}$][*psi*$^{-}$] in 74D-694 background (*S. cerevisiae*)	Lindquist Lab	N/A
African killifish *Nothobranchius furzeri* (GRZ strain)	This paper	N/A
C57BL/6 mice	National Institute on Aging	N/A
Oligonucleotides		
Primers for cloning and sequencing, see Table S4	This paper	N/A
Other		
Cover glass thickness 1 (24 × 60 mm)—for Leica DMI6000	Corning	Cat# 2975-246
Cover glass thickness 1 ½ high performance, D = 0.17mm—for OMX	Zeiss	Cat# 474030-9000-000
Epifluorescence microscope equipped with Leica HC PL APO 100 x 1.4 OIL and HC PL APO 63 x 1.4 OIL objectives	Leica	DMI6000
Glass-bottom plate, 12-well with high performance #1.5 cover glass	Cellvis	P12-1.5H-N
Multi-spot microscope slide (3″ x 1″ with 12 wells, 6 mm dia. wells)	Thermo Shandon	Cat# 9991090
Fusion Pulse 6 Membrane imager	Vilber Lourmat	N/A
iBlot 2	Thermo Scientific	IB21001
iBlot™ 2 Transfer Stacks	Thermo Scientific	IB23001
Stereo binocular microscope	Leica	S9E
3D Structured Illumination microscopy	Applied Precision-GE	DeltaVision OMX BLAZE system
Tissue homogenizer	Biospec	985370–04
TissueLyzer LT	QIAGEN	85600
TissueLyzer Adaptor	QIAGEN	69980
Amicon Ultra 0.5 mL Centrifuge filters, 30 kDa NMWL devices	Millipore	Cat#UFC505024
Amicon Ultra 4 mL Centrifuge filters, 30 kDa NMWL devices	Millipore	Cat#UFC805024
Zeba™ Spin Desalting Columns (7K MWCO, 75 μL)	Thermo Fisher	Cat# 89878
Zeba™ Spin Desalting Columns (7K MWCO, 0.5 mL)	Thermo Fisher	Cat# 89882
Recombinant DNA		
Gateway®pDONR™221	Invitrogen	Cat# 12536017
pcDNA3.1	ThermoFisher	Cat# V79020
pAG415GPD-ccdB-EGFP	(Alberti et al.)[80]	Addgene plasmid # 14194
pAG416GAL-ccdB-EGFP	(Alberti et al.)[80]	Addgene plasmid # 14195
pAG416GAL-ccdB-mRuby3	This paper	N/A
pAG426GAL-ccdB-mRuby3	This paper	N/A
pDEST17-His10-SMT3-ccdB-SNAP	This paper	N/A
Protein-specific yeast expression plasmids, Table S4	This paper	N/A
Software and algorithms		
CellProfiler 3.1.9	(McQuin et al.)[81]	https://cellprofiler.org/

(*Continued on next page*)

Please cite this article in press as: Harel et al., Identification of protein aggregates in the aging vertebrate brain with prion-like and phase-separation properties, Cell Reports (2023), https://doi.org/10.1016/j.celrep.2023.112787

Continued

REAGENT or RESOURCE	SOURCE	IDENTIFIER
DISOPRED 3	(Jones et al.)[54]	http://bioinf.cs.ucl.ac.uk/psipred/?disopred=1
Fiji	NIH	https://imagej.net/Fiji
Leica software package	Leica	N/A
PLAAC	(Lancaster et al.)[53]	http://plaac.wi.mit.edu/
Prism 8.4	GraphPad	https://www.graphpad.com/scientific-software/prism/
Python 2.7.15	Python Software Foundation	https://www.python.org/
R 3.5.1	R Project	https://www.r-project.org/

RESOURCE AVAILABILITY

Lead contact

Further information and requests for resources and reagents should be directed to and will be fulfilled by the lead contact, Anne Brunet (abrunet1@stanford.edu).

Material availability

The plasmids generated in this study are available at Addgene. The killifish DDX5 antibody is available upon request to the lead contact.

Data and code availability

All raw mass spectrometry reads as well as processed datasets can be found in the MassIVE database (https://massive.ucsd.edu/ProteoSAFe/dataset.jsp?task=46e5fed3be0643a6bcb8f5a28d599685). The codes and results are available in the GitHub repository https://github.com/ywrchen/killifish-aging-aggregates as well as in Zenodo: https://zenodo.org/record/7982837. Any additional information required to reanalyze the data reported in this work paper is available from the lead contact upon request.

EXPERIMENTAL MODEL AND STUDY PARTICIPANT DETAILS

S. *cerevisiae*

S. cerevisiae strains were obtained from the sources indicated (key resources table). All S. cerevisiae strains were stored as glycerol stocks at −80°C. Before use, strains were either revived on YPD (10 g/L yeast extract, 20 g/L dextrose, 20 g/L peptone, sterilized by autoclaving) or on defined medium (2% glucose, 6.7 g/L yeast nitrogen base without amino acids, 20 mg/L histidine, 120 mg/L leucine, 60 mg/L lysine, 20 mg/L arginine, 20 mg/L tryptophan, 20 mg/L tyrosine, 40 mg/L threonine, 20 mg/L methionine, 50 mg/L phenylalanine, 20 mg/L uracil, 20 mg/L adenine, sterilized by autoclaving) as necessary. Antibiotics, or defined drop-out media were used as indicated to maintain plasmid selection. All strains were grown at 30°C unless otherwise indicated.

Yeast strains expressing exogenous killifish proteins were generated by transforming laboratory strain BY4741 (either fresh mid-exponential cells or frozen chemically competent cells) with yeast expression plasmids that encoded proteins of interest. Yeast transformation was carried out using a standard lithium-acetate protocol. First, cells were inoculated into 25 mL of liquid rich medium (YPD) and grown to saturation overnight on a shaker at 200 r.p.m and 30°C. The cells were then diluted by 25-fold into 500 mL of liquid rich media (YPD) and regrown on a shaker at 200 r.p.m and 30°C. Once the culture reached mid-exponential phase (OD_{600} ~0.4–0.6), the cells were harvested by centrifugation at 2000xg for 5 min and washed twice in an equal volume of sterile water. The cells were either used directly for yeast transformation or further processed to generate competent cells. To generate chemically competent cells, cell pellets were resuspended in 5 mL of filtered sterile frozen competent cell solution (5% v/v glycerol, 10% v/v DMSO), and 50 μL aliquots were generated in 1.5 mL microcentrifuge tube and stored at −80°C. To ensure good survival rates, aliquots were slowly frozen either using Mr. Frosty freezing container (Thermo Scientific Cat# 5100-0001) or Styrofoam box padded with Styrofoam chips or newspaper (to reduce air space around sample). For yeast transformation, competent cells were thawed in 37°C water bath for 15-30s then centrifuged at 13000xg for 2min to remove supernatant and resuspended in a transformation master mix (260 μL PEG 3500 50% (w/v), 36 μL 1 M Lithium acetate, 50 μL denatured salmon sperm carrier DNA (2 mg/mL), 14 μL plasmid DNA (0.1–1 μg total plasmid), and sterile water to a final volume of 360 μL). Cells were incubated in the transformation master mix at 42°C for 45 min. Following incubation, cells were harvested, resuspended in 1 mL sterile water, and ~100 μL was plated on selective medium and grew at 30°C. Successful transformants typically appeared in 2–3 days and were further propagated in defined liquid drop-out medium (omitted nutrient depending on the plasmid being selected) and stored as glycerol stocks in −80°C.

Mice

All mice used in this study were male C57BL/6 mice obtained from the NIA Aged Rodent colony. We used young (4 months) and old (28 months) male mice. Mice were habituated for more than one week at Stanford before use. At Stanford, all mice were housed in the Comparative Medicine Pavilion or the Research Animal Facility II, and their care was monitored by the Veterinary Service Center at Stanford University under IACUC protocol 8661.

African turquoise killifish strain, husbandry, and maintenance

The African turquoise killifish (GRZ strain) were housed as previously described.[45] Fish were housed at 26°C in a central filtration recirculating system with a 12 h light/dark cycle at the Stanford University facility (Aquaneering, San Diego) or at the Hebrew University of Jerusalem (Aquazone ltd, Israel). In both facilities, fish were fed twice a day on weekdays and once a day on weekends with Otohime Fish Diet (Reed Mariculture). In these conditions, killifish lifespan was approximately 6–8 months. The *TERT*$^{\Delta 8/\Delta 8}$ loss-of-function allele[45] was maintained as heterozygous (due to fertility issues in homozygous) and propagated by crossing with wild-type fish. Following genotyping at the age of one month,[45] fish were single-housed. All turquoise killifish care and uses were approved by the Subcommittee on Research Animal Care at Stanford University (IACUC protocol #13645) and at the Hebrew University of Jerusalem (IACUC protocol #NS-18-15397-2).

METHOD DETAILS

Isolation of tissue lysate (TL) and aggregate-enriched (AGG) fractions from brain tissues

This protocol is described in more depth in Chen, Harel et al. for all tissues49. Briefly, whole brains of 3 young (3.5 months) wild-type, 3 old (7 months) wild-type, and 3 old (7 months) *TERT*$^{\Delta 8/\Delta 8}$ mutant[45] male fish were collected and snap-frozen in liquid nitrogen. All procedures were conducted at 4°C unless stated otherwise. We have used an adaptation of a standard aggregate isolation protocol[50,82] to separate relatively small oligomeric protein aggregates from other membraneless organelles (e.g. stress granules).[83] Our protocol uses multiple differential centrifugation steps to exclude both large membraneless organelles (e.g. stress granules)[84] large defined macromolecular complexes (e.g. ribosomes.[85] Brains were homogenized using a tissue homogenizer in 100 μL of buffer A (30 mM Tris-Cl pH = 7.5, 1 mM DTT, 40 mM NaCl, 3 mM $CaCl_2$, 3 mM $MgCl_2$, 5% glycerol, 1% Triton X-100, protease inhibitor cocktail tablet used at 1x the manufacturer recommended concentration (Roche cOmplete EDTA-free Protease Inhibitor Cocktail, Cat# 11697498001). Homogenization was performed in round-bottom tube (2 mL corning cryogenic vials) to ease lysis and the resulting sample was transferred to 1.5 mL Eppendorf tube for the first centrifugation spin. Lysate was spun at 800 g for 10 min (spin 1) to remove cell debris (Eppendorf Centrifuges 5430 with Eppendorf FA-45-48-11 30-spot 45-degree fixed angel rotor). Supernatants were transferred to a new Eppendorf tube and treated with 100 μg/mL RNase A (Akron Biotech, 89508-840), and 100 μg/mL DNase I (New England Bio, Cat# M0303S) for 30 min on ice. Samples were spun at 10,000 g for 15 min (spin 2 in the same Eppendorf FA-45-48-11 rotor) and the resulting supernatant is the tissue lysate (TL) fraction. A 25 μL aliquot of the TL was kept in a separate tube for protein quantification and mass spectrometry analysis. For isolation of the aggregate (AGG) fraction, all the remaining TL was loaded onto the top of a 1 mL 40% sucrose pad and additional ~750 μL (adjusted to balance all ultra-centrifuge tubes) of buffer A was layered on the top in ultra-centrifugation tube (Beckman Coulter Ultra-Clear centrifuge tubes, thinwall, 2.2 mL, 11 × 34 mm, catalog # 347356). The samples were separated through ultracentrifugation for 1 h at 200,000 g (spin 3 at 49,000 r.p.m. in Beckman TLS-55 rotor). Top layers of supernatants were removed, leaving 15–20 μL of liquid at the bottom. An additional 30 μL of buffer A was added to rigorously re-suspend the pellets. Protein concentration for TL and AGG samples was assessed using standard BCA kit (Pierce BCA Protein Assay Kit – Reducing Agent Compatible, catalog #23250).

Mass spectrometry sample preparation and analysis

Following tissue lysate (TL) extraction and aggregate (AGG) isolation, samples were re-suspended in 8M urea and ProteaseMAX (Promega) and were subsequently subjected to reduction (with 10 mM DTT for 30 min at 55°C) and alkylation (with 30 mM acrylamide for 30 min at room temperature) followed by trypsin digestion (1:50 concentration ratio of sequencing grade trypsin to total protein overnight at 37°C followed by quenching with 25 μL of 50% formic acid to pH below 3.0). The digested peptides from different samples of the same organ were separately quantified and equal amount of peptide samples were labeled with TMT10plex mass tag before mass spectrometry analysis. In particular, equal amount of TL or AGG (3–10 μg of peptide depending on the organ/tissue) from each sample was labeled with 9 different TMT-10plex tags accordingly to the manufacturer's protocols (cat# 90110, Thermo Scientific). The same mass tag and sample assignment was maintained throughout the entire study (old brain samples were labeled with TMT^{10}-126, TMT^{10}-127N, and TMT^{10}-127C respectively; young brain samples were labeled with TMT^{10}-128N, TMT^{10}-128C, and TMT^{10}-129N respectively; and old *TERT*$^{\Delta 8/\Delta 8}$ brain samples were labeled with TMT^{10}-129C, TMT^{10}-130N, and TMT^{10}-130C respectively). One-ninth of each sample (equal amount of peptide across all TL or AGG samples from a tissue/organ) were pooled after trypsin digestion and labeled with the 10th TMT tag to serve as the reference channel for internal normalization. Post-labeling, each set of samples were further cleaned up with C18 peptide desalting columns. Samples were subjected through high pH reverse phase fractionation into 3 or 4 fractions and all fractions were run independently on an Orbitrap Fusion (Thermo Scientific) mass

Please cite this article in press as: Harel et al., Identification of protein aggregates in the aging vertebrate brain with prion-like and phase-separation properties, Cell Reports (2023), https://doi.org/10.1016/j.celrep.2023.112787

spectrometer coupled to an Acquity M-Class nanoLC (Waters Corporation). Data searches were conducted with killifish proteome downloaded from NCBI (available in GitHub repository https://github.com/ywrchen/killifish-aging-aggregates and MassIVE dataset MSV000086315 for this paper).

Data collection was performed using an Orbitrap Fusion Tribrid mass spectrometer (RRID:SCR_018702 Thermo Scientific, San Jose, CA) with an Acquity M-Class UPLC system (Waters Corporation, Milford, MA) for reverse phase separations. Separations were performed on in-house pulled-and-packed fused silica chromatography columns. The fused silica column has an I.D. of 100 μm and is packed with a C18 reprosil Pur 1.8 μm stationary phase (Dr. Maisch) to a length of ~25 cm. The UPLC system was set to a flow rate of 300–450 nL/min, where mobile phase A was 0.2% formic acid in water and mobile phase B was 0.2% formic acid in acetonitrile; it was operated at a typical pressure of ~6500 psi. Peptides were directly injected onto the chromatography column, with a gradient of 2–55% mobile phase B over a 180-min gradient, followed by a high-B wash. CID fragmentation was used in a data-dependent fashion for MS/MS spectral generation.

TMT data were collected in a 10-notch synchronous precursor selection (SPS) fashion, with MS2 using CID and MS3 using HCD as outlined previously.[86] AGC was operated in a predicted mode at a maximum fill time of 150 ms (AGC target of 5000) for MS2 and 250 ms for MS3 (AGC target of 10000), with isolation windows of 0.7 m/z for both MSn dimensions. CID and HCD fragmentation were at 35% and 55% in instrument frame, respectively. Orbitrap resolutions were held to 120k and 60k for precursor and fragment spectra, respectively. Mass spectra were analyzed using Proteome Discoverer v2.0 (Thermo Scientific) for MS3 quantification of tandem mass tag reporter ions and the Byonic v2.6.49 search algorithm node for peptide identification and protein inference. Briefly, a typical mass spectrometry analysis allowed for fully tryptic digestion with up to two missed cleavages. A 12 ppm mass accuracy was tolerated for precursor and MS3 HCD fragments, *i.e.*, reporter ions, and 0.3 Da mass accuracy for CID fragmentation at the MS2 level. Static modifications include cysteine carbamidomethylation and TMT labels on peptide N-termini and lysine residues. Oxidation of methionine and deamidation of aspartate and glutamine were considered as dynamic modifications. Peptides and proteins were cut at the 1% FDR level using the Byonic node. Reporter ion intensities were normalized against a pooled sample containing each of the other samples in a given sample run and reported relative to these pooled samples. These ratios were exported for analysis at both the protein and PSM (Peptide Spectrum Match) level. The mass spectrometry raw data, summary table of the reporter ion ratios at protein and PSM levels, as well as protein sequence FASTA files use for the search were deposited to MassIVE with a dataset id as MSV000086315.

Annotation of the NCBI genes models of turquoise killifish

We used the African turquoise killifish (*N. furzeri*) NCBI annotation release 100 for our analysis. The majority of the gene models in this annotation only have a locus number. Therefore, we re-annotated all the killifish gene model names based on orthology analyses with 40 species including mammals, fish and invertebrates. We selected the consensus symbols for the locus assigned by NCBI as our final symbols and re-annotated the genes using a naming scheme Gene_Name(n of m) if there were duplicates in the killifish genome. For most of the analyses, human homologs were reported or used in database search, unless otherwise noted. The annotation and human homologs used in this killifish study can be found in Table S1D.

Mass spectrometry data normalization and analysis of age-associated changes

The target protein results including the reporter ion ratios and total number of spectra assigned to peptides from this protein (# PSMs) were further processed to infer the abundance of each protein in each sample. First, the human contaminants were removed. Next, the protein abundance of each sample was inferred from its PSM contribution (or equivalently each TMT10plex tag), calculated by multiplying the total number of PSMs for a protein by the fraction of reporter ion signal that came from this channel (ratio of query channel divided by sum of the ratios across all channels, note that the TMT-131 was the normalization channel and contributed as 1 to the overall signal). Because equal amounts (by mass) of peptides were loaded in each channel, we normalized the sum of PSMs for all proteins in a channel to a constant of 100,000. The resulting normalized counts of PSMs for a protein in a sample represent the final reported protein abundance (PSMsNorm). We log2-transformed the protein abundance (log2_PSMsNorm) and the resulting protein abundance for each tissue approximately followed a normal distribution.[49] We then used the log2-transformed protein abundance to perform a parametric statistical test (Student's t-test), as is often done for proteomics datasets.[87–92]

The age-associated changes in a protein in either tissue lysate or aggregate fraction were calculated as the fold change in the average abundance of a protein between the two age groups (Young and Old) (between Old and Old $TERT^{\Delta 8/\Delta 8}$ mutants though these conditions were not analyzed in depth in this manuscript). Both fold change (i.e. OvY_FC for the fold change of old divided by young) and log2-transformed fold change (i.e. OvY_logFC was the log2-transformed fold change of old divided by young) are reported in Table S1A. Age group differences were assessed using a Student's t-test (p values from this test referred to as OvY_pval). The p values were not corrected for multiple hypothesis testing, as is often done for proteomics datasets.[87–92]

We defined the term 'aggregation propensity' (PROP) to infer the intrinsic likelihood of a protein to aggregate, scored by dividing the abundance of a protein in the aggregate fraction (AGG) by its tissue lysate (TL) abundance. Note that this metric can only be reported when a protein is identified in both the TL and AGG fractions. Proteins that were only detected in AGG but not in TL make up about 0.8–1.7% (median 1.3%, average 1.2%) of total AGG signal and their abundance change was analyzed at the AGG level only. Because each channel represents the tissue sample from an individual fish, we reported the aggregation propensity of a protein for each sample. The age-associated changes in aggregation propensity (i.e. OvY_prop_FC) were calculated as the fold change in the

average aggregation propensity of a protein between the two age groups. The log2-transformed fold change (i.e. OvY_prop_logFC) was reported as well. Student's t-tests were performed on the log2-transformed aggregation propensities of the different age groups. The resulting p values were reported (OvY_prop_pval) to assess whether the changes between conditions were statistically significant.

Principal component analysis (PCA)

Standardized log2-transformed normalized protein abundance (peptide spectral count for each protein) for young, old, and *TERT*$^{\Delta 8/\Delta 8}$ mutant brain samples (TL and AGG) were used as input for principal component analysis (PCA). PCA was performed in R (version 3.5.0) using autoplot function implemented in R package ggfortify (version 0.4.6) and plotted using ggplot2 (version 3.1.1).

Gene ontology enrichment analysis

Enriched Gene Ontology (GO) terms associated with proteins from old versus young brain samples (AGG and TL) were identified using Gene Set Enrichment Analysis (GSEA) implemented in R package clusterProfiler (version 3.10.1).[93] All the proteins identified in the brain were ranked and sorted in descending order based on multiplication of $\log_2$ transformed fold change and $-\log_{10}$(p value). This metric prioritizes proteins with both large absolute fold changes and small p values. Note that due to random seeding effect in GSEA, the exact p value and rank of the enriched terms may differ for each run. These random seeds did not qualitatively affect the enrichment analyses.

Statistics for enrichment for PLAAC and DISOPRED

We calculated the normalized prion score (NLLR) predicted by PLAAC[53] and the fraction of disordered residues with DISOPRED 3[54] for each protein that showed significant age-associated increase in aggregation in the brain and other tissues (paired t test p value <0.05 and t-value of log2 transformed fold change of AGG or PROP from old over young animals greater than 0.75). The p values were not corrected for multiple hypothesis testing, as is often done for proteomics datasets.[87–92] We considered a protein to contain a prion-like domain (PrD) if it had a positive NLLR score in the primary sequence by PLAAC. We considered a protein to contain an intrinsically disordered region (IDR) if the fraction of disordered residues for that protein was greater than 0.3. Residues are considered disordered if their scores were greater than 0.5 based on DISOPRED 3 prediction. We then performed a Fisher's exact test on the age-associated aggregates that contain either PrD or IDR, respectively, in comparison to the total detected aggregates in each tissue. The p values were reported.

CRISPR/Cas9 target prediction and gRNA synthesis

CRISPR/Cas9 genome-editing was performed according to.[44,45] In brief, for targeting DDX5, we identified conserved regions in the coding sequence using multiple vertebrate orthologs using http://genome.ucsc.edu/. Conserved regions that were upstream of functional or active protein domains were selected for targeting in exon 5 and 7 of *DDX5*. gRNA target sites were identified using CHOPCHOP (https://chopchop.rc.fas.harvard.edu/),[94] and were as follows (PAM sites are in bold, in modified nucleotides, from C to G, are in square brackets):

Exon5: [C]GACCATGTCTTTTCCACTC**AGG;** G[C]ATCGCTCAAACGGGGTCT**GGG;**

GGGTGGCCCATTGTCCTGAG**TGG.** Exon7: GGTGGCTGCTGAGTACGGCA**GGG;** GGTGCATGTACTCTTGAGAC**GGG;** GGATG TACTCTTGAGACGGG**AGG;** GGTGGCACCAACCCGTGAGC**TGG.** Hybridized oligonucleotides, according to 44,45, were used as an *in vitro* transcription template. gRNAs were *in vitro* transcribed and purified using the MAXIscript T7 kit (ThermoFisher # AM1312), according to the manufacturer's protocol.

Production of Cas9 mRNA

Experiments were performed according to 44,45. The pCS2-nCas9n expression vector was used to produce Cas9 mRNA (Addgene, #47929).[95] Capped and polyadenylated Cas9 mRNA was *in vitro* transcribed and purified using the mMESSAGE mMACHINE SP6 ULTRA (ThermoFisher # AM1340).

Microinjection of turquoise killifish embryos and sequencing of targeted sites

Microinjection of turquoise killifish embryos was performed according to.[44,45] Cas9-encoding mRNA (300 ng/μL) and gRNA (30 ng/μL) were mixed with phenol red (2%) and co-injected into one-cell stage fish embryos. Three days after injection, genomic DNA was extracted from 5 to 10 pooled embryos. The genomic area encompassing the targeted site (~600bp) was PCR-amplified, using the following primer sequences: Exon5F1: TTGGATAAGACACTCACTGCCA; Exon5F2: ACACTCACTGCCAAAGTCTTCC. Exon5R1: CTGATGTTGGATGTGAACGACT; Exon5R1: GTGAACTTACAATAGGCCCGTC. Exon7F1: CCAGAAAAGAGAGAGCG AGTTT; Exon7F2: TCATTATCGGACTCAGTTGCTT; Exon7R1: CTATCTTGCGGATCTGAGGTTC; Exon7R2: TCCGATACACGGTT TTTGAATA. DNA sequencing was used for analysis. Perturbing the DDX5 gene led to embryonic lethality in the F0 generation, resulting in failure to obtain germline-transmission and an F1 generation.

Please cite this article in press as: Harel et al., Identification of protein aggregates in the aging vertebrate brain with prion-like and phase-separation properties, Cell Reports (2023), https://doi.org/10.1016/j.celrep.2023.112787

Generation of DDX5-GFP transgenic fish

The *Tg(DDX5p:DDX5-GFP)* transgenic animals (F0 founders) were generated at the Stowers Institute via the Tol2 system 43,44. A 7.8 kb cassette that includes 5.2 kb *DDX5* promoter sequence and 2.3 kb encoding a DDX5-GFP fusion protein was cloned into pDest-Tol2 vector[96] through Gibson assembly (#E5510, NEB). Gibson assembly primers were designed using NEBuilder Assembly Tool (http://nebuilder.neb.com/), and primer sequence in lowercase mark the homology arm. A 5.4kb region was identified around the *DDX5* promoter to be positive for the active chromatin marks H3K27ac and H3K4me3.[97] This fragment also included the first the first intron and exon of *DDX5*. This entire region was PCR amplified using Platinum PCR SuperMix High Fidelity (Thermo Fisher Scientific), genomic DNA as template, and the following primers: DDX5-PromoterGibson-F: aacatatccagtcactatggACCTGGAGTCACTGCTTG; DDX5-Intron1Gibson-R: acccccatacCCTGTGGTGAAAAAAGGAC. The PCR product was gel purified and sequence verified by comparing it to the killifish genome using BLAST. To amplify the DDX5-GFP gene cassette we used the DDX5-GFP yeast expression vector we generated as a PCR template (reference Yiwen's section). The following primers were used (omitting the first exon which was included in the promoter fragment): DDX5-GFPGibson-F: tcaccacaggGTATGGGGGTGGCCCCCC; DDX5-GFPGibson-R: tggatcatcatcgatggtacTTACTTGTACAGCTCGTCCATGCCG. The PCR product was gel-purified and sequence-verified. The pDest-Tol2CV vector was digested with KpnI-HF and SalI-HF (NEB), removing the eye marker expression cassette (crystallin:Venus). The linearized plasmid was gel-purified. All three fragments were assembled using NEBuilder HiFi (NEB) according to the manufacturer's protocol. The transposase expression vector was obtained from the Tol2Kit (http://tol2kit.genetics.utah.edu/index.php/Main_Page). 20 pg of plasmid DNA and 30 pg of transposase mRNA were co-injected into one-cell stage killifish embryos. Injected embryos were maintained at 26°C and hatched at 15 days post injection. Overexpression of DDX5 protein in the F0 generation caused growth retardation and defects, resulting in failure to obtain germline transmission and an F1 generation. Therefore, only chimeric F0 animals with GFP expression in the brain were used in this study.

GFP antibody staining in brain tissue

Three 7-month old F0 *Tg(ddx5:DDX5-GFP)* animals (males) with GFP expression in the brain were used for GFP antibody staining. Fish were euthanized in 500 mg/mL MS-222 and the brain tissue were dissected out and subjected to overnight fixation with 4% PFA at 4°C. Brain cryosections were prepared as previously described.[98,99] Antibody staining was done on 10 μm brain cryosections according to published protocol with modifications.[100] Briefly, brain cryosections were bleached with 5% H_2O_2 and 0.1% Formamide in PBS. Before primary antibody incubation, samples were treated with Trueblack Lipofuscin Autofluorescence Quencher (Biotium) for 30 s and no detergent was used in all follow-up steps. Anti-GFP antibody (ab13970, Abcam) and the goat anti-chicken secondary antibody Alexa 647 (Thermo Fisher) were used as 1:500. Samples were mounted in ProLong Gold Antifade Mount and imaged under PerkinElmer Ultraview spinning disk.

Generation of killifish DDX5 antibodies

Custom made antibodies aging the killifish DDX5 protein (XP_015809881.1) were generated in rabbits and performed by Bethyl, using their standard protocol that peptide synthesis, conjugation of antigen to carrier, subcutaneous immunizations of 2 rabbits, followed by ELISA testing results and affinity purification. The following peptide (corresponding to the C terminus of killifish DDX5) was used as an immunogen: DDX5-625: 625-PYPIPPPFPQ-634. Antibodies were used at a dilution of 10,000 for Western blot, and 1:500 for immunofluorescence.

Tissue extracts and western-blot for DDX5 antibodies

Three young (2.5 months old) and three old (5.5 months old) *Nothobranchius furzeri* (GRZ strain) male fish were sedated in 200 mg/L of Tricain (Sigma-Aldrich, A5040), and then euthanized in 500 mg/L of Tricain in system water. Dissections were carried out under a stereo binocular (Leica S9E) at room temperature. Brains were dissected, and whole brains were placed in cold, slightly modified Buffer A (see Mass-Spec section: 30 mM Tris-HCl pH = 7.5, 40 mM NaCl, 3 mM $CaCl_2$, 3 mM $MgCl_2$, 5% glycerol, 1% Triton X-100) with freshly added protease inhibitors: pepstatin A at a final concentration of 1μM (Abcam, ab141416) and N-Ethylmaleimide at a final concentration of 10mM (Sigma-Aldrich, E3876). Homogenization was performed in a conical eppendorf tube to allow full homogenization of brain tissue with 3mm-metal beads (Eldan Israel, Cat# RC55 420). Homogenization was carried out with mechanical disruption using TissueLyzer LT (QIAGEN, #85600) with a dedicated adaptor (QIAGEN, #69980) at 50Hz for 4 min. No centrifugation was performed, and whole brain lysate were used to avoid loss of DDX5 protein. Protein concentration was measured with BCA (Sigma-Aldrich), according to manufacture instructions. Brain homogenate was then mixed with a pre-heated (95°C) Sample Buffer with Urea (SB + U) (Tris-HCl pH6.8 62.5mM, Glycerol 10%, SDS 2%, 0.00125% and Urea 8M) at a ratio of 1:6 (sample to SB + U), boiled at 95°C for 5 min and placed on ice.

Standard Western blot was performed. Briefly, 23μg of protein was resolved using Novex WedgeWell 4–20% Tris-Glycine gel (Thermo Fisher XP04205BOX), at 220V for 45 min. Transfer to a Nitrocellulose membrane was performed using the iBlot 2 (Thermo Scientific, IB21001). Membranes were then stained with Ponceau Red (Sigma, P7170-1L), and imaged with regular white light. Membranes were then washed in TBST 0.1% (Tris-HCl 10mM pH 8.0, NaCl 150mM, Tween 0.1%) 3 times for 5 min to remove Ponceau staining, and blocked in 5% BSA (sigma-aldrich) for 1 h at room temperature. Next, anti-DDX5 (1:1000, custom-made, this paper)

was incubated in 5% BSA blocking solution at 4°C overnight. Following washes, membranes were incubated with HRP secondary antibodies. For DDX5, we used anti-rabbit HRP (Abcam, ab6721). Membranes were treated with EZ-ECL kit and chemiluminescence was detected using Fusion Pulse 6 (Vilber Lourmat).

Immunostaining of DDX5 in killifish brain sections

Fish were euthanized with MS222 (500 mg/L) for 10 min at room temperature, and then the brains of 4 young (3.5 months), and 4 old (7 months) male fish were dissected immediately into cold PBS (pH 7.4, Gibco). The dissected brains were fixed with 4% paraformaldehyde (PFA) in PBS at 4°C overnight. The next day brain samples were transferred into 30% sucrose at 4°C overnight, followed by standard cryo-sectioning protocol. Samples were sectioned at 10 μm thickness and stained as previously described.[98,99] Briefly, following three 10 min wash with PBST (PBS +1% Tween), sections were blocked for 1h with serum-free block (Dako, X0909), and incubated over-night with our custom-made DDX5 antibodies (1:500) diluted in the blocking solution. Following subsequent washes with PBST, sections were incubated for 1 h at room temperature with 1:300 goat anti-rabbit Alexa 488 secondary antibody (Abcam, ab150077)) and 2 μg/mL Hoechst. Samples were mounted in ProLong Gold Antifade Mount and imaged under Nikon Eclipse confocal microscope, using either X40 or X60 objectives.

Immunostaining of DDX5 in mouse brain sections

All immunostainings were performed on young (4 months) and old (28 months) C57BL/6 male mice obtained from the NIA. Mice were subjected to intracardiac perfusion with 5mL of PBS containing heparin followed by 20mL of 4% paraformaldehyde (PFA, Electron Microscopy Sciences, RT 15714) in PBS. Brains were post-fixed for 24 h in 4% PFA. They were then subjected to dehydration in 30% sucrose (Sigma-Aldrich, S3929) for 72 h. Brains were subsequently embedded in Tissue-Tek optimal cutting temperature (O.C.T.) compound (Electron Microscopy Sciences, 62550) and sectioned using a cryostat in 12μm coronal sections that were mounted on glass slides. To perform immunofluorescent staining, sections were first washed with PBS, followed by permeabilization with ice-cold methanol with 0.2% Triton X- for 10 min at room temperature. Sections were blocked with 5% Normal Donkey Serum (ImmunoReagents Inc., SP-072-VX10) and 1% BSA (Sigma Aldrich A8806) in PBS for 30 min at room temperature. Primary antibody staining was performed overnight at 4°C in 5% Normal Donkey Serum and 1% BSA in PBS. Primary antibodies used were the following: DDX5 (Atlas Antibodies, HPA020043, [1:200]) and NeuN (Millipore, MAB377, clone A60 [1:500]). Sections were washed with PBS with 0.2% Tween and then with PBS three times for 5 min at room temperature. Secondary antibody staining was performed at room temperature for 2 h in 5% Normal Donkey Serum and 1% BSA in PBS. Secondary antibodies used were the following: donkey anti rabbit-AF568 (ThermoFisher [1:500]) and donkey anti mouse-AF488 (ThermoFisher [1:500]). Sections were washed with 0.2% Tween and then with PBS only three times for 5 min at room temperature. Sections were stained with DAPI (ThermoFisher 62248) at 1 μg/mL for 10 min at room temperature. Sections were mounted with ProLong Gold (ThermoFisher, P36930) and visualized with a Nikon Eclipse Ti confocal microscope equipped with a Zyla sCMOS camera (Andor) and NIS-Elements software (AR 4.30.02, 64-bit) using the 60× objective. No blinding was done for picture taking. For visualization of images displayed in this manuscript, brightness and contrast were adjusted in Fiji to enhance visualization. The same settings were applied to all images shown for each experiment.

Cloning of killifish cDNAs

Brain, liver, and muscle tissues from male African turquoise killifish *N. furzeri* were individually homogenized in RLT buffer (RNeasy Kit, # 74104 QIAGEN) using 0.5 mm Silica disruption beads (RPI-9834) and a tissue homogenizer (FastPrep-24, 116004500 - MP Biomedicals). Total RNA was isolated from the lysed tissues according to the RNeasy Kit protocol. cDNA for DDX5 was prepared from the total RNA from pooled brain, liver, and muscle tissues with high-capacity cDNA RT kit (Applied Biosystems, 4368814) using random primers, and according to the manufacturers' protocol. cDNA was amplified using custom DNA oligonucleotides (IDT) and AccuPrime Pfx DNA Polymerase (Thermo Fisher Scientific). The following primers were used to clone killifish DDX5: DDX5-F: ATGCCTGGATTTGCAGACAG; DDX5-R: TTATTGTGGAAACGGTGGTG. PCR products were gel-purified, cloned using Zero Blunt TOPO PCR Cloning Kit (Thermo Fisher Scientific), and sequence-verified. Similarly, selected proteins with statistically significant increase in aggregation propensity in old brains compared to the young brains (HNRNPH1, MARK4, PABPN1, SCARB2) were cloned from the pooled cDNA (brain, liver, and muscle) using sequence-specific primers (available in Table S4C) and sequence-verified.

Cloning and exogenous expression of killifish proteins in 293T cells

The sequence-verified ORFs of the full length untagged and C-terminally GFP-tagged and truncated GFP-tagged versions of killifish DDX5 (kfDDX5) (1–483 [ΔIDR] or 1–535 [ΔPrD]) and full length GFP-tagged human DDX5 (huDDX5) were cloned into pcDNA3.1 plasmid (ThermoFisher, V79020) and transfected into human embryonic kidney 293T cells (HEK293T, ATCC, CRL-11268). Plasmids were purified using GeneJet Plasmid Minirep kit (Thermo Fisher Scientific, K0503), according to the manufacturer's protocol. The HEK293T cell line (hereafter 293T) was not authenticated in-house. Mycoplasma testing was conducted every 3 months. Glass bottom 12 well plates (Cellvis, P12-1.5H-N) were coated with poly-D-lysine (Sigma Aldrich, P7886-10MG) for 2h at room temperature, washed 3 times with PBS and either directly used for seeding of cells or stored at 4°C for up to 2 weeks. The day before transfection, 3 x 10^5 293T cells per well were plated in 12 well plates in 293T medium (Dulbecco's modified Eagle medium (DMEM, Invitrogen, 11965-092) supplemented with 10% fetal bovine serum (FBS Gibco, 16000-044), 1% penicillin–streptomycin–glutamine (PSQ)

Please cite this article in press as: Harel et al., Identification of protein aggregates in the aging vertebrate brain with prion-like and phase-separation properties, Cell Reports (2023), https://doi.org/10.1016/j.celrep.2023.112787

(Gibco, 10378). The next day, cells were transfected as follows: in each well of a 12 well plate, medium was replaced by 500 μL of fresh medium, and 4 μL of 1 mg/mL polyethylenimine (PEI; Polysciences, 23966-2, linear 25 kDa) was added to 100 μL of DMEM and incubated for 10 min at room temperature. The plasmid of interest (1 μg) was added to the PEI–DMEM mixture and incubated for 15 min at room temperature. The PEI–DMEM–DNA mixture was then added dropwise to the 293T cells and the medium was replaced with 1 mL fresh 293T medium 20h after transfection. Cell were fixed 28-36h after transfection using 4% PFA (Electron Microscropy Sciences, 15710) in PBS for 20 min at room temperature. For GFP-tagged constructs, cells were washed 3 times with PBS, incubated with DAPI (ThermoFisher, 62248) (1:1000 in PBS) for 20 min at RT and washed 2 times more before imaging. For the untagged constructs, cells were washed 3 times with PBS after fixation and incubated for 10min with PBS + Triton (Fisher BioReagents, BP151500) (0.2%). This was followed by 3 washes with PBS, blocking in 5% Donkey Serum (ImmunoReagents, SP-072-VX10) in PBS-T (PBS + Tween 20 (Sigma-Aldrich, P1379-1L), 0.1%) for 30 min at RT and incubation with the custom-made killifish DDX5 antibody (1:500 in PBS-T + 1% BSA (Sigma, A7979) overnight at 4°C. Afterward, cells were washed 3 times with PBS and incubated with secondary antibody donkey anti rabbit-AF568 (ThermoFisher [1:500]) in PBS-T + 1% BSA for 1 h at room temperature in the dark. This was followed by one wash with PBS, incubation with DAPI (1:10,000) in PBS for 10 min and two further washes with PBS for 5 min, each before imaging on a ZEISS LSM 980 confocal microscope. DAPI and GPF were imaged using the 20× objective. No Z-stacks were used. Analysis was done in ImageJ by applying a minimal threshold filter to assess all GFP expressing (or immunocytochemically stained for killifish DDX5) cells followed by manual selection of individual cells showing fluorescent punctate areas above a preset maximal intensity value. Cell presenting with an area above the maximal intensity value were divided by all cells expressing GFP (or immunocytochemically stained for killifish DDX5) to obtain the ratio of cells containing DDX5 puncta.

Cloning of DDX5 wild-type and mutants in yeast vectors

Using the DDX5 fragment we cloned from killifish cDNA, we designed primers to amplify either the region spanning amino acid residues 1–483 (ΔIDR) or 1–535 (ΔPrD). We then cloned the truncated mutants into a gateway entry vector pDONR221 (Invitrogen Cat# 12536017). We verified the sequence by sequencing and subcloned it into a yeast gateway vector to allow GAL-inducible expression of the ORF with a C-terminal EGFP or mRuby3 tag (pAG416GAL-ccdB-EGFP in Lindquist Advanced Gateway Vector Collection, 80 or pAG426GAL-ccdB-mRuby3 generated for this paper) or a yeast gateway vector to allow constitutive expression of the mutant with a C-terminal EGFP tag (pAG415GPD-ccdB-EGFP in Lindquist Advanced Gateway Vector Collection, 80) in yeast.

Exogenous expression of killifish proteins in *Saccharomyces cerevisiae* (one color overexpression assay)

The sequence-verified ORFs were then cloned into yeast gateway vector for GAL-inducible yeast expression with a fluorescent C-terminal EGFP tag (pAG416GAL-ccdB-EGFP in Lindquist Advanced Gateway Vector Collection, 80). The yeast expression plasmid (all low-copy centromeric-based) for each protein was transformed into BY4741 respectively and successful transformation was confirmed through prototrophy selection. The strains bearing the plasmids were inoculated overnight in 2% raffinose media (0.77 g of CSM-URA (Sunrise # 1004-010), 6.7 g of yeast nitrogen base without amino acid (BD 291920), and 20 g raffinose (RPI, #R20500–500.0) in 1 L media), then washed, diluted and switched to 2% galactose media (0.77 g of CSM-URA (Sunrise # 1004-010), 6.7 g of yeast nitrogen base without amino acid (BD 291920), and 20 g galactose (Fisher BioReagents, # BP656-500) in 1 L media) to induce protein expression. The overnight culture generally reached an OD_{600} of 0.9–1 and was further diluted back to OD_{600} ~0.1 and induced for 6–8 h where the OD_{600} reach mid-log ~0.4–0.6. We typically aliquot 2 μL of the mid-log phase yeast onto an imaging spot of a multi-spot microscope slide (6 mm diameter cell Thermo Cat# 9991090), mounted with cover glass (thickness 1 from Corning, Cat# 2975-246) and sealed with nail polish. Microscopy images were taken using a Leica inverted fluorescence microscope with a Hammamatsu Orca 4.0 camera. Exposure times in the DIC channel was 100ms and 50, 250, 500, and 1000 ms in the GFP channel (GFP excitation: 450–490 nm; emission: 500–550 nm; software: LASX DMI6000B; refraction index: 1.518; aperture: 1.4).

Exogenous expression of killifish proteins in *Saccharomyces cerevisiae* (two-color seeding assay)

The full-length African killifish DDX5 and other proteins (PAPBN1, SNRNP70, ELAVL2, CK2A, Human DDX5, PolyQ, NONO, MAGI2, MARK4) were cloned into two yeast advanced gateway destination vectors: one with a constitutive GPD-promoter and a C-terminal EGFP-tag low copy number plasmid (p415GPD-ccdB-EGFP), another one with a galactose-inducible GAL-promoter and a C-terminal mRuby3-tag high copy number plasmid (p426GAL-ccdB-mRuby3). The two plasmids were co-transformed into BY4741 following standard lithium-acetate protocol. First, cells were inoculated and grown to saturation in rich media (YPD). The saturated cultures were then diluted by 10-fold and grew to mid-log. The cells were harvested, washed in sterile water twice, and resuspended in a transformation master mix (240 μL of PEG 3500 50% w/v, 36 μL1 M LiOAc, 50 μL boiled salmon sperm carrier DNA (2 mg/mL), 14 μL plasmid DNA (0.1–1 μg), and sterile water to a final volume of 360 μL). Cells were incubated in the transformation master mix at 42°C for 45 min. Following the heat shock, cells were pelleted, and resuspended in 100 μL of sterile water and plated on respective selective medium.

The BY4741 strain co-transformed with the two fusion protein plasmids was first grown overnight to stationary phase in SD-URA-LEU. Images of the overnight culture were taken as pre-induction phase. The strains were then washed with 1x PBS three times and diluted to OD_{600} = 0.1 in SGAL-URA-LEU (2% galactose). The induction took approximately 6–10 h depending on when the culture reached mid-log (OD_{600} ~ 0.4) and images were taken immediately after this induction phase. After induction, the strains were diluted

Please cite this article in press as: Harel et al., Identification of protein aggregates in the aging vertebrate brain with prion-like and phase-separation properties, Cell Reports (2023), https://doi.org/10.1016/j.celrep.2023.112787

by 200-fold (1 μL of SGAL-URA-LEU induction phase culture into 199 μL of SD-URA-LEU) SD-URA-LEU (2% glucose) and imaged after 24 h of growth as the outgrowth phase. We typically aliquoted 2 μL of the mid-log phase yeast onto an imaging spot of a multi-spot microscope slide (6 mm diameter cell Thermo Cat# 9991090), mounted with cover glass (thickness 1 from Corning, Cat# 2975-246) and sealed with nail polish. Microscopy images were all taken using a Leica inverted fluorescence microscope with a Hammamatsu Orca 4.0 camera. Exposure times in the DIC channel was 100ms and in the fluorescent channel around 50–500 ms (GFP excitation: 450–490 nm and emission: 500–550 nm; Cy3 excitation: and emission; software: LASX DMI6000B; refraction index: 1.518; aperture: 1.4; exposure time: 50, 250, and 500ms for both fluorescent channels). In some specific cases (Figure S4G), we used a two-plasmid system in which the EGFP construct is constitutively on (GPF-ORF-EGFP) and a second construct without a fluorescent tag and inducible with galactose (GAL-ORF).

The microscopy images were quantified using customized CellProfiler script (available in GitHub https://github.com/ywrchen/killifish-aging-aggregates or at this DOI: https://zenodo.org/record/7982837) followed by extensive visual inspection and independent verification. We used the CellProfiler output to primarily identify and quantify total number of cells as well as total number of cells with positive GFP or Cy3 signals. Because the proteins we tested have heterogeneity in protein expression and GFP/Cy3 morphology, we used the CellProfiler foci scoring output as a reference (unified scoring code was difficult to implement) and counted all fluorescent images manually followed by blind counting done by two additional independent lab members on 20% of randomly selected raw images. The reported percentage of cells with foci was quantified as number of cells with GFP or Cy3 foci divided total number of cells with positive GFP or Cy3 signals. We only scored a cell as 'foci-positive' if it either had at least one focus along with diffuse GFP or Cy3 signals or had at least two foci inside a single cell. We considered each half of a budded yeast cells as two cells in the quantification.

Fluorescence recovery after photo bleaching

The yeast samples used for the fluorescence recovery after photo bleaching (FRAP) experiment were prepared following the same procedure as the yeast one-color overexpression assay described above. Briefly, laboratory strain BY4741 transformed with pA416-GAL-DDX5(killifish)-EGFP and [*RNQ*$^{+}$][*psi*$^{-}$] strain transformed with pAG416GAL-Sup35NM(yeast)-EGFP were inoculated in 1 mL of 2% raffinose media (0.77 g of CSM-URA (Sunrise # 1004-010), 6.7 g of yeast nitrogen base without amino acid (BD 291920), and 20 g raffinose (RPI, #R20500–500.0) in 1 L media). The next day, the overnight culture was spun down (3000 g × 5 min at room temperature), washed with 1X PBS twice, diluted by ~10-fold (typical OD600 for overnight culture can reach 0.8–1 and the dilution aimed to dilute the culture to OD600–0.1) and switched to 1 mL of 2% galactose media (0.77 g of CSM-URA (Sunrise # 1004-010), 6.7 g of yeast nitrogen base without amino acid (BD 291920), and 20 g galactose (Fisher BioReagents, # BP656-500) in 1 L media) to induce protein expression. We typically waited 6–8 h, allowing the culture to undergo 2–3 rounds of doubling (mid-log OD_{600} ~0.4–0.6) for sufficient protein induction before imaging.

We prepared thin agar pad for the samples where 8 μL of semi-cooled 1.5% agarose solution (add low melting temperature Nu-Sieve GTG Agarose (Lonza, Cat# 50081) to 2% galactose media (0.77 g of CSM-URA (Sunrise # 1004-010), 6.7 g of yeast nitrogen base without amino acid (BD, 291920), and 20 g galactose (Fisher BioReagents, # BP656-500) in 1 L media), heat it to ~60°C and cool for 1 min) was loaded to each imaging spot of a multi-spot microscope slide (6 mm diameter cell Thermo Cat# 9991090). Typically, 2 μL of the mid-log phase yeast was loaded onto the freshly made agar pad, mounted with high performance cover glass #1.5 (0.17mm +/− 5.0 μm thick, Zeiss #474030-9000-000) and sealed with nail polish. Images were acquired through 3D Structured Illumination microscopy (SIM) with the DeltaVision OMX BLAZE system (Applied Precision-GE, Inc.) equipped with 3 emCCDs (Evolve, Photometrics Inc.) using an Olympus UPlanApo 100x (NA 1.40) oil-immersion objective. SIM excitation was with 100 mW lasers (405nm 488nm, 568nm), widefield epifluorescence excitation for deconvolution datasets was with InsightSSI illuminator (405nm, 488nm, 568 nm) and standard emission filter sets (528/48 nm and 609/37 nm). We used DeltaVision OMX's built-in FRAP and photo kinetic module to set up the time-series experiment. Before each photobleaching experiment, we first drew rectangles around the desired photobleaching areas and recorded their sizes and coordinates. We acquired 3 frames before the actual photobleaching event at the same exposure (FITC-GFP in emCCD-mode with a gain of 500 at 100% intensity for total 100 ms excitation time) and interval (every 20 s) as the recovery stage. The single photobleaching event occurred at frame #4 in the 488-laser channel (GFP) at 31.3% intensity for 0.1 s. We continuously imaged throughout the fluorescence recovery stage for a total of 5 min at 20 s interval.

We analyzed the FRAP time-series images in Fiji. The images were exported as virtual stacks and went through a registration step to minimize drift that would contribute to signal fluctuation. Registration was done with Fiji plugins RegStack or TurboStack followed by manual inspection and the resulting image stacks were used for downstream analysis. Next, we drew the exact photobleaching area (with location and size information recorded at the image acquisition time) and recorded them as region of interests (ROIs). We drew 2X additional areas (ROIs) that were the same size as the photobleached areas in the background as well as inside cells where no photobleaching event occurred. Last, the intensity values of all these ROIs including minimum, mean, and maximum intensity values were exported using the ROI Manager in Fiji. We used the average intensity values of the image background as baseline and subtract that from the photobleached as well as un-bleached ROIs. The FRAP curve was constructed from all photobleached areas after background subtraction (done for each timepoint) and the average as well as standard error of mean were shown. All images for the FRAP experiments were acquired at Stanford Cell Sciences Imaging Facility.

Please cite this article in press as: Harel et al., Identification of protein aggregates in the aging vertebrate brain with prion-like and phase-separation properties, Cell Reports (2023), https://doi.org/10.1016/j.celrep.2023.112787

DDX5-SNAP *E. coli* expression and purification

The full-length African killifish DDX5 was cloned into the pDEST17 vector containing an N-terminal His10-Smt3-tag and a C-terminal SNAP-tag (New England BioLabs). *E. coli* LOBSTR-BL21(DE)-RIL (kerafast) host cells were transformed with the killifish DDX5 plasmid and were grown to an OD of ~0.4, induced by 0.1 mM IPTG overnight at 17°C in LB medium supplemented with 100 μg/mL ampicillin and 25 μg/mL chloramphenicol. Cells were pelleted and resuspended in lysis buffer (50 mM Tris-HCl pH 7.4, 250 mM NaCl, 10% (vol/vol) glycerol, 1 mM DTT, and 10 mM imidazole) containing 200 μg/mL lysozyme and an EDTA-free protease inhibitor cocktail (Roche Diagnostics, cOmplete, EDTA-free Protease Inhibitor Cocktail). After 30 min of lysozyme digestion at 4°C with constant mixing, cells were lysed by sonication, and cellular debris was pelleted at 30,000 g for 30 min. Cleared lysate was incubated with Ni-NTA agarose resin (Qiagen), washed well with Ni-Wash buffer (50 mM Tris-HCl, pH 7.5, 500 mM NaCl, 1 mM DTT, 10% (vol/vol) glycerol, and 25 mM imidazole), and eluted with Ni-Elution buffer (50 mM Tris-HCl, pH 7.5, 500 mM NaCl, 1 mM DTT, 10% (vol/vol) glycerol, and 200 mM imidazole). The eluted protein was dialyzed in high salt storage buffer (50 mM Tris-HCl, pH 7.5, 1 M NaCl, 10% (vol/vol) glycerol, and 1 mM DTT) and digested overnight with 2 μg/mL His6-Ulp1 (Smt3/SUMO-specific protease, purified from *E. coli* with nickel affinity resin) at 4°C to remove the N-terminal His10-SMT3 tag. The digested protein was incubated with Ni-NTA agarose resin again for a second round of native affinity purification, washed well with Ni-Wash high salt buffer (50 mM Tris-HCl, pH 7.5, 1 M NaCl, 1 mM DTT, and 10% (vol/vol) glycerol), and eluted with Ni-Elution high salt buffer (50 mM Tris-HCl, pH 7.5, 1 M NaCl, 1 mM DTT, 10% (vol/vol) glycerol, and 25 mM imidazole). We performed size exclusion chromatography on the eluted proteins in a Superdex 200 Increase 10/300 GL column (GE Healthcare) using an Akta Ettan fast protein liquid chromatography (FPLC) system (GE Healthcare) to further separate the desired protein from contaminants. The resulting protein was concentrated (Amicon Ultra 0.5 mL and 4 mL Centrifuge filters, 30 kDa NMWL devices, Millipore Cat#UFC505024 and UFC805024) and flash frozen in liquid nitrogen for future use.

DDX5(1–535)-SNAP *E. coli* expression and purification

The DDX5 mutant 1–535 lacking the putative C-terminal prion-like domain (PrD) was cloned into the pDEST17 vector containing an N-terminal His10-Smt3-tag and a C-terminal SNAP-tag (New England BioLabs). The same purification scheme was used to purify DDX5(1–535)-SNAP than DDX5-SNAP, except the native affinity purification were done with medium salt concentration and the protein was flash-frozen in medium salt storage buffer (50 mM Tris-HCl, pH 7.5, 500 mM NaCl, 1 mM DTT, and 10% (vol/vol) glycerol).

DDX5(1–483)-SNAP *E. coli* expression and purification

The DDX5 mutant 1–483 lacking the intrinsically disordered region (IDR) was cloned into pDEST17 vector containing an N-terminal His10-Smt3-tag and a C-terminal SNAP-tag (New England BioLabs). The exact same purification scheme for DDX5(1–535)-SNAP was used to purify DDX5(1–483)-SNAP and the protein was flash frozen in medium salt storage buffer (50 mM Tris-HCl, pH 7.5, 500 mM NaCl, 1 mM DTT, and 10% (vol/vol) glycerol).

His10-DDX5-SNAP *E. coli* expression and purification

The full-length African killifish DDX5 was cloned into the pDEST17 vector containing an N-terminal His10-tag and a C-terminal SNAP-tag (New England BioLabs). *E. coli* LOBSTR-BL21(DE)-RIL (kerafast) host cells were transformed with the killifish DDX5 plasmid and were grown to an OD of ~0.4, induced by 0.1 mM IPTG overnight at 17°C in LB medium supplemented with 100 μg/mL ampicillin and 25 μg/mL chloramphenicol. Cells were pelleted and resuspended in lysis buffer (50 mM Tris-HCl pH 7.4, 250 mM NaCl, 10% (vol/vol) glycerol, and 1 mM DTT) containing 200 μg/mL lysozyme and an EDTA-free protease inhibitor cocktail (Roche Diagnostics, cOmplete, EDTA-free Protease Inhibitor Cocktail). Keep a 1:20 lysis buffer to culture volume ratio. After 30 min of lysozyme digestion at 4°C with constant mixing, cells were lysed by sonication (five 2 min cycle, 2s on 2s off, at 100% amplitude, all performed on ice), and cellular debris was pelleted at 30,000 x g (Beckman JA25.25 rotor) for 30 min. Cleared lysate was incubated with Ni-NTA agarose resin (Qiagen), washed well with Ni-Wash buffer (50 mM Tris-HCl, pH 7.5, 200 mM NaCl, 0.5 mM DTT, and 10% (vol/vol) glycerol), and eluted with Ni-Elution buffer (50 mM Tris-HCl, pH 7.5, 200 mM NaCl, 0.5 mM DTT, 10% (vol/vol) glycerol, and 200 mM imidazole). The eluted protein was dialyzed at 4°C to remove imidazole (dialysis buffer: 50 mM Tris-HCl, pH 7.5, 200 mM NaCl, 200 mM arginine, 10% (vol/vol) glycerol, and 0.5 mM DTT) and concentrated to ~5 mg/mL (Amicon Ultra 4 mL Centrifuge filters, 30 kDa NMWL devices, Millipore Cat# UFC805024). Last, we performed size exclusion chromatography on the concentrated proteins in a Superdex 200 Increase 10/300 GL column (GE Healthcare) using an Akta Ettan fast protein liquid chromatography (FPLC) system (GE Healthcare) to further separate the desired protein from contaminants. The resulting protein was further concentrated (Amicon Ultra 0.5 mL and 4 mL Centrifuge filters, 30 kDa NMWL devices, Millipore Cat#UFC505024 and UFC805024) and flash frozen in liquid nitrogen for future use.

Protein labeling reaction

Recombinant proteins were labeled with SNAP-Surface 549 dye (New England BioLabs, Cat# S9112S) for visualization. The labeling reaction was performed in the high salt storage buffer (for DDX5-SNAP) or medium salt storage buffer (for DDX5(1–535)-SNAP and DDX5(1–483)-SNAP) described above while keeping the SNAP-Surface dye at 2x the final concentration of the protein. To minimize protein degradation and photobleaching of the dye, we followed the following order of the reagent addition was: 1) recombinant protein, 2) 4x storage buffer, 3) 5% Tween 20, 4) 100 mM DTT, and 5) 2x SNAP Surface 549 dye to minimize proteolysis. The labeling

reaction was incubated overnight in dark (to avoid photobleaching) at 4°C. To remove excess non-covalently linked SNAP dye, we used a standard desalting column (Zeba spin desalting columns pre-equilibrated with high salt buffer (1 M NaCl, 50 mM Tris-HCl, pH 7.5, 1 mM DTT for DDX5-SNAP) or medium salt buffer (500 mM NaCl, 50 mM Tris-HCl, pH 7.5, 1 mM DTT for DDX5(1–535)-SNAP and DDX5(1–483)-SNAP), Thermo Fisher, Cat# 89882). In case of preparing purified recombinant protein inputs for the ATPase activity assay, we used dialysis exclusively to remove excess dye while adjusting the salt concentration to a desired level (50 mM NaCl) at the same time (Slide-A-Lyzer 20K MWCO Mini dialysis cassette were used, Thermo Cat#69590). Successful labeling was verified by running SDS-PAGE and image the gel directly using Bio-Rad Universal Hood II Gel Doc Molecular Imaging System CFW-1212M (using the protein blot DyLight 550 setting, excitation/emission: 550/518). We ran a small amount (1 μL) of Bio-Rad Precision Plus Protein WesternC standards along with the labeled protein while keeping at least one open lane in between the protein ladder and sample to avoid signal bleed-through. We imaged immediately after gel electrophoresis to obtain the best signal.

Phase diagrams

Purified proteins were labeled overnight (the same protein storage buffer with additional 2x dye for every 1x protein, 1mM DTT, 5% Tween 20) with SNAP DyLight 549 dye. After labeling, proteins were resolved on SDS-PAGE and imaged on a gel doc system with excitation/emission at 550/518nm (see protein labeling reaction section for details) to ensure the correct protein was labeled and there was minimum degradation. Phase diagrams were generated through dialysis using Slide-A-Lyzer MINI Dialysis Device (20K MWCO, 0.1 mL, Thermo Cat#69590) and the resulting protein was further diluted to respective protein/salt mixture (no inclusion of glycerol, DNA, RNA, or ATP in any condition) when necessary. The protein concentration for each condition was measured directly from 1 μL aliquot of the sample using NanoDrop (record A280nm measurements and use the exact same protein sample buffer as blank) and the Bradford assay (Biorad). After incubation for different amounts of time (1 h after dialysis or dilution to allow droplet maturation) at different temperatures (either 4°C or 25°C), 1–2 μL of the protein/salt mixtures was aliquoted onto a coverslip/glass slide (multi-spot microscope slide (6 mm diameter cell Thermo Cat# 9991090) mounted with cover glass (thickness 1 from Corning, Cat# 2975-246)) and sealed with nail polish. Microscopy images were taken using a Leica inverted fluorescence microscope with a Hamamatsu Orca 4.0 camera. Exposure times in the DIC channel was 100ms and in the fluorescent channel around 50–500 ms (GFP excitation: 450–490 nm and emission: 500–550 nm; Cy3 excitation: and emission; software: LASX DMI6000B; refraction index: 1.518; aperture: 1.4; exposure time: 50, 250, and 500ms for both fluorescent channels). Scoring for droplet formation was based on DIC and Cy3 imaging using a 100× oil objective on an inverted Leica microscope. If spherical-shaped droplets were observed in both DIC and Cy3 channel, we noted that query protein can phase separate under the particular protein and salt concentrations. We used results conducted at 4°C to construct the phase diagram.

Salt, protein concentration, temperature, and time effects on DDX5 assembly

We assessed the spontaneous assembly of DDX5 at different salt and protein concentrations at different temperatures in the absence of nucleic acids (DNA or RNA) and ATP. We focused on four conditions where DDX5 was shown to phase separate. Specifically, full length DDX5 stock protein (~24 μM stored in 1 M NaCl, 50 mM Tris-HCl, pH 7.4, 10% glycerol, 1 mM DTT at −80°C) was labeled overnight at 4°C (see labeling reaction for detail) with SNAP DyLight 549 dye. After labeling, proteins were resolved on SDS-PAGE and imaged on a gel doc system with excitation/emission at 550/518nm (see protein labeling reaction section for details) to ensure the correct protein was labeled and there was minimum degradation. Next, we dialyzed 20 μL of purified proteins using Slide-A-Lyzer MINI Dialysis Device (20K MWCO, 0.1 mL) in 250 mL medium salt buffer (500 mM NaCl, 50 mM Tris-HCl, pH 7.4, 1 mM DTT) and 250 mL low salt buffer (150 mM NaCl, 50 mM Tris-HCl, pH 7.4, 1 mM DTT), respectively, for a total of 1 h with constant stirring (200 r.p.m.) at 4°C. After dialysis, protein concentration in either sample were estimated from nanodrop A280nm measurements (the exact same protein sample buffer was used as blank to zero the reads). We further diluted the proteins to the following 4 conditions (condition 1: [NaCl] = 500 mM and [DDX5] = 9.8 μM; condition 2: [NaCl] = 250 mM and [DDX5] = 4 μM; condition 3: [NaCl] = 150 mM and [DDX5] = 6 μM; condition 4: [NaCl] = 50 mM and [DDX5] = 2.8 μM all in 50 mM Tris-HCl, pH 7.4, 1 mM DTT, no RNA/DNA/ATP) and prepared 5 μL sample for each condition for incubation at either 4°C or room temperature (~25°C) with no shaking/agitation. At 2 h and 24hr timepoints, we aliquoted 1 μL of protein from each condition onto a coverslip (multi-spot microscope slide (6 mm diameter cell Thermo Cat# 9991090) mounted with cover glass (thickness 1 from Corning, Cat# 2975-246)), sealed with nail polish, and imaged them. Microscopy images were taken using a Leica inverted fluorescence microscope with a Hammamatsu Orca 4.0 camera using a 100× oil objective. Exposure times in the DIC channel was 100ms and in the fluorescent channel around 50–500 ms (GFP excitation: 450–490 nm and emission: 500–550 nm; Cy3 excitation: and emission; software: LASX DMI6000B; refraction index: 1.518; aperture: 1.4; exposure time: 50, 250, and 500ms for both fluorescent channels). The microscopy images of *in vitro* assembled protein condensate were quantified using CellProfiler. Specifically, we used a customized CellProfiler script (available in GitHub https://github.com/ywrchen/killifish-aging-aggregates or at this DOI: https://zenodo.org/record/7982837) to identify and quantify the total number of condensates and characterize their shape (form factor) and intensity.

In vitro seeding

Full length killifish DDX5 stock protein (~24 μM of DDX5-SNAP stored in 1 M NaCl, 50 mM Tris-HCl, pH 7.4, 10% glycerol, 1 mM DTT at −80°C) was labeled overnight at 4°C (see labeling reaction for detail) with SNAP DyLight 549 dye. A killifish DDX5 variant

with an N-terminal His10-tag (~16 μM of His10-DDX5-SNAP stored in 1 M NaCl, 50 mM Tris-HCl, pH 7.4, 10% glycerol, 1 mM DTT at −80°C) was labeled overnight at 4°C (see labeling reaction for detail) with SNAP Alexa 488 dye. After labeling, proteins were resolved on SDS-PAGE and imaged on a gel doc system with excitation/emission at 550/518nm (see protein labeling reaction section for details) to ensure the correct protein was labeled and there was minimum degradation. The labeled DDX5-SNAP protein was subjected to desalting where the column (Zeba spin desalting columns, Thermo Fisher, Cat# 89882) was pre-equilibrated with high salt buffer (1 M NaCl, 50 mM Tris-HCl, pH 7.4, and 1 mM DTT) and the resulting protein was diffuse serving as "recipients" (final stock concentration was 4.35 μM determined by Bradford). The N-terminal His10-tagged DDX5-SNAP was dialyzed in low salt buffer (150 mM NaCl, 50 mM Tris-HCl, pH 7.4, and 1 mM DTT) to induce the formation of amorphous aggregates which served as the "seed" (final stock concentration was 8.7 μM determined by Bradford). We set up the *in vitro* assembly with equal volume of diffuse DyLight 549 labeled DDX5-SNAP and equal volume of three 5-fold serial dilutions (diluent was the same low salt buffer) of Alexa 488 labeled His10-DDX5-SNAP aggregates in the absence of DNA/RNA/ATP. We also included a control where the diffuse DyLight 549 labeled DDX5-SNAP was mixed with equal volume of low salt buffer only. All samples were incubated at room temperature (~25°C) with no shaking/agitation. At 1 h, 24hr, and 72 h timepoints, we aliquoted 1 μL of protein from each condition onto a coverslip (multi-spot microscope slide (6 mm diameter cell Thermo Cat# 9991090) mounted with cover glass (thickness 1 from Corning, Cat# 2975-246)), sealed with nail polish, and imaged them. Microscopy images were all taken using a Leica inverted fluorescence microscope with a Hamamatsu Orca 4.0 camera using a 100× oil objective. Exposure times in the DIC channel was 100ms and in the fluorescent channel around 50–500 ms (GFP excitation: 450–490 nm and emission: 500–550 nm; Cy3 excitation: and emission; software: LASX DMI6000B; refraction index: 1.518; aperture: 1.4; exposure time: 50, 250, and 500ms for both fluorescent channels).

ATPase assay

DDX5 is an ATP-dependent helicase.[101] To test the ATPase activity of DDX5, ATPase assays were set up in 96-well PCR plate on ice where fresh ATP stock was added last. A 10 μL reaction was set up with final condition of 50 mM Tris-HCl pH 7.5, 150 mM NaCl, 5 mM $MgCl_2$, 2 mM ATP, variable amount of protein, and 500 ng/μL of yeast total RNA (unless otherwise noted). Reactions were conducted at room temperature for 30 min (or for variable amount of time specified in the time-course experiments), diluted to a final volume of 50 μL by addition of 40 μL nuclease-free water and quenched with 100 μL of BIOMOL GREEN (molybdate/malachite green-based colorimetric phosphate assay). The rate of ATP hydrolysis was reported as amount of free phosphate released in a unit time and volume. The free phosphate is inferred from $OD620_{nm}$ reading upon 20 or 30 min of color development after BIOMOL GREEN addition. A phosphate standard curve is constructed beforehand in the exact reaction buffer condition to relate $OD620_{nm}$ reading and the amount of free phosphate in solution. In all experiments, we set up > 4 technical replicates for each condition. All experiments were independently repeated for at least three times and the average and standard error of mean were shown.

Droplet and diffuse protein activity comparison

Full-length DDX5 or ΔPrD or ΔIDR mutants were labeled overnight at 4°C the night before use. To induce robust formation of droplets, full-length DDX5 or ΔPrD or ΔIDR mutants were subjected to dialysis in droplet induction buffer (50 mM NaCl, 50 mM Tris-HCl, 0.5 mM DTT) at 4°C for 15 min. Dialysis (a 100 μL dialysis cassette was used at maximum 40% volume capacity, Slide-A-Lyzer 0.1 mL MINI Dialysis Device 20K MWCO, Thermo Cat#69590) was done in 10000:1 buffer to sample volume ratio (or even larger) to ensure rapid equilibration of salt to the desired 50 mM concentration without drastic increase in sample volume. For a 30 μL aliquot, 15 min of dialysis was generally enough to equilibrate the salt in our setup, which included a stir bar and rotation speed at 200 r.p.m. The dialyzed sample was imaged right away to confirm the presence of droplets. For samples that require droplet as starting material, the dialyzed sample served as the protein input. Diffuse sample was obtained by selecting the supernatant after a spin at 13,000 g for 20 min at 4°C for experiments described in Figures 4A and 4B. For experiments described in Figures 4C–4G, the resulting pre-steady state diffuse sample were divided in half where one was further incubated at 4°C to allow enough time for new droplet to mature. This second experimental setup ensured that the total protein concentration of the diffuse and droplet samples remained the same. Protein concentration was estimated from nanodrop A280nm measurements for each condition (using the same protein sample buffer as blank to zero the reads). We did not observe that the presence of droplet upon thorough mixing significantly altered the nanodrop reading. The ATPase activity assay on droplet and diffuse protein was performed as described above in the ATPase reaction section.

QUANTIFICATION AND STATISTICAL ANALYSIS

For proteomics, we used the log2-transformed protein abundance to perform a parametric statistical test (Student's t-test). We verified that the protein abundance for each tissue approximately followed a normal distribution.[49] The p values were not corrected for multiple hypothesis testing, as is often done for proteomics datasets.[87–92] All the proteins identified in the brain were ranked and sorted in descending order based on multiplication of $\log_2$ transformed fold change and $-\log_{10}$(p value). This metric prioritizes proteins with both large absolute fold changes and small p values. Note that due to random seeding effect in GSEA, the exact p value and rank of the enriched terms may differ for each run. These random seeds did not qualitatively affect the

enrichment analyses. P-values were not FDR-corrected. To determine the enrichment for PLAAC or DISOPRED, p values were calculated using a Fisher's exact test on the age-associated aggregates that contain either PrD or IDR, respectively, in comparison to the total detected aggregates in each tissue. To test statistical significance for differences in protein aggregations in human 293T cells, p values were calculated with the Kruskal-Wallis test with Dunn's correction. To test statistical significance for differences in protein aggregations in yeast and for differences in the form factor of protein condensates *in vitro*, p values were calculated using a Student's t-test.

Cell Reports, Volume ■ ■

Supplemental information

Identification of protein aggregates in the aging vertebrate brain with prion-like and phase-separation properties

Itamar Harel, Yiwen R. Chen, Inbal Ziv, Param Priya Singh, Daniel Heinzer, Paloma Navarro Negredo, Uri Goshtchevsky, Wei Wang, Gwendoline Astre, Eitan Moses, Andrew McKay, Ben E. Machado, Katja Hebestreit, Sifei Yin, Alejandro Sánchez Alvarado, Daniel F. Jarosz, and Anne Brunet

Figure S1

A GSEA enrichment (biological processes) for age-related changes in the brain

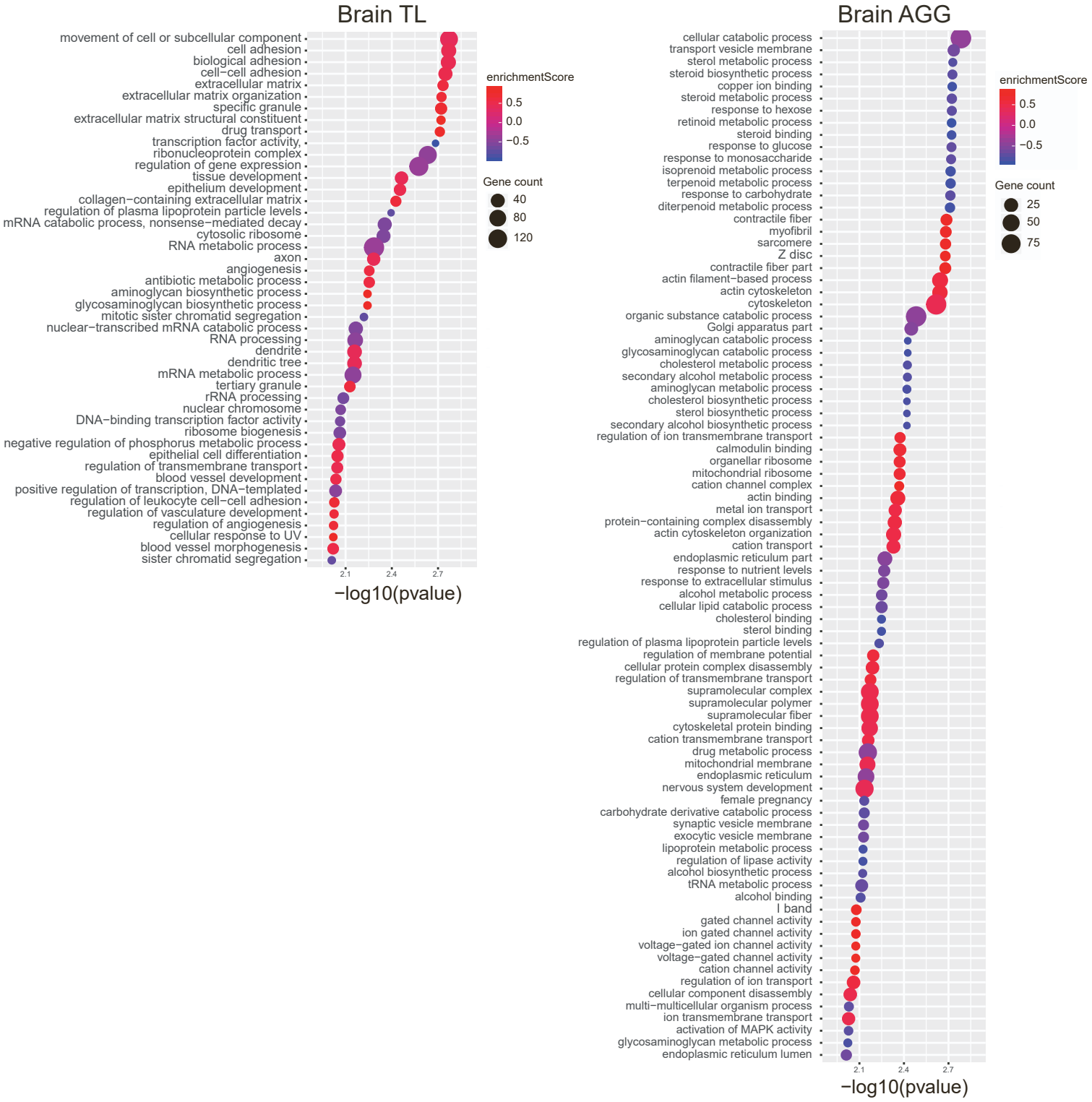

B Enrichment for disordered domains

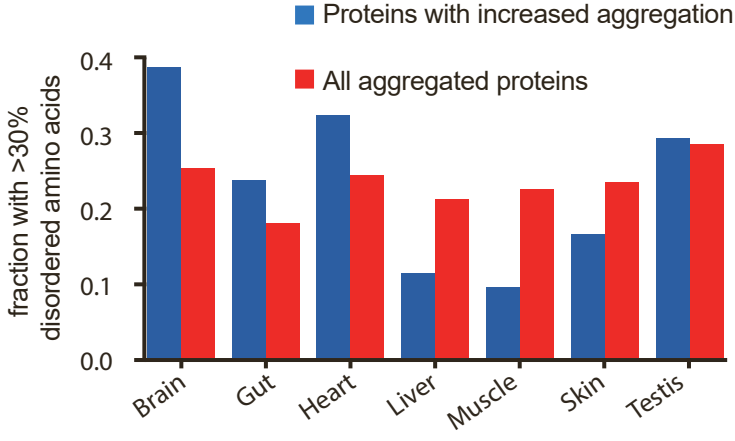

* More than 30% of amino acid residues are predicted to be disordered

Figure S1 – Characteristics of protein aggregates in old killifish brains, Related to Figure 1
(A) GO enrichment using Gene Set Enrichment Analysis (GSEA) for proteins with increased age-related changes in the brain, for either tissue lysate (TL, left), or aggregate fraction (AGG, right). Enrichment score = score for enrichment/depletion of GO terms in this gene set. Counts = number of genes. P-values were not FDR-corrected.
(B) Enrichment for intrinsically disordered regions in proteins with increased aggregation propensity with age in the brain. Proteins with more than 30% of amino acid residues that are predicted to be disordered are considered here. Red: all detected aggregated proteins; Blue: proteins with an age-related increase in aggregation propensity are in blue. No significant difference between the two groups in each organ (Fisher's exact test). Numbers in Table S3.

Figure S2

A DDX5 in the killifish brain

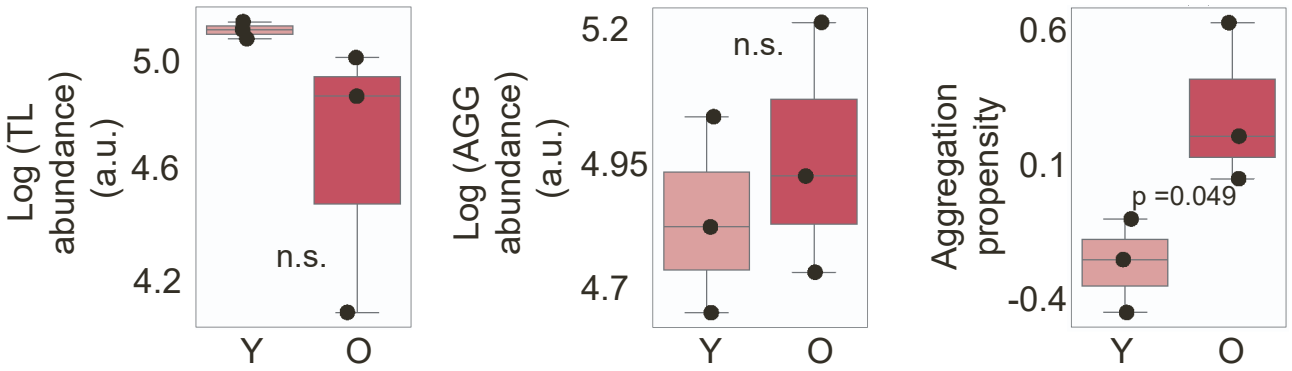

B Prion-like domains in DEAD-box helicase family members identified in this study

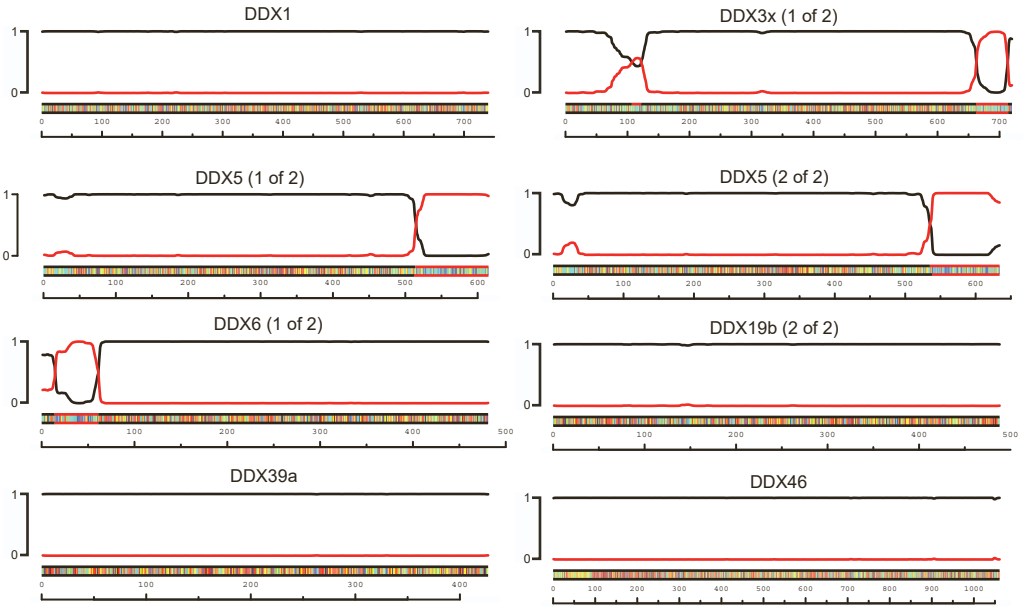

Killifish final Symbol	PrD score
DDX1	-15.70
DDX39a	-20.53
DDX3x (1 of 2)	12.35
DDX46	-10.67
DDX5 (1 of 2)	37.47
DDX5 (2 of 2)	34.82
DDX6 (1 of 2)	12.31
DDX3x (2 of 2)	12.87
DDX19b (2 of 2)	-5.92

Color-coded amino acid visualization N Q Y G M S P A H T F R V I D L K C W E — Background — Prion-like domain (PrD)

C Amino acid composition of PrD and IDR domains in DDX5

DDX5 (2 of 2) PrD (Putative):
535-634 (end)

GSKAQNSGNYGGNSGNSCGSYGNN
NYNNSNGQGSFSGPPNQGGFGNQGF
QAPPQFGGMQRAAQNGVNHPPFPFN
AQPPPPQNQQPPPPMVPYPIPPPFPQ

DDX5 (2 of 2) IDR domain:
483-535 is RGG-righ

RGGRGRGGRGGYKD
DRRDRYSGGRSNFGG
SGFRDRDHDRGFGNG
PKTTFG

D Western blot of killifish brain with C-term DDX5 antibody

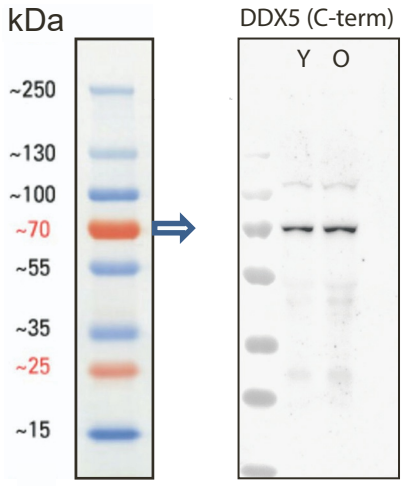

DDX5 (C-term) antigen: 625-PYPIPPPFPQ-634

E Immunohistochemistry of killifish brain sections using C-term killifish-specific DDX5 antibody

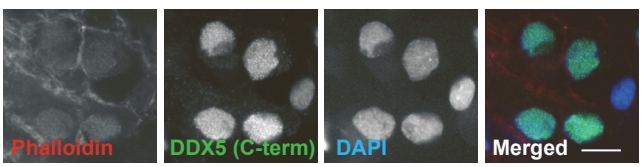

F Blinded quantification of DDX5 puncta in killifish brain sections

Speckles	Young brain	Old brain
More nuclear	50%	38%
More cytoplasmic	50%	62%

* Data from 3 animals for each condition. A total of 43 sections.

Figure S2 – DDX5 forms aggregates in old vertebrate brains, Related to Figure 2

(A) DDX5 levels in the tissue lysate (TL) and aggregate fraction (AGG) as well as DDX5 propensity to aggregate with age in the killifish brain. The box shows the quartiles of the data while the whiskers extend to show the rest of the distribution on protein abundance (y-axis) in young (Y) or old (O) samples. Each dot represents the protein abundance of an individual fish sample. Unit for y-axis a.u. stands for arbitrary units. P-values: Student's t-tests; n.s.: $p>0.05$.

(B) Location of the predicted prion-like (PrD) domain in DEAD-box helicase family members identified in this study. Red line: score of the PrD domain. Amino-acid numbers are indicated at the bottom. PrD score (PLAAC) is indicated (bottom right). Amino-acid composition is color-coded.

(C) Amino acid composition of PrD and RGG (motifs rich in arginines and glycines) domains in the primary DDX5 paralog in this study, DDX5 (2 of 2). The DDX5 (1 of 2) is more prevalent in the liver. Amino-acid numbers of each domain are indicated.

(D) Production and validation of killifish DDX5 C-terminus antibody using a Western blot for brain lysates, extracted from either young (~3 months old) or old (~7 months old) killifish. The peptide sequence used as an antigen for immunization is indicated at the bottom.

(E) Immunohistochemistry of killifish brain sections using C-term DDX5 antibody (green) and phalloidin, which recognizes actin filaments (red). Blue: DAPI. Scale bar: 10μm.

(F) Qualitative quantification of the localization of DDX5 puncta in brain sections from young (3.5 months old) and old (7 months old) killifish. Data from 3 animals for each condition, with a total of 43 sections.

Figure S3

A Generation of *Tg(ddx5:DDX5-GFP)* transgenic fish

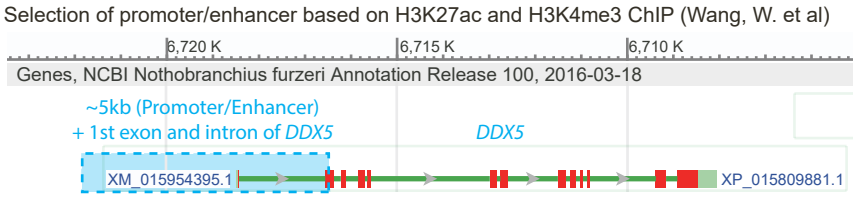

B Generation of *DDX5* mutant using CRISPR

1) Target selection

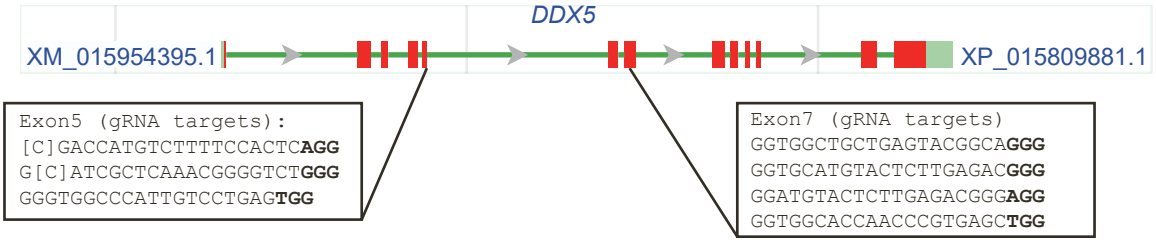

2) Detected germline transmission (in embryos)

```
DDX5 locus, exon 5 (Δ7)
GAGCGATGCCGACCATGTCTTTTCCACTCAGGACAATGGGCCAC
||||||||||||||||||||||||        ||||||||||||
GAGCGATGCCGACCATGTCTTTTCC-------ACAATGGGCCAC

DDX5 locus, exon 7/8 (Δ4)
CTGCTGAGTACGGCAGGGCCTCCCGTCTCAAGAGTACATGCATC
||||||||||||||||||||||||||||||||||||||||||||
CTGCTGAGTACGGCAGGGCCTC----CTCAAGAGTACATGCATC
```

3) No stable line (embryonic lethal)

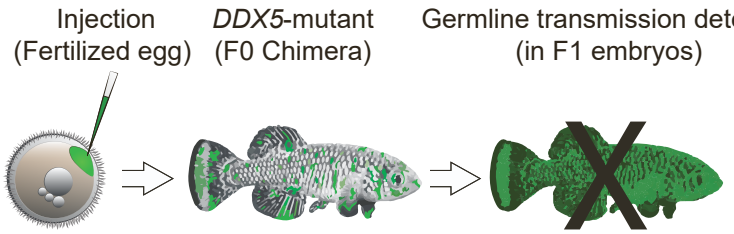

C Generating truncations in the killifish DDX5

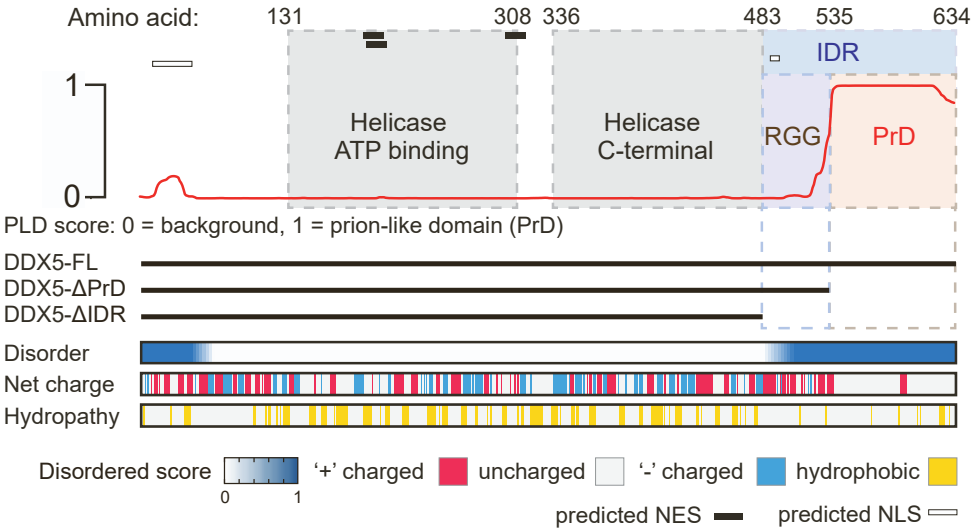

D Localization of DDX5 and polyQ(97) puncta in 293T cells

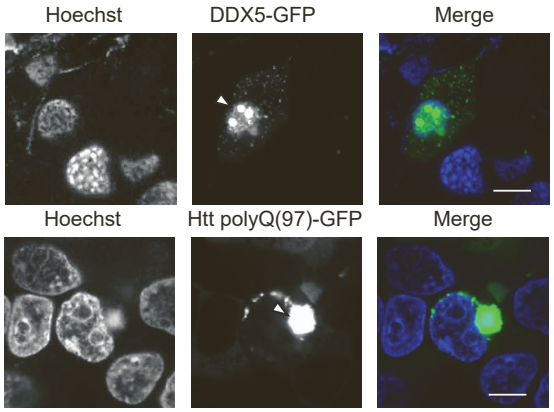

E Aggregation of human DDX5 in human 293T cells

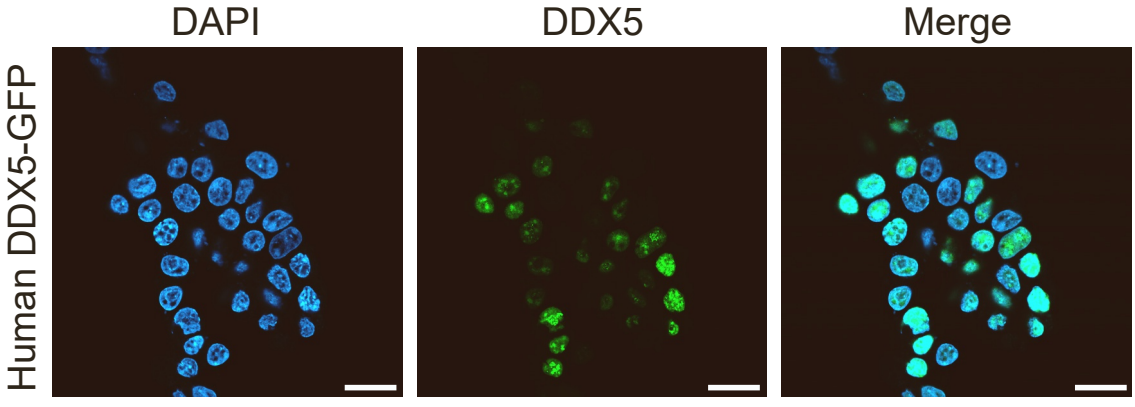

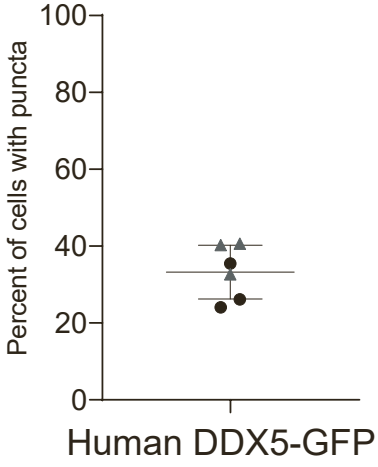

Figure S3 – Killifish mutants for DDX5 and expression in human cells, Related to Figure 2
(A) The *Tg(ddx5:DDX5-GFP)* transgenic founder F0 fish were generated by using 5kb surrounding the transcriptional start site of the *DDX5* gene (including the first exon) to drive the expression of DDX5-GFP fusion protein (dashed blue line). Exons are indicated in red. This construct did not go germline and no stable line could be generated.
(B) Generation of DDX5 CRISPR killifish mutant, including (1) gRNA target design for exons 5 and 7, and (2) evidence for successful germline transmission in F1 embryos. (3) F1 fries were never detected, even as heterozygous. Therefore, no stable line could be generated.
(C) Generation of killifish DDX5 mutants with truncation of the prion-like domain (DDX5-ΔPrD) or truncation of the intrinsically disordered region (DDX5-ΔIDR) tagged with EGFP for expression in mammalian cells. FL: full length. Red line: PLAAC score of the protein sequence. Bottom: Color-coded distribution of the disordered region (DISOPRED3, blue), net charge (sliding window of 5 amino acids), and hydropathy (sliding window of 5 amino acids) in the killifish DDX5 protein.
(D) Localization of DDX5-GFP (left) or polyQ(97)-GFP puncta in 293T cells. DDX5 puncta are primarily nuclear, whereas polyQ(97) puncta are primarily perinuclear (white arrowheads). Green: GFP-tag of the indicated protein; Blue: Hoechst. Images are representative of 2 experiments, each performed in triplicates. Scale bar: 5μm.
(E) Percentage of aggregate-like puncta for GFP tagged human DDX5 in human 293T cells. Puncta were assessed using fluorescence (green, GFP-tagged). Left: Representative images from two independent experiments, each performed in triplicate. Scale bar: 10μm. Right: Mean +/- SD of the percentage of transfected cells with DDX5 aggregates. Each dot represents the average of ~240 cells from 3 fields of view in a well, over two independent experiments. Circles: experiment #1, Triangles: experiment #2.

Figure S4

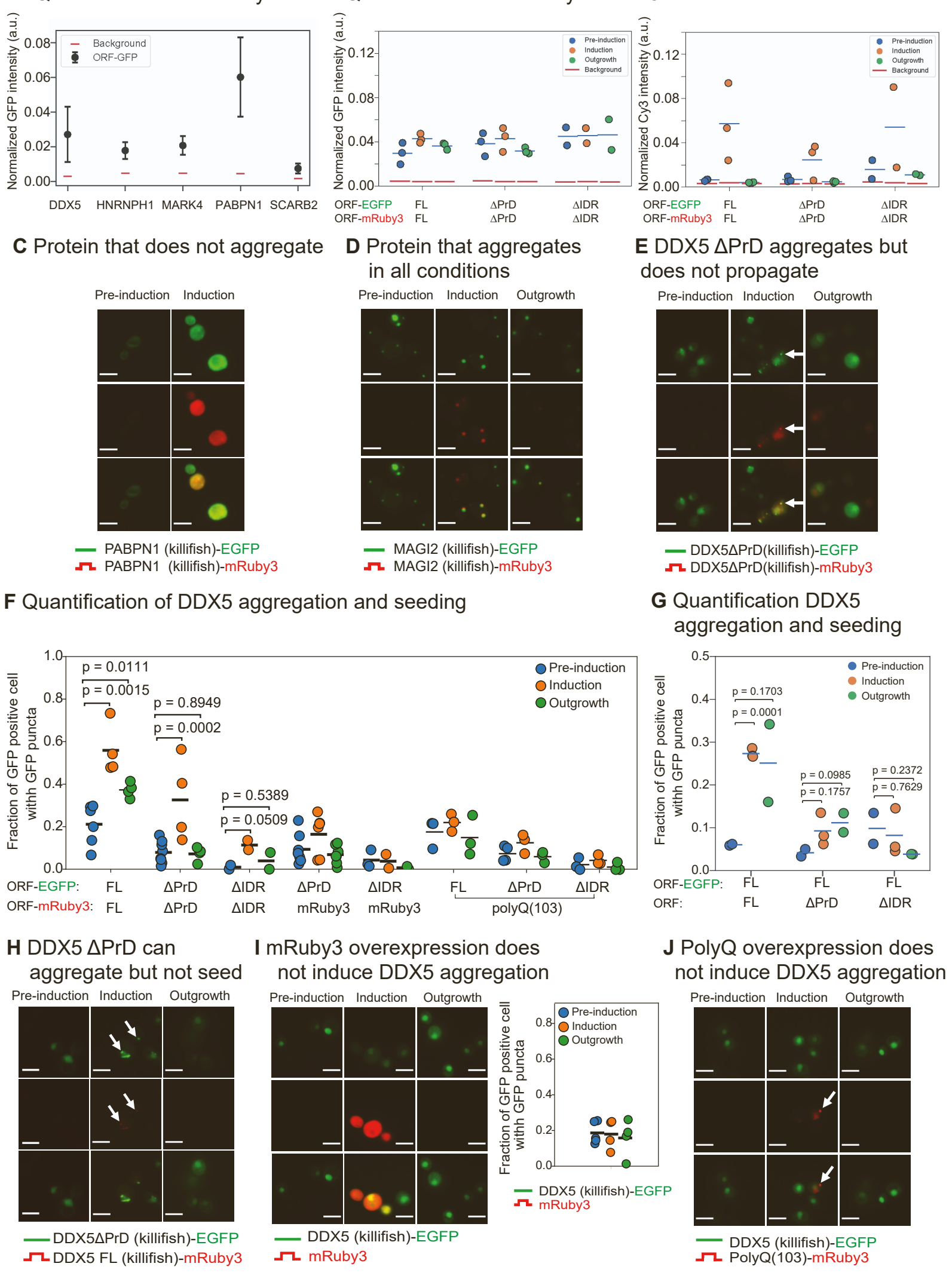
A Quantification of intensity
Normalized GFP intensity (a.u.)
Background
ORF-GFP
DDX5
HNRNPH1
MARK4
PABPN1
SCARB2
B Quantification of intensity of DDX5 and its truncation mutants
Normalized GFP intensity (a.u.)
Normalized Cy3 intensity (a.u.)
Pre-induction
Induction
Outgrowth
Background
ORF-EGFP FL ΔPrD ΔIDR
ORF-mRuby3 FL ΔPrD ΔIDR
C Protein that does not aggregate
D Protein that aggregates in all conditions
E DDX5 ΔPrD aggregates but does not propagate
Pre-induction
Induction
Outgrowth
PABPN1 (killifish)-EGFP
PABPN1 (killifish)-mRuby3
MAGI2 (killifish)-EGFP
MAGI2 (killifish)-mRuby3
DDX5ΔPrD(killifish)-EGFP
DDX5ΔPrD(killifish)-mRuby3
F Quantification of DDX5 aggregation and seeding
Fraction of GFP positive cell withh GFP puncta
p = 0.0111
p = 0.0015
p = 0.8949
p = 0.0002
p = 0.5389
p = 0.0509
ORF-EGFP: FL ΔPrD ΔIDR ΔPrD ΔIDR FL ΔPrD ΔIDR
ORF-mRuby3: FL ΔPrD ΔIDR mRuby3 mRuby3 polyQ(103)
G Quantification DDX5 aggregation and seeding
p = 0.1703
p = 0.0001
p = 0.0985
p = 0.1757
p = 0.2372
p = 0.7629
ORF-EGFP: FL FL FL
ORF: FL ΔPrD ΔIDR
H DDX5 ΔPrD can aggregate but not seed
DDX5ΔPrD (killifish)-EGFP
DDX5 FL (killifish)-mRuby3
I mRuby3 overexpression does not induce DDX5 aggregation
DDX5 (killifish)-EGFP
mRuby3
J PolyQ overexpression does not induce DDX5 aggregation
DDX5 (killifish)-EGFP
PolyQ(103)-mRuby3

Figure S4 – Quantification of aggregation and prion-like behavior, Related to Figure 3
(A) Quantification of overall fluorescence intensity for experiments presented in Figures 3B and C. Each dot represents the mean of the normalized GFP intensity for all cells expressing the protein fused with EGFP in one experiment. Whisker is +/- one standard deviation of the normalized GFP intensity across all cells expressing protein fused with EGFP in one experiment. The red bar is the mean normalized GFP intensity of the background of all corresponding fields of view in one experiment. Note that all proteins were tested in different experiments.
(B) Quantification of overall fluorescence intensity for experiments presented in Figures 3E-G and Figure S4F. Each dot represents the quantification of an independent experiment. The blue bar is the mean across experiments.
(C,D) Identification of killifish candidate proteins that do not aggregate (C), and proteins that aggregate under basal expression levels (D).
(E) Following overexpression of DDX5ΔPrD-mRuby3, DDX5ΔPrD-GFP form aggregates (white arrows), which become diffuse and nuclear-localized after propagation. Representative of 4 independent experiments (quantified in D). Scale bar: 5μm.
(F) Quantification of DDX5 aggregates and prion-like seeding potential by calculating the fraction of GFP positive cells with EGFP puncta in the indicated systems during pre-induction, induction, and outgrowth. Mean values from 3 or more independent experiments are indicated by the black bar, and each dot represents the average value within each experiment (induction and outgrowth phase results were selected when overexpression of mRuby3-tagged protein was robust. An average of 135 GFP-positive yeast cells are quantified for each strain under each experimental condition). P-values: from unpaired t-test between indicated experimental phases.
(G) Quantification of DDX5 aggregates and prion-like seeding potential by calculating the fraction of EGFP positive cells with EGFP puncta during pre-induction, induction, and outgrowth. Mean values from 2-3 independent measurements of 1 independent experiment are indicated by the black bar. Each dot represents 1 independent measurement for one experiment. P-values: Student's t-test.
(H) The prion-like domain of DDX5 is necessary for propagation. Following overexpression of DDX5FL-mRuby3, DDX5ΔPrD-GFP forms aggregates (white arrows) in the induction phase but becomes diffuse (nuclear) in the outgrowth phase. Representative of 4 independent experiments (quantified in H). Scale bar: 5μm.
(I) Left: following expression of mRuby3 alone, killifish DDX5-EGFP remains diffuse (and nuclear-localized). Representative images of 4 independent experiments (quantified on the right). Scale bar = 5 μm. Right: Quantification of DDX5 aggregation and prion-like seeding potential by calculating the fraction of EGFP positive cells with EGFP puncta during pre-induction, induction, and outgrowth. Mean values from 4 independent experiments are indicated by the black bar. Each dot represents the average value within each experiment (an average of 135 GFP-positive yeast cells were quantified for each strain under each experimental condition). Difference across groups were assessed using Student's t-test.
(J) Following expression of the toxic and aggregation-prone PolyQ(103) repeat, killifish DDX5-EGFP remains diffuse (and nuclear-localized). White arrows: PolyQ(103)-mRuby3 aggregates. Scale bar: 5 μm.

Figure S5

A Purification of recombinant killifish DDX5 full length and truncation mutants

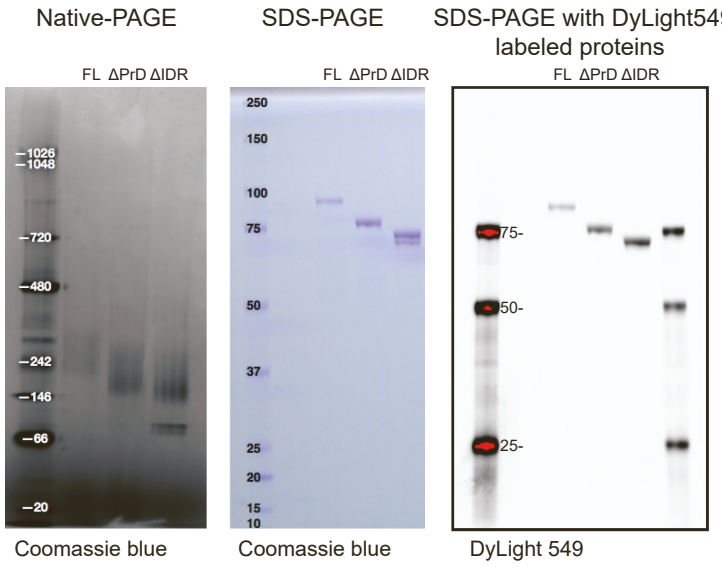

B Activity of DDX5 condensates

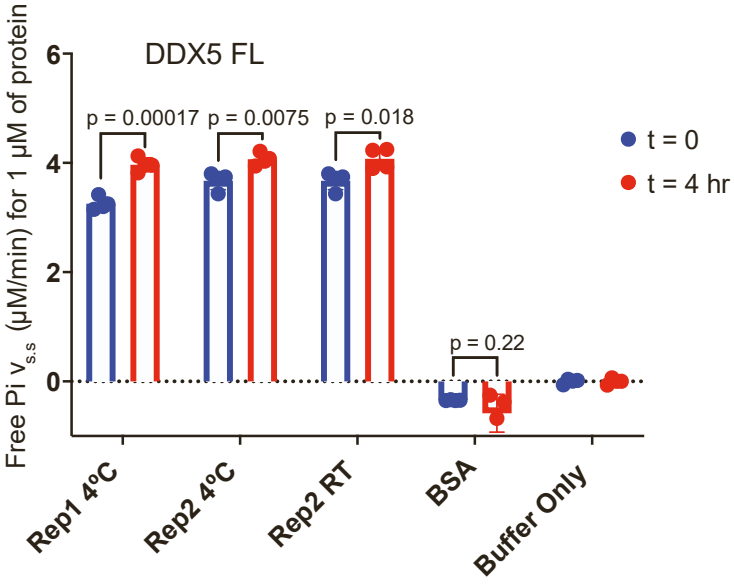

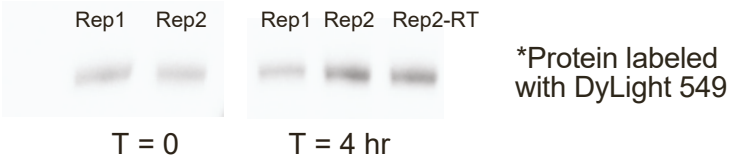

*Protein labeled with DyLight 549

C DDX5 ΔPrD has RNA-stimulated ATPase activity

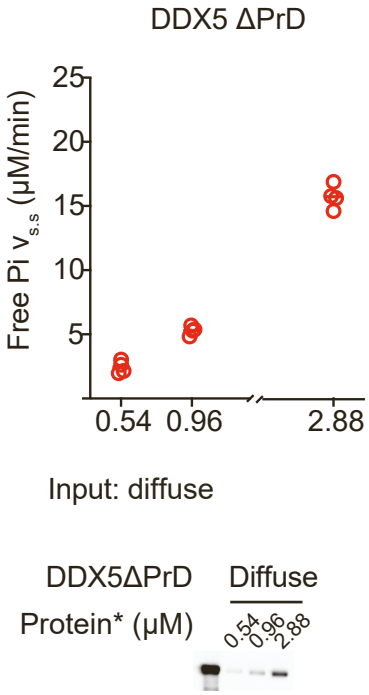

D Activity of diffuse DDX5 full length and truncation mutants

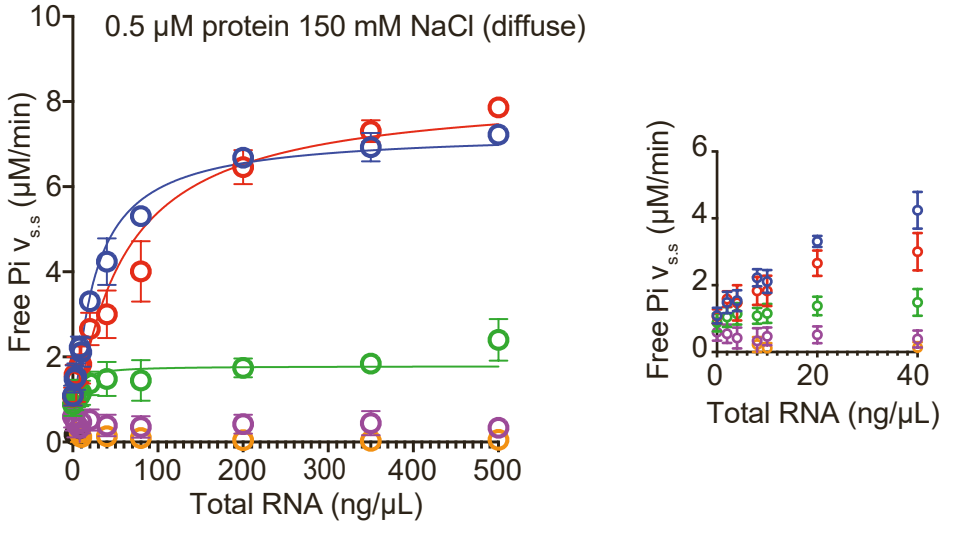

*Protein labeled with DyLight 549

DDX5 DDX5 ΔPrD DDX5 ΔIDR BSA Buffer

E Michaelis-Menten fit for ATPase activity of diffuse DDX5 full length and truncation mutants

Michaelis-Menten fit

Killifish protein	V_{max} (μM/min) free Pi	Km (ng/μL) yeast total RNA	r^{2*}
DDX5 FL	7.3 (6.8-7.9)	22.8 (16.5-31.3)	0.9
DDX5 ΔPrD	8.3 (7.2-9.7)	53.3 (31.1-92.1)	0.9
DDX5 ΔIDR	N/A	N/A	N/A

*Non-linear regression

Figure S5 – DDX5 ATPase activity, Related to Figure 4

(A) Purified recombinant killifish DDX5 FL and mutants (ΔPrD and ΔIDR), as seen by Native-PAGE stained with coomassie blue (left), SDS-PAGE stained with coomassie blue (center), and SDS-PAGE visualized with DyLight 549 (SNAP-tagged protein was labeled with DyLight 549 dye prior to gel electrophoresis) (right).

(B) ATPase assay results from an additional independent experiment (similar to Figure 4C). Killifish DDX5 protein in diffuse (red circles) or condensate (blue circles, above 2 μM) forms were used to induce ATP hydrolysis in the presence of yeast total RNA. The ATPase activity is measured as a function of free phosphate (Pi) release rate (μM/min), controlling for the same total DDX5 protein concentrations (μM). Values of 4 technical replicates are shown along with western blot to confirm a similar level of total DDX5 protein.

(C) Killifish DDX5ΔPrD shows concentrations dependent ATPase activity in the presence of RNA (red circles). At these consecrations, the DDX5ΔPrD protein was in its diffuse form. ATPase activity is measured as a function of free phosphate (Pi) production rate (μM/min) at the indicated protein concentrations (μM). Values of 4 replicates from one representative experiment are shown along with SDS-PAGE of the reaction mixture. Two independent experiments were performed.

(D) Left: ATPase activity for the killifish DDX5 full length (FL) and mutants (ΔPrD and ΔIDR). As negative controls, BSA (Bovine Serum Albumin) or buffer alone was used. Activity is measured under diffuse conditions (0.5 μM protein, 150 mM NaCl) as a function of free Pi production rate (μM/min) at the indicated RNA concentrations (ng/μL). Right: Inset displays activity at lower concentration with higher resolution. Mean +/- SEM from 3 independent experiments (3-4 replicates in each experiment) were shown.

(E) Michaelis-Menten fit for the activity of DDX5 full length (FL) and mutants (ΔPrD and ΔIDR), as measured in (C). The Michaelis–Menten equation describes the rate of ATP hydrolysis by relating the rate of free Pi production (μM/min) induced by DDX5 to the concentration of the RNA substrate (yeast total RNA) (ng/μL). The estimated maximum reaction rate (Vmax) and the Michaelis constant Km (a measure of the substrate-binding affinity) are provided.